Università degli Studi di Ferrara

DOTTORATO DI RICERCA IN
FISICA

CICLO XXIII

COORDINATORE Prof. Filippo Frontera

Study of aerosol scavenging processes in atmosphere

Settore Scientifico Disciplinare FIS/06

Dottorando
Dott. Lorenza Di Matteo

Tutore interno
Prof. Federico Porcù

Tutore esterno
Prof. Angelo Piano

Anni 2008/2010

Contents

List of Figures

INTRODUCTION

The study of aerosol is interesting for a number of reasons: direct (scatters and absorbs solar and infrared radiation) and indirect effects (modifies microphysics of clouds serving as condensation nuclei and ice nuclei) on climate, effects on human health and ecological hazard, just to mention some.

In recent decades it is worth taking into consideration two events in which the concentration of aerosol influenced the climate. In 1991, the violent eruption of the volcano Pinatubo has scattered 15 million to 30 million tons of sulfur dioxide in the atmosphere, causing a decrease in average global temperature of the planet within two years. In 2001, the interruption of air traffic in North America, following the attack on the Twin Towers in New York, coincided with an increase in daytime temperature ($\sim$ 1 °C). This shows that the effect of the reduction of aerosol and contrails of the aircraft was to increase the incoming solar radiation on the Earth's surface. Aerosol concentrations and forcing will change in the future, as a result of changing emissions, related to the growth of the population. The uncertainties associated with our knowledge of the present day distribution of aerosols will have consequences to the analysis of future scenarios. Seen in context, a better understanding of the scavenging of aerosol in the atmosphere is of crucial importance.

The aim of this thesis is to increase the knowledge of aerosol removal through processes linked to clouds (thermophoresis, ice nuclei, cloud condensation nuclei and impaction scavenging), by means of experimental studies.

Thermophoresis describes a phenomenon in which particles suspended in a fluid with no uniform temperature are subject to a force, named thermophoretic force, which is counteracted by the fluid drag on the particle. Thermophoresis plays a role in the scavenging of aerosol particles in clouds.

This process happen in cloud because during processes like condensation or evaporation, temperature gradients are formed in clouds. In normal gravity it is not possible to study the phoretic effect alone, as particles move due to gravity and due to natural convection resulting from temperature gradients established to study thermophoresis. So experiments were performed in microgravity conditions. Concerning the study of the thermophoresis I carried out preliminary studies in normal gravity regarding aerosol generation and characterization and many experiments to test the apparatus for the microgravity campaigns. Measurements of the thermophoretic velocities of aerosol particles in different carrier gases (helium, nitrogen, argon, xenon) were performed in microgravity conditions (the drop tower facility, in Bremen). The experiments permitted the study of thermophoresis in conditions which minimize the impact of gravity. Particle trajectories, and consequently particle velocities, were reconstructed by analyzing the sequence of particle positions.

Cloud condensation nuclei are atmospheric aerosol that serves as particle upon which water vapor condenses to form droplets that are activated and grow by condensation to form cloud droplets at the supersaturations achieved in clouds. As to this study, I helped in the realization of the thermal diffusion chamber, used in the experimental campaign performed in S. Pietro Capofiume (in which I took part). Then experiments to test the chamber and the acquisition system were carried out. Subsequently we analyzed data correlating them with meteorological conditions recorded during the experimental campaign.

Ice forming nuclei (IFN or IN) are aerosol particle that catalyze the formation of ice crystals in cloud. They can form ice through different thermodynamic mechanisms or modes: deposition, condensation-freezing, immersion and contact. The existence of these multiple heterogeneous mechanisms during both the activation of IN both in the atmosphere and in the various different IN detections instruments, leads to a large degree of uncertainty and sometimes contradictory results. Because few measurements of IN at the ground level in low polluted area are reported, two experimental campaigns, in which I took part, were carried out; various aerosol fractions and total suspended particles were sampled on nitrocellulose membrane, four times a day (period 06-22 h), at 3 m above ground level. Finally we used a replica of the Langer dynamic developing chamber housed in a refrigerator

to detect and determine the concentration of aerosol particles active as IN at different supersaturations with respect to ice and water.

Removal of dust by precipitations event is also known by the common people, but not all rainfalls have the same effect: duration, intensity and types have different influences on aerosol removal. For this study I performed indoor measurements of aerosol concentration and relating these results with r.h, a parameter that influence the aerosol distribution. Subsequently I carried out experimental campaign outdoor, during rain events. Finally data were analyzed drawing conclusions.

This work is structured as follows. Chapter 2 is about studies of thermophoresis; theoretical background and results concerning experiment in microgravity conditions. In chapter 3 results concerning studies of cloud condensation nuclei are presented. Chapter 4 deals with studies of Ice Nuclei; a description of measurements techniques and results obtained. Chapter 5 concerns with studies of aerosol scavenging by precipitations. In this chapter are presented indoor measurements concerning aerosol distributions (and related with relative humidity) and outdoor measurements during rain events. Finally, the last chapter includes conclusions and perspectives of my work.

Chapter 1

AEROSOLS: DEFINITIONS AND DYNAMICS

1.1 Introduction

Aerosol are tiny particles suspended in the atmosphere, at number concentrations depending upon factors such as location, atmospheric conditions, annual and diurnal cycles and presence of local sources. Atmospheric aerosols originate from a wide variety of natural (vulcanic eruption, mineral dust, sea salt) and anthropogenic sources (industrial emission, biomass burning). Average particle compositions vary with size, time and location, and the bulk compositions of individual particles of a given size also vary significantly (McMurry, 2000).

The study of aerosol is interesting for a number of reasons: direct and indirect effect on climate, effects on human health, visibility reduction, optical effects, ecological hazards, influence in atmospheric chemistry.

Atmospheric aerosols influence the radiation balance of the Earth atmosphere directly through scattering and absorption of incoming solar radiation and outgoing terrestrial radiation (Shen et al., 2005; Zhang, Han, and Zhu, 2007) and indirectly by serving as cloud condensation nuclei and ice nuclei (IN) and thereby influencing microphysics of clouds (Lohmann, 2005; Sun & Ariya, 2006). Clouds, in turn, play a key role in the Earth's radiation budget through absorption of terrestrial infrared radiation and reflection of solar irradiation (Sun & Ariya, 2006)

There are also concerns about the effects of aerosol on human health.

In general, human beings come into direct contact with atmospheric aerosol by breathing or via their skin (Salma et al., 2001). The smallest aerosol are small enough to get into the human respiratory system. The health impact of exposure to ultrafine particles (less than 100 nm) can manifest itself in a variety of symptoms (Kennedy, 2007).

The optical properties of aerosols are responsible for many spectacular atmospheric effects,such as richly colored sunsets, halos around the sun or moon, and rainbows. For two years after the eruption of volcano Krakatau (1883), that has scattered tons of aerosol in the atmosphere, the moon appeared blue. Horvath et al. (1994) say that the appearance of a blue sun it is due to unusual optical properties of the atmosphere, which are caused by suspended aerosol particles.

Visibility reduction due to aerosol has been the subject of numerous studies (Trijonis, 1980; Malm and Pitchford, 1997 and many others). A volcano erupted close to Iceland's Eyjafjallajokull Island (April 2010); the volcanic ashes caused several flights to be delayed due to visibility reduction.

Aerosol has a number of properties such as size, chemical composition, hygroscopycity, density and shape. Size is normally used to classify aerosol because it is the most easily measured property and because inferences about the other properties can be drawn from size information.

Atmospheric aerosol particles range in size over more than four orders of magnitude (McMurry, 2000) from 0.01 μm as a lower limit to approximately 100 μm as the upper limit.

1.2 Definitions

All liquid or solid particles suspended in air are defined as *aerosol* particles (Curtius, 2006) and they are are two-phase systems, consisting of the particles (liquid or solid) and the gas in which they are suspended.

Dust are particles of matter regarded as the result of disintegration(from submicroscopic to microscopic); the wind erosion from desert regions gives a considerable contribution to the global aerosol budget (Borbèly-Kiss et al., 2004).

Fumes are particles produced by many manufacturing processes; e.g manufacture or carbon black(Cameron& Goerg-Wood, 1999); they are below 1 μm in size.

Smoke are fine particles resulting from the burning of organic material; smoke particles are in the same size range as fume particles).

Mists and fog are particles of aerosol produced e.g by the disintegration of liquid).

Haze are particles with some water vapor incorporated into them or around them.

Smog is a combination of smoke and fog, usually containing photochemical reaction products combined with water vapor; it is less than 1 μm in diameter).

Spray is formed by the mechanical breakup of a liquid; particles are larger than a few micrometers.

A *monodisperse* aerosol contains particles of only a single size; a *polydisperse* aerosol contains particles of more than one size.

An *homogeneous* aerosol contains particles that are chemically identical. In an *inhomogeneous* aerosol there are particles which have different chemical compositions.

Moreover many shapes are possible for aerosol particles:

Isometric particles are those for which all three dimensions are roughly the same (e.g spherical). *Platelets* are particles that have two long dimensions and a small third dimension (e.g leaves or leaf fragments). *Fibers* are particles with great length in one dimension compared to much smaller lengths in the other two (From Parker C. Reist, 1984).

1.3 Size

Aerosol sizes are usually reported as diameters. Commonly used effective diameters are:

Aerodynamic diameter The diameter of a unit density sphere (density = 1g/cm^3) that has the same terminal falling speed in air as the particle under consideration

Stokes diameter Diameter of a sphere of the same density as the particle in question having the same settling velocity as that particle.

Optical diameter Obtained by light scattering detectors, depends on particle refractive index, shape, and size

Vacuum aerodynamic diameter Diameter of a sphere, in the free molecular regime, with unit density (density = 1g/cm^3) and the same terminal falling speed in air as the particle under consideration.

Electrical mobility diameter Diameter of a charged sphere with the same migration velocity of the charged particle under consideration in a constant electric field at atmospheric pressure.

Atmospheric aerosol particles range in size over more than four orders of magnitude (McMurry, 2000) from 0.01 μm as a lower limit to approximately 100 μm as the upper limit (see Table 1). The lower limit approximates roughly the point where the transition from molecule to particle takes place. Particles much greater than about 100 μm or so do not normally remain suspended in the air for a sufficient length of time to be of much interest in aerosol science.

Particles much greater than 5 to 10 μm in diameter are usually removed by the upper respiratory system. An increasing attention has been devoted to submicron and ultrafine particles because these particles can penetrate to the deeper part of the respiratory tract and they are generate in abundance by the most significant pollution sources (Morawska et al, 2005). Within the size range of 0.01 μm to 100 μm lie a number of physical dimensions which have a significant effect on particle properties. For example, the mean free path of an "air" molecule is about 0.07 μm. This means that the air in which a particle is suspended exhibits different properties, depending on particle size. Also, the wavelengths of visible light lie in the narrow band of 0.4 μm to 0.7 μm. Particles smaller than the wavelength of light scatter light in a distinctly different manner than do larger particles. Particle size is the most important descriptor for predicting aerosol behavior (From Parker C. Reist, 1984).

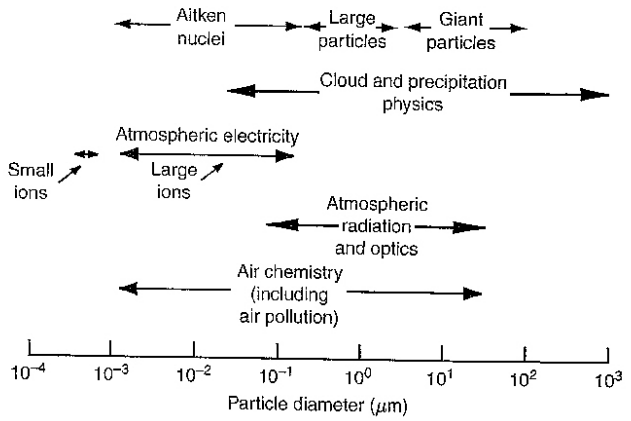

Figure 1.1: Size range of particles in the atmosphere and their importance; [From Wallace & Hobbs, 2006]

Tab. 1 Typical particle diameters (μm)

Tobacco smoke	0.25	Lypocodium	20
Ammonium chloride	0.1	Atmospheric fog	2-50
Sulfuric acid mist	0.3-5	Pollens	15-70
Zinc oxide fume	0.05	Aerosol spray products	1-100
Flour dust	15-20	Talc	10
Pigments	1-5	Photochemical aerosols	0.01-1

[Source: From Parker C. Reist]

1.4 Aerosols Concentrations and Size Distributions

Figure 1.1 shows the ranges of particle sizes that play a role in the atmosphere.

The range of particle number concentrations observed in the atmosphere is considerable: number concentrations of less than 10 particles cm^{-3} are found in the stratosphere at 20 km altitude (Curtius et al., 2005), several thousand particles per cubic centimeter are typically observed in modestly polluted continental areas near the ground more than 1 x 10^5 particles cm^{-3} are often observed in urban areas (Jaenicke, 1993).

The averages of numerous measurements of *particle number distributions* in continental, marine, and urban polluted air are shown in Fig 1.2. The

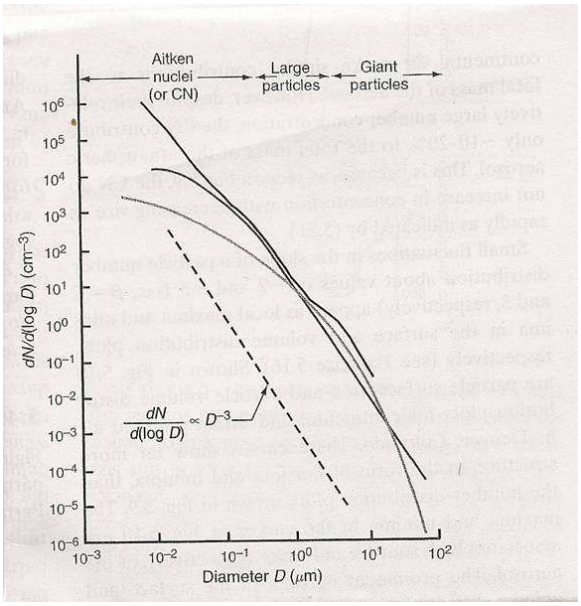

Figure 1.2: Number distributions of tropospheric particles obtained from averaging many measurements in continental, marine and urban polluted air. Also plotted is Eq. 1.2 with β=3 [From Wallace & Hobbs, 2006]

measurements are plotted in the form of a number distributions in which the ordinate [dN/d(log D)] and the abscissa (D) are plotted on logarithmic scales, where dN is the number concentration of particles with diameters between D and D+dD. Several conclusions can be drawn from the results shown in Fig 1.2:

- The concentration of particles fall off very rapidly as they increase in size. Therefore, the total number concentration is dominated by particles with diameters $< 0.2\mu m$, which are therefore referred to as *Aitken nuclei*.

- Those portion of the number distribution curves can be represented by an expression of the form

$$log\frac{dN}{d(logD)} = const - \beta logD \tag{1.1}$$

or taking antilogs,

$$\frac{dN}{d(logD)} = CD^{-\beta} \tag{1.2}$$

where C is a constant related to the concentration of the particles and the values of β (slope of the number distribution curve) generally lies between 2 and 4. Continental aerosol particles with diameters larger than $\sim 0.2\mu m$ follow quite closely with $\beta \simeq 3$. A size distribution with $\beta = 3$ is called a *Junge distribution*.

- The number distributions of particles shown in Fig.1.2 confirm CN measurements which indicate that the total concentrations of particles are, on average, greatest in urban polluted air and least in marine air (From Wallace & Hobbs, 2006).

1.5 Sources

1.5.1 Biological aerosol

Solid and liquid particles are issued into the atmosphere from animals and plants. These emissions, which include seeds, pollen, spores, and fragments of animals and plants, are usually 1-250 μm in diameter (From Wallace & Hobbs, 2006). Different fractions of plant material are broken up my mechanical and/or decay process, and the resulting particles become airborne due to air motion (Winiwarter et al., 2009).

Bacteria, algae, protozoa, fungi, and viruses are generally $< 1\mu m$ in diameter. Some characteristic concentrations are: maximum values of grassy pollens $> 200\ m^{-3}$; fungal spores (in water) $\sim 100 - 400m^{-3}$; bacteria over sewage treatment plants $\sim 10^4 m^{-3}$. (From Wallace & Hobbs, 2006)

1.5.2 Marine aerosol

Marine aerosol accounts for the majority of the global aerosol flux [$\sim$ 1000-5000 Tg per year, although this includes giant particles ($\sim 2 - 20\mu m$ diameter) that are not transported very far]. Just above the ocean surface in the remote marine atmosphere, sea salt generally dominates the mass of both supermicrometer and submicrometer particles (From Wallace & Hobbs, 2006). Primary aerosol particles are produced by sea spray involving a *bubble bursting* mechanism (Fig.1.3). It has been well documented that marine aerosol particle have a complex composition and contain bacteria, virus-like particles, fragments of marine organisms, and amorphous gel-like material

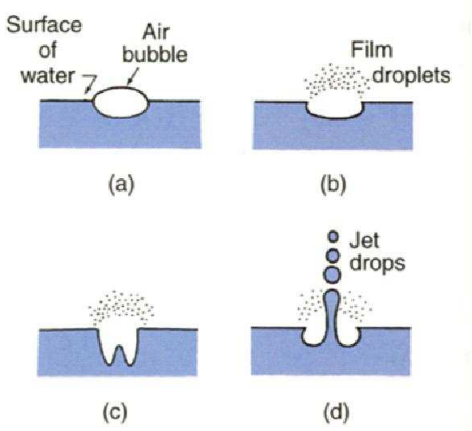

Figure 1.3: Schematics to illustrate the manner in which film droplets and jet drops are produced when an air bubble bursts at the surface of water. Over the oceans some of the droplets and drops evaporate to leave sea-salt particles and other materials in the air. The time between (a) and (d) is $\sim 2ms$. The film droplets are $\sim 5 - 30\mu m$ diameter before evaporation. The size of the jet drops are $\sim 15\%$ of the diameter of the air bubble.[From Wallace & Hobbs, 2006]

similar to exopolymer secretions of algae and bacteria (Leck& Biggs, 2005a, 2005b).

Sea spray primary particles are produced as a result of breaking waves processes occurring on ocean surface. Wind generated waves braking at wind speed higher than $4ms^{-1}$; the formed bubbles rise and burst upon reaching the surface, thereby producing the so-called film and jet drops. (Fuentes et. al, 2010).

The average rate of production of sea-salt particles over the oceans is $\sim 100\ cm^{-2}s^{-1}$. Hygroscopic salts [NaCl (85%), KCl, $CaSO_4$ $(NH_4)_2SO_4$] account for $\sim 3.5\%$ of the mass of seawater. These materials are injected into the atmosphere by bubble bursting over the oceans. In addition, organic compounds and bacteria in the surface layers of the ocean are transported to the air by bubble bursting.

Dry sea-salt particles will not form solution droplets until the relative humidity exceeds 75%. Ambient gases (e.g., SO_2 and CO_2) are taken up by these droplets, which changes the ionic composition of the droplets. For example, the reaction of OH(g) with sea-salt particles generates OH^- (aq)

in the droplets, which leads to an increase in the production of SO_4^{2-} (aq) by aqueous-phase reactions and a reduction in the concentrations of Cl^- (aq). Consequently, the ratio of Cl to Na in sea-salt particles collected from the atmosphere is generally much less than in seawater itself. The excess of SO_4^{2-} (aq) over that of bulk seawater is referred to as *non-sea-salt sulfate* (nss). The oxidation of Br^- (aq) and Cl^- (aq) in solutions of sea-salt particles can produce BrO_x and ClO_x species. Catalytic reactions involving BrO_x and ClO_x, similar to those that occur in the stratosphere, destroy O_3. This mechanism has been postulated to explain the depletion of O_3, from $\sim$ 40 to 0.5 ppbv, that occurs episodically over periods of hours to days in the Artic boundary layer starting at polar sunrise and continuing through April.(From Wallace & Hobbs, 2006).

1.5.3 Biomass burning

Smoke from forest fires is a major source of atmospheric aerosols. Small smoke particles (primarily organic compounds and elemental carbon) and fly ash are injected directly into the air by forest fires.

Several million grams of particles can be released by the burning of 1 hectare ($10^4 m^2$). It is estimated that about 54 Tg of particles (containing $\sim$ 6 Tg of elemental carbon) are released into atmosphere each year by biomass burning. The number distribution of particles from forest fires peak at 0.1 μm diameter, which makes them efficient *cloud condensation nuclei*. Some biogenic particles (e.g., bacteria from vegetation) may nucleate ice in cloud (From Wallace & Hobbs, 2006).

1.5.4 Solid Earth

The transfer of particles to the atmosphere from the Earth's surface is caused by winds and atmospheric turbolence. To initiate the motion of particles on the Earth's surface, surface wind speeds must exceed certain threshold values, which depend on the size of the particle and the type of surface. The threshold values are at least $\sim 0.2 ms^{-1}$ for particles 50-200 μm in diameter (smaller particles adhere better to the surface) and for soils containing 50% clay or tilled soils. To achieve a frictional speed of 0.2 ms^{-1} requires a wind speed of several meters above ground level. A major source for particles with diameter $\sim 10 - 100 \mu m$ is *saltation* (From Wallace &

Hobbs, 2006). Saltation abrades immobile surface clods and crusts to create both additional suspension-size ($> 106\mu m$ diameter) and saltation/creep aggregates (Hagen et al., 2010).

On the global scale, semiarid regions and deserts (which cover about one-third of the land surface) are the main source of particles from the Earth's surface. They provide ~ 2000 Tg per year of mineral particles. Dust from these sources can be transported over long distance (From Wallace & Hobbs, 2006). Volcanoes inject gases and particles into the atmosphere. The composition of these aerosols is given by typical earth crust elements and some compounds from gas to particle conversion. The large particles have short residence times, but the small particles (produced primarily by gas-to-particle (g-to-p) conversion of SO_2) can be transported globally, particularly if they reach high altitudes (From Wallace & Hobbs, 2006).

1.5.5 Anthropogenic

The global input of particles into the atmosphere from anthropogenic activities is $\sim 20\%$ (by mass) of that from natural sources. The main anthropogenic sources of aerosols are dust from roads, wind erosion of tilled land, biomass burning, fuel combustion, and industrial processes. For particles with diameters $> 5\mu m$, direct emissions from anthropogenic sources dominate over aerosols that form in the atmosphere by g-to-p conversion (referred to as *secondary particles* of anthropogenic gases. However, the reverse is the case for most of the smaller particles, for which g-to-p conversion is the over-whelming source of the number concentration of anthropogenically derived aerosols.

In 1997 the worldwide direct emission into the atmosphere of particles $< 10\mu m$ diameter from anthropogenic sources was estimated to be $\sim 350Tg$ per year (excluding g-to-p conversion). About 35% of the number concentration of aerosols in the atmosphere was sulfate, produced by the oxidation of SO_2 emissions. Particles emissions worldwide were dominated by fossil fuel combustion (primarily coal) and biomass burning. These emissions are projected to double by the year 2040, due largely to anticipated increases in fossil fuel combustions, with the greatest growth in emissions from China and India.

During the 20th century, the emissions of particles into the atmosphere from anthropogenic sources was a small fraction of the mass of particles

from natural sources. However, it is projected that by 2040 anthropogenic sources of particles could be comparable to those from natural processes (From Wallace & Hobbs, 2006).

1.5.6 In situ formation

In situ condensation of gases (i.e, g-to-p conversion) is important in the atmosphere. Gases may condense onto existing particles, thereby increasing the mass (but not the number) of particles, or gases may condense to form new particles. The former path is favored when the surface area of existing particles is high and the supersaturation of the gases is low. If new particles are formed, they are generally $< 0.01\mu m$ diameter. The quantities of aerosols produced by g-to-p conversion are comparable to direct emission in the case of naturally derived aerosols. Three major families of chemical species are involved in g-to-p conversion: sulfur, nitrogen, and organic and carbonaceous materials. Various sulfur gases [e.g, H_2S, CS_2, COS, dimethylsulphide (DMS)] can be oxidized to SO_2. The SO_2 is then oxidized to sulfate (SO_4^{2-}).

Over the oceans, sulfates derived from DMS contribute to the growth of existing particles. Sulfates are also produced in and around clouds, and nitric acid can form from N_2O_5 in cloud water. Subsequent evaporation of cloud water releases these sulfate and nitrate particles into the air.

Organic and carbonaceous aerosols are produced by g-to-p conversion from gases released from the biosphere and from volatile compounds such as crude oil that leak to the Earth's surface (From Wallace & Hobbs, 2006).

1.5.7 Direct emissions and in situ production

Table 2 summarizes estimates of the magnitudes of the principal sources of direct emission of particles into the atmosphere and *in situ* sources.

Anthropogenic activities emit large numbers of particles into the atmosphere, both directly and through g-to-p conversion. For particles $\geq 5\mu m$ diameter, human activities worldwide are estimated to produce $\sim 15\%$ of natural emissions, with industrial processes, fuel combustion, and g-to-p conversion accounting for $\sim 80\%$ of the anthropogenic emissions.

However, in urban areas, anthropogenic sources are much more important. For particles $< 5\mu m$ diameter, human activities produce $\sim 20\%$ of

natural emissions, with g-to-p conversion accounting for $\sim 90\%$ of the human emissions (From Wallace & Hobbs, 2006).

Tab 2 Estimates (in Tg per year) for the year 2000 of (a) direct particle emissions into the atmosphere and (b)*in situ* production

(a) Direct emissions

	Northern hemisphere	**Southern hemisphere**
Carbonaceous aerosols		
Organic matter (0-2 μm)		
Biomass burning	28	26
Fossil fuel	28	0.4
Biogenic ($> 1\mu m$)	-	-
Black carbon ($0 - 2\mu m$)		
Biomass burning	2.9	2.7
Fossil fuel	6.5	0.1
Aircraft	0.005	0.0004
Industrial dust, etc. ($> 1\mu m$)		
Sea salt		
$< 1\mu m$	23	31
$1 - 16\mu m$	1,420	1,870
Total	1,440	1,900
Mineral (soil) dust		
$< 1\mu m$	90	17
$1 - 2\mu m$	240	50
$2 - 20\mu m$	1,470	282
Total	1,800	349

(b) In situ

	Northern hemisphere	**Southern hemisphere**
Sulfates (as NH_4HSO_4)	145	55
Anthropogenic	106	15
Biogenic	25	32
Volcanic	14	7
Nitrate (as NO_3^-)		
Anthropogenic	12.4	1.8
Natural	2.2	1.7
Organic compounds		
Anthropogenic	0.15	0.45
Biogenic	8.2	7.4

[From Wallace & Hobbs, 2006]

1.6 Chemical Composition

Except for marine aerosols, the masses of which are dominated by sodium chloride, sulfate is one of the prime contributors to the mass of atmospheric aerosols. The mass fractions of SO_4^{2-} range from $\sim 22-45\%$ for continental aerosols to $\sim 75\%$ for aerosols in the Artic and Antarctic. Because the sulfate content of the Earth's crust is too low to explain the large percentages of sulfate in atmospheric aerosols, most of the SO_4^{2-} must derive from g-to-p conversion of SO_2. The sulfate is contained mainly in submicrometer particles. Ammonium ($NHSO_4^+$) is the main cation associated with SO_4^{2-} in continental aerosol. It is produced by gaseous ammonia neutralizing sulfuric acid to produce ammonium sulfate [$(NH_4)_2SO_4$](From Wallace & Hobbs, 2006). The ratio of the molar concentration of NH_4^+ to SO_4^{2-} ranges from $\sim$ 1 to 2, corresponding to an aerosol composition intermediate between that for NH_4HSO_4 and $(NH_4)_2SO_4$. The average mass fractions of submicrometer non sea-salt sulfates plus associated NH_4^+ range from $\sim$ 16 to 54% over large regions of the world.

In marine air the main contributors to the mass of inorganic aerosols are the ions Na^+, Cl^-, Mg^{2+}, SO_4^{2-}, K^+, and Ca^{2+}.
Apart from SO_4^{2-}, these compounds are contained primarily in particles a few micrometers in diameter because they originate from sea salt derived

from bubble bursting (see Fig. 1.3). Sulfate mass concentrations peak from particles with diameters $\sim 0.1 - 1\mu m$. Particles in this size range are effective in scattering light (and therefore reducing visibility) and as cloud condensation nuclei.
Nitrate NO_3^- occurs in larger sized particles than sulfate in marine air. Because seawater contains negligible nitrate, the nitrate in these particles must derive from the condensation of gaseous HNO_3, possibly by g-to-p conversion in the liquid phase.

Nitrate is also common in continental aerosols, where it extends over the diameter range $\sim 0.2 - 20\mu m$. It derives, in part, from the condensation of HNO_3 onto larger and more alkaline mineral particles. Organic compounds form an appreciable fraction of the mass of atmospheric aerosols. The most abundant organics in urban aerosols are higher molecular weight alkenes (C_xH_{2x+2}), $\sim 1000{-}4000ng\,m^{-3}$, and alkenes C_xH_{2x}, $\sim 2000ng\,m^{-3}$. Many of the particles in urban smog are by-products of photochemical reactions involving hydrocarbons and nitrogen oxides, which derive from combustions.

Elemental carbon (commonly referred to as "soot"), a common component of organic aerosols in the atmosphere, is a strong absorber of solar radiation. For example, in polluted air masses from India, elemental carbon accounts for $\sim 10\%$ of the mass of submicrometer sized particles (From Wallace & Hobbs, 2006).

1.7 Transport

Aerosols are transported by the airflows they encounter during the time they spend in the atmosphere (From Wallace & Hobbs, 2006).

The transport along the trajectories depends on the history of the transported air masses; it is affected by meteorological conditions and by the nature of emission sources touched along the transport path (Borbèly-Kiss et al., 2004).

The transport can be over intercontinental, even global, scales. Thus, Saharan dust is transported to the Americas, and dust from the Gobi Desert can reach the west coast of North America (From Wallace & Hobbs, 2006). The long-range transport of continental aerosols from natural and anthropogenic sources to the marine environment has been recognized as a major source for many biogeochemically important trace metals and nutrients to

the world oceans (Kumar et al., 2008). If the aerosols are produced by g-to-p conversion, long-range transport is likely because the time required for g-to-p conversion and the relatively small sizes of the particles produced by this process lead to long residence times in the atmosphere. This is the case for sulfates that derive from SO_2 blasted into the stratosphere by large volcanic eruptions. It is also the case for acidic aerosols such as sulfates and nitrates, which contribute to *acid rain*. Thus, SO_2 emitted from power plants in the United Kingdom can be deposited as sulfate far inland in continental Europe (From Wallace & Hobbs, 2006).

1.8 Aerosols: direct and indirect effects on climate

The imbalance of the net radiation (solar and terrestrial) received and emitted by the Earth is the ultimate driving force of the terrestrial climate system. The global energy budget of our planet changes in response to variations in both concentrations of the atmospheric radiatively-active constituents and surface reflectance characteristics. Changes in atmospheric gaseous composition and particle content (including *aerosols* and *clouds*) are expected to produce radiative forcing processes leading to regional warming or cooling effects.

Aerosols have *direct effects*, due to scattering and absorption of solar and terrestrial radiation and *indirect effects* by modifying microphysics, the radiative properties and the lifetime of clouds.

The radiative effects of aerosol particles vary as a function of the sizes of the particle relative to the energy wavelength of interest (Arimoto, 2001).

The quantification of aerosol radiative forcing is more complex than the quantification of radiative forcing by greenhouse gases because aerosol mass and particle number concentrations are highly variable in space and time and there is limited information on their global distribution. This variability is due to the much shorter atmospheric lifetime of aerosols compared with the important greenhouse gases (IPCC, 2007). In Europe and North America, where anthropic sources of aerosols are intense, the columnar particulate matter content mainly consists of sulphates and some soot substances, presenting rather high values of AOD (aerosol optical depth) at VIS and NIR wavelengths (see Fig. 1.4).

Black carbon absorbs solar radiation and can lead to a warming of the

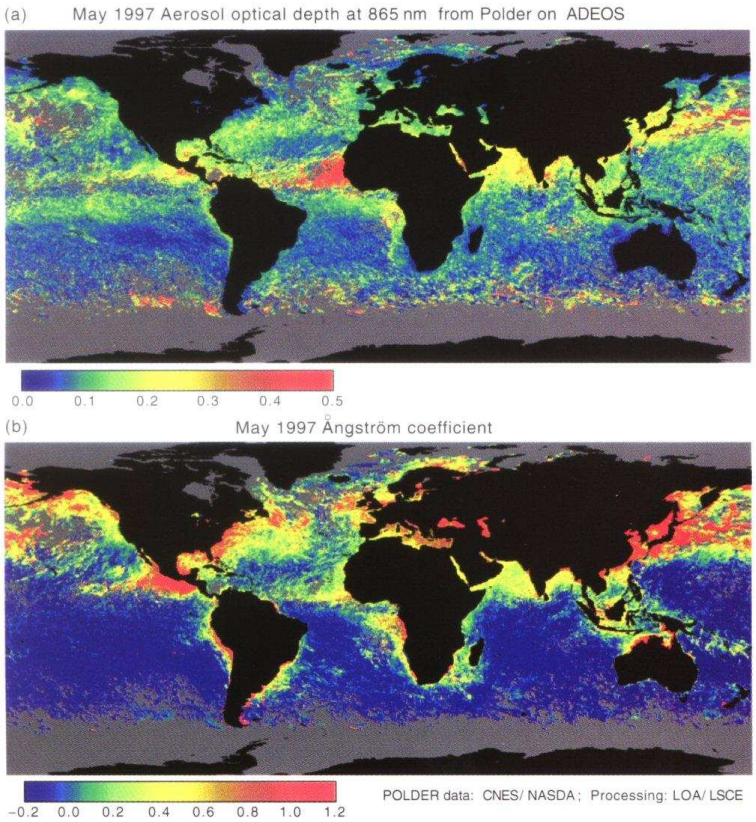

Figure 1.4: (a) Aerosol Optical Depth; (b)Ångström exponent from POLDER satellite data for May 1997 Deuzé et al., G.R.L.,1999.

surrounding air; this warming can prevent cloud formation.

Aerosols also act as condensation centers for cloud droplets and ice crystals, thereby changing cloud properties. If more aerosol particles compete for the uptake of water vapor, the resulting cloud droplets do not grow as large. More smaller cloud droplets have a larger surface area than fewer larger cloud droplets for the same amount of cloud water (Lohmann, 2005).

Changes in cloud microstructure due to aerosols are associated with increases in cloud albedo (Brenguier et al., 2000; see Fig. 1.5); a polluted cloud reflects more solar radiation back to space, resulting in a negative radiative forcing at TOA.

In addition, these more numerous but smaller cloud droplets collide less efficiently with each other, which reduces the precipitation efficiency of polluted clouds and presumably prolongs their lifetime (cloud lifetime effect). It also implies more scattering of solar radiation back to space, thus reinforc-

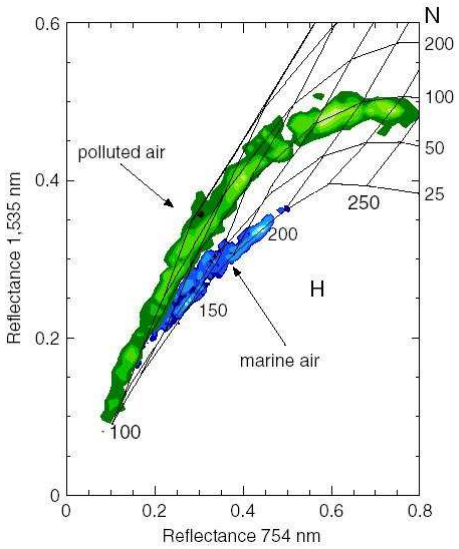

Figure 1.5: Changes in cloud microstructure due to aerosols; Brenguier et al., 2000.

ing the cloud albedo effect (Lohmann, 2005). The global mean magnitude of the cloud albedo effect since pre-industrial times is estimated between -0.5 and -1.9 Wm^{-2} from different climate models and the cloud lifetime effect to be between -0.3 and -1.4 Wm^{-2} (Lohmann and Feichter, 2005). The semi-direct effect, which could in principle counteract part of this negative forcing at TOA, is predicted to be only between -0.5 and +0.1 Wm^{-2}, where the negative values result from black carbon being located above the cloud. If the individual indirect effect values are summed up, the indirect effect could amount to almost -3 Wm^{-2} (Lohmann, 2005)

In South Asia, absorbing aerosols in atmospheric brown clouds may have played a major role in the observed South Asian climate and hydrological cycle changes and may have masked as much as 50% of the surface warming due to the global increase in greenhouse gases; their simulations raise the possibility that, if current trends in emissions continue, the South Asian subcontinent may experience a doubling of the drought frequency in future decades (Lohmann, 2005).

1.9 Aerosol removal

Once aerosol is suspended in the atmosphere, it is altered or removed; it cannot stay in the atmosphere indefinitely, and average lifetimes are of the order of a few days to a week.

For particulate pollutants, removal fates are strongly related to particle size (Zheng M. et al., 2005). Larger aerosol settle out of the atmosphere very quickly under gravity (see Fig. 1.6), and some surfaces are more efficient at capturing aerosol than others. Small particles can be converted into larger particles by *coagulation*. Coagulation is strictly related to *Brownian diffusion*. Coagulation does not remove particles from the atmosphere but changes features of the size distribution of the particle population; shifts small particles into size ranges where they can be removed by other mechanisms.

Dry and *wet deposition* are the two major removal mechanisms for atmospheric aerosols; dry deposition is the removal process through which aerosol particles are taken up by the Earth's surface without the aid of precipitation (Zhang et al., 2006).

The process of particle dry deposition includes several mechanisms: Brownian diffusion, phoretic effects, inertial impaction interception and sedimentation. Brownian diffusion is the most important mechanisms for very small particles ($< 0.1\mu m$ in diameter), but its importance decreases rapidly as particle size increases.

Sedimentation (gravitational settling) dominates over other mechanisms for particles larger than $10\mu m$, although interception and impaction can also be as important as gravitational settling for large particles under certain conditions. Impaction and interception are the dominant mechanisms for particles of sizes 2-10 μm (Zhang et al., 2006). There is *impaction* when small particles interfacing a bigger obstacle are not able to follow the curved streamlines of the flow due to their inertia, so they impact the droplet. There is *interception* when small particles follow the streamlines, but if they flow too close to an obstacle, they may collide.

As cloud particles grow, aerosol tend to be driven to their surface by the diffusion field associated with the flux of water vapor to the growing cloud particles, called the *diffusiophoretic force* (From Wallace & Hobbs, 2006). The particle motion is commonly termed diffusiophoresis; the mechanism of

diffusiophoresis occurs in different flow regimes which can be characterized by the Knudsen number (Prodi et al., 2002).

In the process of wet deposition, there are always atmospheric hydrometeors which scavenge aerosol particles. Precipitation plays an important role in determing the fluxes of ambient trace species to the earth surface.

The scavenging of particles in the air by precipitation is one of the major processes by which the atmosphere is cleansed and the balance between the sources and sinks of atmospheric aerosol particles is maintained (Chang et al., 2003). It is estimated that, on global scale, precipitation processes account for about 80-90 % of the mass of particles removed from atmosphere (From Wallace & Hobbs, 2006).

Different types of wet deposition include: nucleation scavenging (serving as CCN or ice nuclei) or impaction scavenging (being collected by falling hydrometeors) and then delivered to the Earth's surface. Impaction scavenging depends on the net action of various forces influencing the relative motions of aerosol particles and hydrometeors. It is usually split into two categories: in-cloud scavenging and below-cloud scavenging (Zhang et al., 2006). The mechanisms of impaction scavenging for in-and below-cloud scavenging are basically the same. The only difference is that cloud droplets inside a cloud are generally much smaller than raindrops descending below the cloud.

1.10 Aerosol dynamics

1.10.1 Equation of motion of the individual, spherical particle suspended in a gas

By determing the path of a single particle it is possible to predict particle position and behavior. This can be done by solving force balance equations (see eq. 1.3). The forces may include those which are generally functions of time and the position of the particle, such as electrical forces, or they can be forces which are constant, such as gravity. The net difference of the forces acting on the particle is equal to the rate of change of particle momentum:

$$m\frac{dv_p}{dt} = F_g + F_r + F_{th} + F_d + F_e + F_f \tag{1.3}$$

$$F_g = m \cdot g \cdot (\rho_p - \rho)/\rho_p \tag{1.4}$$

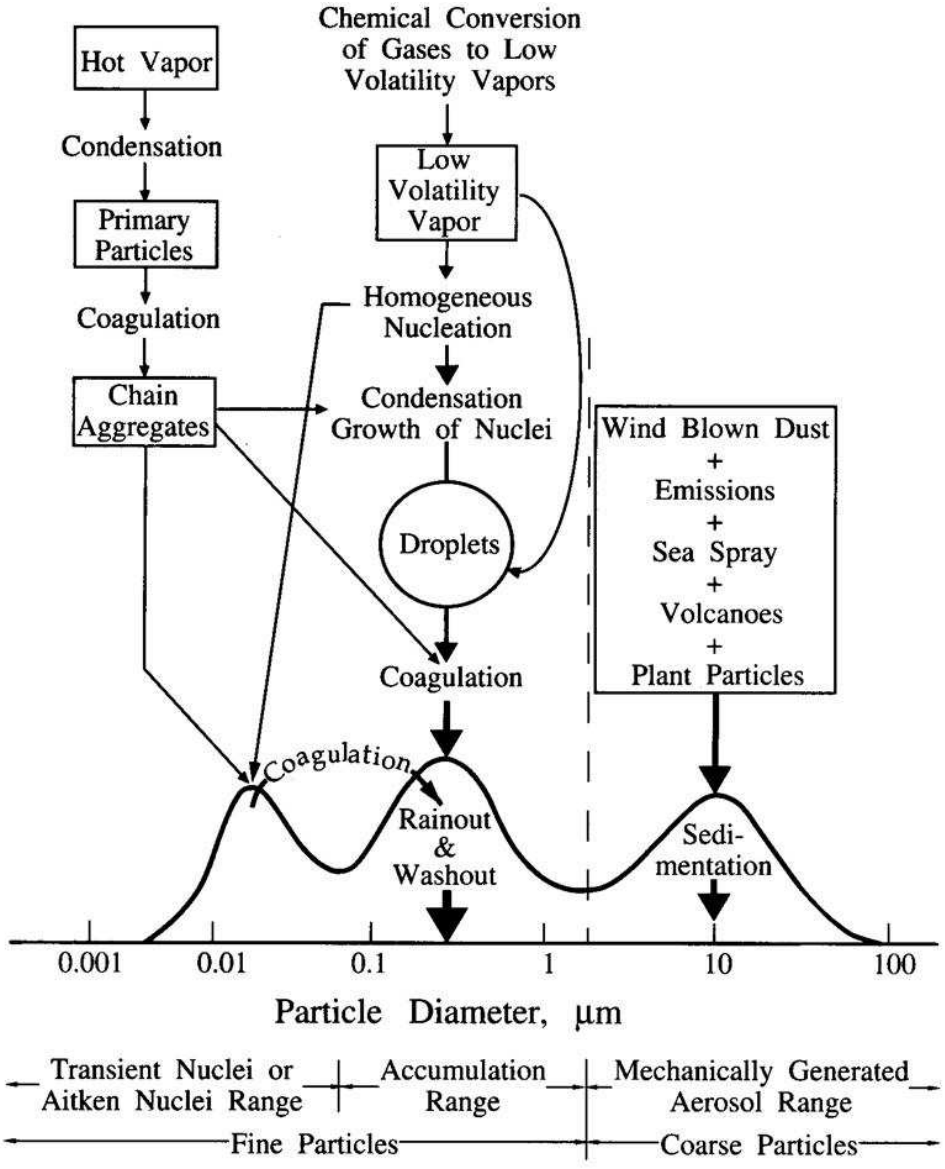

Figure 1.6: Aerosol distribution and removal[(Whitby and Sverdrup, 1980), reproduced from Seinfeld and Pandis, 1998]

where m is the mass, g is the acceleration due to gravity ρ is the fluid density and ρ_p density of particle. F_g is the gravitational force with a correction for the buoyancy.

$$F_r = 6 \cdot \pi\mu \cdot r \cdot \frac{V - V_p}{1 + \alpha \cdot K_n}; N_{KN} \leq 1 \tag{1.5}$$

is the force resisting the motion of a sphere moving through a fluid, as in the Stoke's equation, with Cunningham correction factor (α). where: μ viscosity of the medium r= radius v= fluid velocity v_p = particle velocity

The Cunningham correction factor is an important correction to Navier-Stokes' law and should always be used when particles are less than 1 μm in diameter. It represents the mechanism for transition from the continuum to the molecular case.

$$\alpha = 1.257 + 0.400exp(-\frac{1.10}{N_{Kn}}) \tag{1.6}$$

The force resisting the motion of a sphere moving through a fluid for small particles, in the molecular regime ($K_n \to \infty$) is the Waldmann's relation:

$$F_r = \frac{32}{3}r^2(1 + \frac{\pi}{8a})\frac{p(\nu - \nu_p}{\overline{c}}; N_{KN} \geq 1 \tag{1.7}$$

where $\overline{c}$ is the mean thermal velocity of molecules, p is the pressure of the fluid e a a reflection parameter.

F_{th} Termophoretic force

F_d Diffusiophoretic force

F_e Electrostatic force

F_f Basset term

The Basset force is difficult to implement and is usually neglected. This force include effects of fluid acceleration, caused by pressure gradient of gas surrounding particles. The interaction between fluid molecules and particles depends on the Knudsen number. This number it is important for F_r, F_{th}, F_d, F_e, F_f.

$$K_n = \frac{\lambda}{r} \tag{1.8}$$

where λ is the gas mean free path. The mean free path is defined a sthe average distance a molecule will travel in a gas before it collides with another

molecule; r is the characteristic length scale of the particle. The appropriate particle length scale is assumed to be the equivalent-volume radius of the particle. In case of spherical particle, the characteristic length scale of the particle is the radius. There are several cases:

- $K_n \to 0$ Continuum regime
- $0 < K_n < 0.1$ Slip-flow region
- $0.1 < K_n < 10$ Transition region
- $K_n \to \infty$ Free molecular region

In the *continuum regime* the gas surrounding a particle can be regarded as a continuum and consequently the transport processes to and from the particle can be analysed consequently.

In the *slip-flow region* the continuum theory applies, except in a very thin layer of gas next to the gas-particle boundary surface, where non continuum effects are assumed to be present; in this case the continuum regime theory applies with specific boundary conditions called slip-flow.

In the *free molecular regime* ($K_n \to \infty$) the velocity distribution function of the incoming molecules is not affected by the presence of the particle (Zheng F., 2002), because the mean free path of the molecules of gas is larger than the size of the particle.

In the *intermediate regime*, interactions are difficult to analyze and none of the theoretical approaches have provided a completely satisfactory explanation. Unfortunately, many processes occur in this regime.

1.10.2 Phoretic forces

Small particles suspended in non-isothermal gas and/or in an isothermal gas mixture with concentrations gradients of chemical species, experience a force that is inducted by thermal (*thermophoresis*; see chapter 2) or concentrations gradients (*diffusiophoresis*). Such phenomena play a crucial role in the scavenging of aerosol particles in clouds, when droplets and/or ice crystals grow or evaporate, and below clouds, during the fall of hydrometeors (Prodi et al, 2006). A competition between thermo-and diffusiophoresis exists in the scavenging of atmospheric aerosol during growing or evaporating processes of ice crystals and droplets. Diffusiophoresis was studied theoretically and experimentally by Waldmann (1959), Kousaka and Endo (1993),

Prodi et al. (2002). In the free molecular region ($K_n \to \infty$) Waldmann found:

$$\vec{F_d} = -\frac{32}{3} r^2 \sum_i^n (1 + \frac{\pi}{8}\alpha_i) p_i \frac{\vec{V_p} - \vec{V_i}}{\vec{c_i}} \tag{1.9}$$

In a binary gas mixture the diffusive molecular velocity W_i is defined by the diffusion law as a function of the molar fraction of the components and of the coefficient of molecular diffusion D_{12}: $\gamma_1 \vec{W_1} = \gamma_2 \vec{W_2} = -D_{12} \nabla \gamma_1$ In the case of fluid with zero average molecular velocity of the mixture, there is only diffusion. In these conditions, the particle velocity is given by

$$\vec{V_d} = -\frac{m_1 - m_2}{m + \sqrt{m_1 m_2}} D_{12} \nabla \gamma_1 \tag{1.10}$$

In the case of one of the components with $v_i = 0$ and the other diffusing in it, the gradient of concentration of the diffusing component generates a pressure gradient which is counteracted by a hydrodynamic flow of the mixture (Stefan flow). The velocity of the particle in the mixture is:

$$v_d = -\frac{m_1}{\gamma_1 m_1 + \gamma_2 \sqrt{m_1 m_2}} \frac{D_{12}}{\gamma_2} \nabla \gamma_1 \tag{1.11}$$

In the transition region Waldmann found:

$$\vec{F_d} = -6\pi\mu r \sigma_{12} D_{12} \nabla \gamma_1 \tag{1.12}$$

σ_{12}=Diffusion slip factor In motionless gas in the presence of a diffusing component, the velocity of the particle results from the sum of Stefan flow velocity and diffusiophoretic velocity:

$$v_d = -(1 + \sigma_{12}\gamma_2) \frac{D_{12}}{\gamma_2} \nabla \gamma_1 \tag{1.13}$$

On the basis of Maxwellian distribution of the velocity of the molecules:

$$\sigma_{12} = \frac{m_1 - m_2}{m + \sqrt{m_1 m_2}} \tag{1.14}$$

1.10.3 Electrostatic force

The aerosol capture by hydrometeors is affected by electrostatic forces, determined by electrostatic charge of hydrometeors. Davis (1964) dealt the

problem using the interaction between two charged spheres:

$$\vec{F_{e,r}} = -[\epsilon r^2 E_0^2 (F_1 \cos^2\gamma + F_2 \sin^2)\gamma + E_0 \cos\gamma (F_3 Q_A + F_4 Q_r) +$$

$$\frac{1}{\epsilon r^2}(F_5 Q_A^2 + F_6 Q_A Q_r + F_7 Q_r^2) + E_0 Q_r \cos\gamma]\hat{e_r}$$

$$+[\epsilon r^2 E_0^2 F_8 \sin 2\gamma + E_0 \sin\gamma (F_9 Q_A + F_{10} Q_r) + E_0 Q_r \sin\gamma]\hat{e_\gamma} \qquad (1.15)$$

$$\vec{F_{e,A}} = E_0(Q_A + \vec{Q_r}) - \vec{F_{e,r}} \qquad (1.16)$$

r, A= radius spheres ($r < A$); $\vec{F_{e,r}}$ force on sphere of radius r; γ angle between vertical axis and the line between centers of spheres; F_i Davis coefficients.

Chapter 2

THERMOPHORESIS

2.1 Introduction

Thermophoresis describes a phenomenon in which particles suspended in a fluid with non uniform temperature are subject to a force, named thermophoretic force, which is counteracted by the fluid drag on the particle. In steady state, particles move at a constant velocity due to equal thermophoretic and drag forces, known as thermophoretic velocity.

In addition to intrinsic theoretical interest, thermophoresis plays a role in the *scavenging of aerosol particles in cloud*, and is of considerable importance in many industrial processes: scale formation on the surfaces of heat exchangers, with the consequent reduction of heat transfer efficiency; micro-contamination control in the semiconductor industry; chemical vapour deposition processes for the manufacture of high-quality optical fibers; the performance of thermal precipitators in removing small particles from gas streams; the increase in the deposition of diesel or gasoline car exhaust particles on the surface of the oxidation catalyst.

Experiments to measure the thermophoretic force or velocity have mainly been performed in normal gravity, with monoatomic (Ar, He) and polyatomic gases (Air, N_2, CO_2), employing a variety of experimental methods.

In normal gravity it is not possible to study the phoretic effect alone, as particles move due to gravity and due to natural convection resulting from temperature gradients established to study thermophoresis.

Such difficulties can be overcome by utilizing a microgravity environment, e.g. parabolic flights or drop tower facilities (see Figure 2.1).

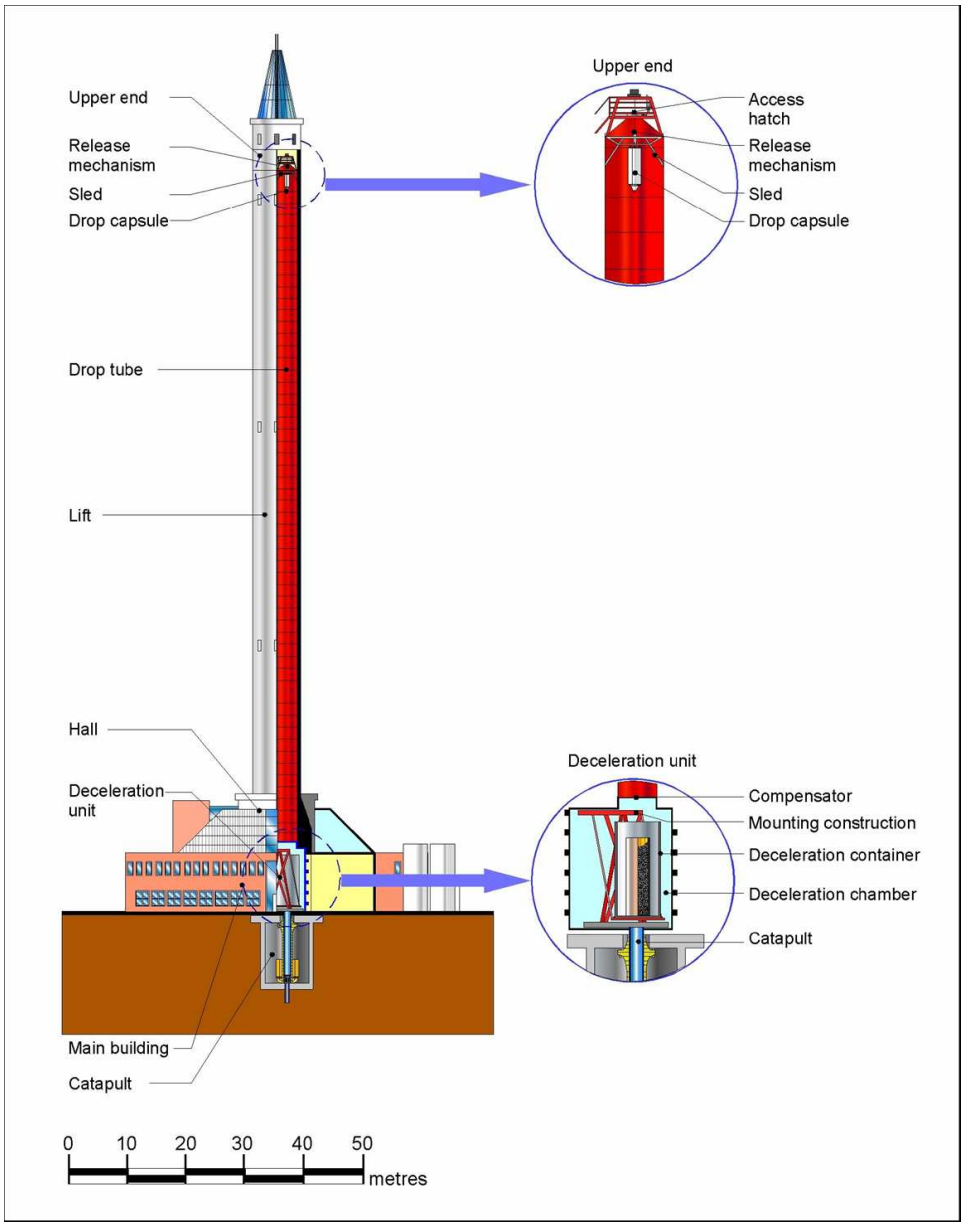

Figure 2.1: The droptower scheme

2.2 Theoretical background and previous experiments in microgravity

Theoretical investigations suggest that thermophoretic velocity depends on many factors, i.e. the temperature gradient, thermal conductivities of gases and particles, Knudsen number (defined as the ratio λ/r, where λ is the molecular mean free path of the fluid surrounding an aerosol particle, and r is the radius of the particle), and momentum and energy accommodation coefficients of gas molecules on the particle surface.

Such parameters influence the thermal and viscous slip flow and the flow induced by thermal stress. Momentum and energy accommodation coefficients are defined by

$$\alpha_t = \frac{(M_i - M_e)}{(M_i - M_s)} \tag{2.1}$$

and

$$\alpha_e = \frac{(E_i - E_e)}{(E_i - E_s)} \tag{2.2}$$

where M stands for the average tangential component of momentum of the gas molecules, and E for the average energy flux of the molecules. Subscripts e, i and s refer, respectively, to molecules emerging from the surface, incident molecules, and molecules leaving the surface in equilibrium with the surface.

Values of $\alpha_E = \alpha_t = 1$ correspond to the situation where incident molecules achieve complete thermodynamic equilibrium with the surface before leaving; $\alpha_E = \alpha_t = 0$ correspond to the complete specular reflection of the incident molecules. Intermediate values of α_E and α_t mean that the molecules partially adapt to the particle surface temperature.

In the free-molecule regime ($K_n \ll 1$), Waldmann's theory (Waldmann, 1959) gives a thermophoretic velocity independent of particle diameter.

In the slip-flow regime (or near-continuum regime, Kn < 0.1), Brock (1962) was the first to derive a near-continuum solution with the complete set of slip conditions, based on Navier-Stokes-Fourier theory.

The transition region ($0.1 \leq K_n < 10$) is more difficult to analyze. Talbot, Cheng, Schefer, and Willis (1980) recognized that when $K_n \to \infty$,

Brock's thermal force differs from the free-molecule solution of Waldmann only for the multiplicative factor

$$\frac{c_s}{cm}$$

which is about unity. Therefore, Talbot (1980) suggested the use of Brock's equation in the entire range of Knudsen number and suggested for the thermal sleep coefficient c_s , the coefficient of temperature jump c_t , and the velocity slip coefficient c_m , the values 1.17, 2.18 and 1.14, respectively, for complete thermal and momentum accommodation (Ivchenko & Yalamov, 1971; Loyalka, 1968; Loyalka & Ferziger, 1967).

Approaches based on the linearized Bhatnagar-Gross-Krook (BGK) model (Bhatnagar, Gross, & Krook, 1954) of the Boltzmann equation have been attempted (Law, 1986; Loyalka, 1992).

Yamamoto and Ishihara (1988) solved numerically the BGK model of the Boltzmann equation by assuming a complete accomodation of the molecules on the surface of the aerosol. They obtained the thermophoretic forces and velocity over a wide range of Knudsen number for arbitrary values of the particle's heat conductivity. The BGK model is the lowest-order approximation to the Boltzmann equation and gives an incorrect Prandtl number ($\mathrm{P}_r = 1$) for monoatomic gas.

Beresnev and Chernyak (1995) proposed a kinetic theory for the thermophoretic force and velocity of a spherical particle in a rarefied gas carried out on the basis of the S model (a third-order model of the linearized collision operator) kinetic equations (Shakhov, 1968). Beresnev's theory considers among the boundary conditions the possibility of arbitrary energy (α_E) and tangential momentum accommodation (α_T) of the gas molecules on the particle surface.

The works of Dwyer (1967), Sone and Aoki (1981, 1983), Yamamoto and Ishihara (1988), Loyalka (1992) and Ohwada and Sone (1992) predict negative thermophoresis for large values of the ratio between thermal conductivities of the particle and gas and for $K_n < 0.2$, although their predictions are not confirmed experimentally.

In order to compare experimental data obtained in different experimental conditions with the same carrier gas against the values calculated from theoretical studies it is useful to introduce the reduced thermophoretic velocity,

a dimensionless parameter defined as

$$V_{thr} = -V_{th}T/(\nu\nabla T) \tag{2.3}$$

where V_{th} is the thermophoretic velocity, T is the mean gas temperature in the vicinity of the aerosol particle, the kinematic viscosity of the gas, and ∇T the temperature gradient in the gas.

In order to compare the experimental thermophoretic velocities obtained with different gases, it is convenient to introduce a velocity V_s, normalized to a standard temperature T_0:

$$V_s = -V_{th}(T/T_0)/(\nu_0/\nu)/\nabla T \tag{2.4}$$

Concerning microgravity conditions, Toda, Ohi, Dobashi, and Hirano (1996), Toda, Ohnishi, Dobashi, and Hirano (1998) and Oostra (1998) performed experiments in the drop tower facilities of JAMIC ($g_0 = 10^{-5}$g, t = 10 s) and Zarm, in Bremen and the results are shown in Fig. 2.2

Toda et al. (1996, 1998) carried out experiments in Knudsen number range of 0.008-0.15, using SiO_2, MgO and PMMA particles in air at atmospheric pressure.

Toda's microgravity experiments gave values of V_{thr} as much as two or three times higher than those predicted by Talbot's equation, in experiments performed with SiO_2, and about seven times higher with MgO (k = 1.4 and 42 $Wm^{-1}K^{-1}$, respectively).

Oostra's results obtained with TiO_2 , M1200 (silica powder, Merk, Germany) and glass (k=11.7, 1.01 and 0.93 W $m^{-1}K^{-1}$, respectively) are lower than the values predicted by Talbot's equation. These experimental results have a large uncertainty due to the fact that the aerosol used in the experiments has a broad particle size distribution.

Prodi et al. (2006) performed experiments in microgravity conditions so as to obtain measurements of thermophoretic velocities in the transition region, using aerosol particles with different thermal conductivities (carnauba wax, paraffin and sodium chloride) and nitrogen as carrier gas. The aim was to evaluate the influence of the thermal conductivity of the particles in the thermophoresis.

The present work reports on the last test series of experiments (October 2005) whose main goal was to obtain thermophoretic velocities in mi-

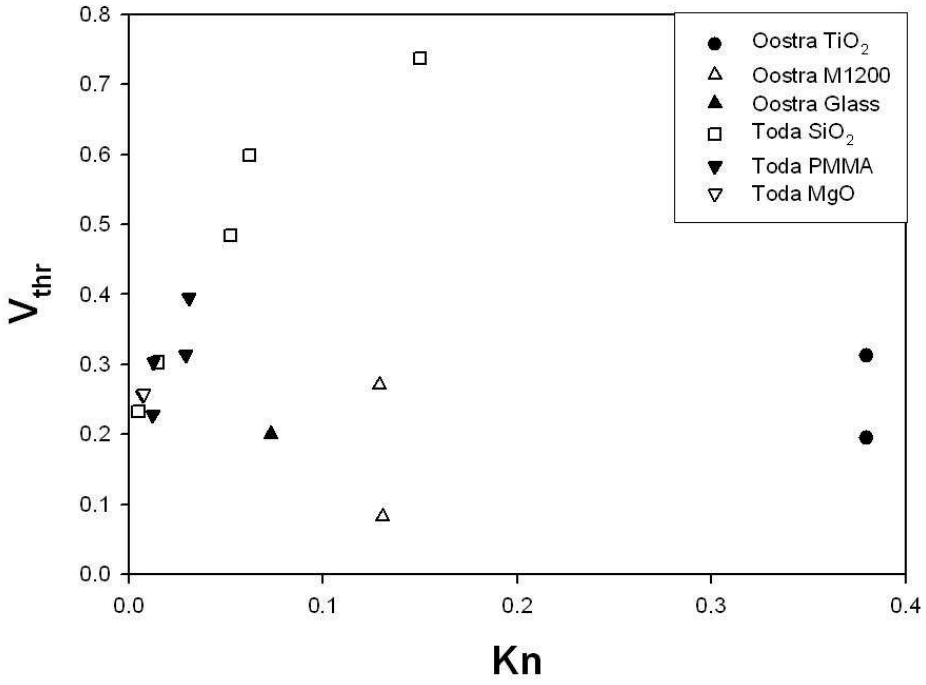

Figure 2.2: Reduced thermophoretic velocity as a function of the Knudsen number. Experimental data of Oostra (1998) and Toda et al. (1996, 1998) are reported.

crogravity conditions for gases with different thermal conductivities. Such experiments were never done before.

The data were compared with the theories of Talbot et al.(1980), Yamamoto and Ishihara (1988), and Beresnev and Chernyak (1995).

These theories, as shown above, have a different approach to the thermophoresis phenomenon.

2.3 Experimental set-up

As told in the introduction, in normal gravity it is not possible to study the phoretic effect alone, as particles move due to gravity and due to natural convection resulting from temperature gradients established to study thermophoresis. So experiments were performed in microgravity conditions.

The microgravity experiments were carried in the drop tower facility, which provides a weightlessness stage of about 4.7 s under free fall conditions with residual acceleration of about $10^{-6} g_0$. The experimental apparatus is housed in a special pressurized capsule (see Fig 2.3).

The electronic system of the Bremen drop tower comprises a ground station computer system, a telemetry remote control-transmission line, and a capsule computer system inside the capsule itself, allowing the control and automation of the experiment.

The cell used for the experiments consists of two plane plates (18.5 x 18.5 mm^2), one at the top and one at the bottom of the square mono-block vessel of optically polished Pyrex. The distance between the plates was 7 mm (see Fig. 2.4)

The upper plate was heated by an electric heater, and the lower one was maintained at ambient temperature. The temperature of the bottom and top of the cell was measured and recorded 2 times per second with two thermocouples inserted in the plates as sensors.

The heating of the upper plate started 3 min before the beginning of the microgravity condition and switched off 5 s after the fall. As the time required to heat the upper plate is about 1 min, when the capsule begins to drop, the temperature of the plate is completely stabilized. The standard deviation of temperature measured during the falls is about 0.1 and 0 °C for the upper and bottom plate, respectively.

The inlet and outlet of the aerosol occurs through two small holes in the

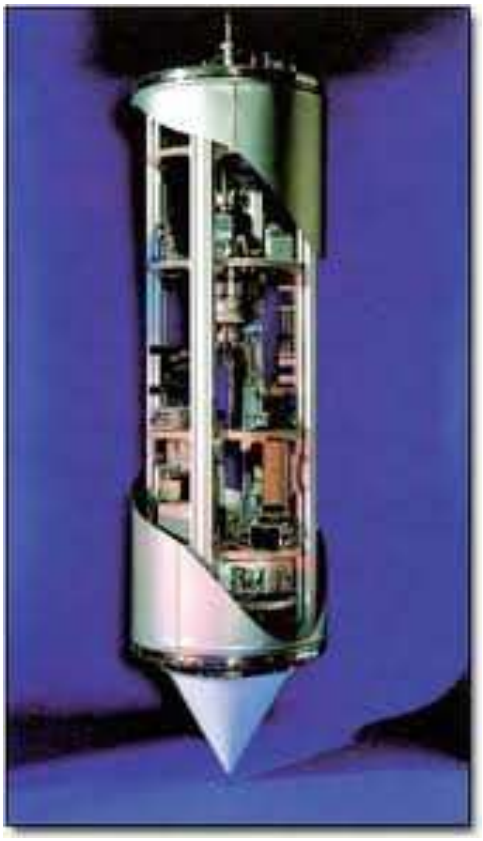

Figure 2.3: The pressurized capsule of the Bremen drop tower

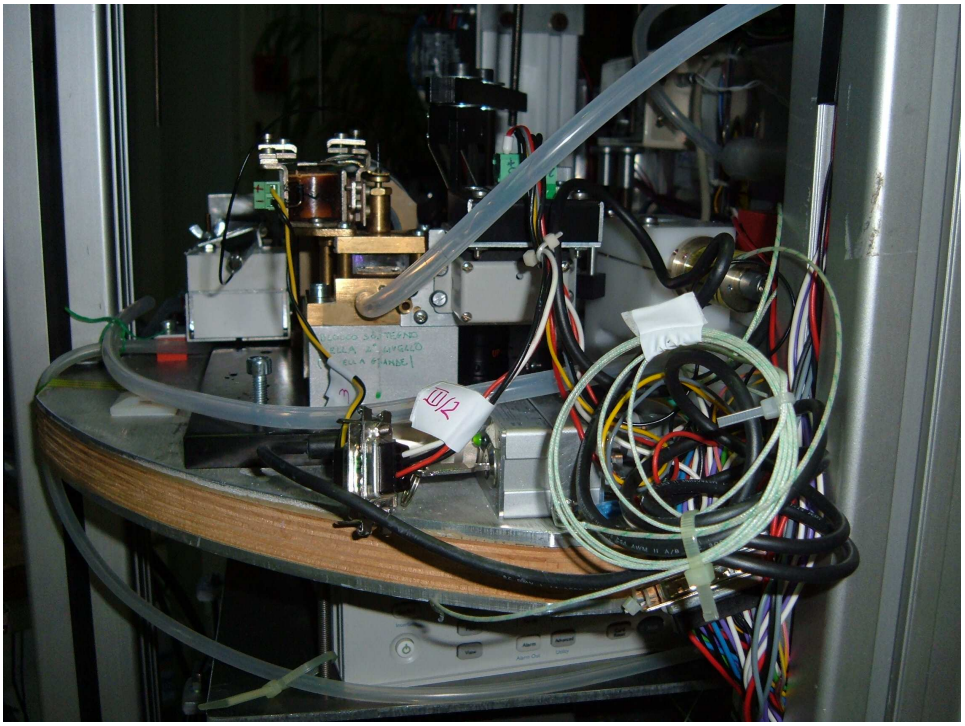

Figure 2.4: An example of cell used for experiments

bottom plate, which shut immediately after the introduction of the aerosol assuring a good seal. Using the electronic system of the drop tower, the aerosol was automatically injected into the cell about 15 s before the free fall (beginning of microgravity), and the flow was stopped about 2 s prior to the capsule drop.

The temperature and pressure inside the capsule were continuously monitored. N_2, Ar, He and Xe were supplied during the runs with small pressurized bottle (1 or 10 l). The temperature gradient in the cell during the runs performed with N_2 as carrier gas was in the range 4215-5730 K m^{-1} , with He in the range 1270-1900 K m^{-1}, Ar in the range 4760-5060 K m^{-1} , and Xe in the range 4790-5310 K m^{-1}.

The aerosol inside the cell was observed through the digital holographic velocimeter (Dubois, Joannes, & Legros, 1999), a device allowing the determination of 3-D coordinates of particles (30 frames/s; space resolution of about 0.2 m) in the viewing volume of 0.5 x 0.5 x 0.5 mm^3. Particle trajectories were reconstructed through the analysis of the sequence of particle positions, and a mean velocity for each particle was calculated by dividing

the length of the trajectory of each considered particle by the time employed. For each drop the number of frames recorded in microgravity conditions was about 130.

In order to calculate the velocity of each particle, the initial frame was considered to be that in which the gas motion was stopped and the movement of particles was vertical, i.e. in the direction of the thermal gradient.

The characteristic time of momentum transfer, i.e. the time necessary to allow the velocity of the gas inside the cell to be negligible when microgravity conditions are established, is theoretically related to δ^2/ν(δ, distance between the plate; ν, kinematic viscosity), and should be theoretically about 1 s for Xe and lower for N_2, He, and Ar (Dressler, 1981).

It is important to note that it was possible to check the actual relaxation time for momentum by observing the recorded images; from this inspection it turned out that the time was lower than 0.4 s for He, N2 and Ar, while it was about 2 s for Xe. Therefore, for Ar, He, N_2, it was possible to measure in each run the velocity of an individual particle for a maximum time of 4 s, and for Xe for about 2.5 s.

The relaxation time for aerosol particle was much lower than the momentum relaxation time.

Tab. 3 Values of physical parameters for Ar, Xe, He, N_2

Gas	λ, μm at T=293.15K	T_{mean},K	$\lambda, \mu m$ at T_m	$k_g, Wm^{-1}K^{-1}$ at T_{mean}	η,N s m^{-2} at T_{mean}	v,m^2s^{-1} (at T_{mean})
A_r	0.069	315.79	0.07582	0.0185	2.388E-5	1.54E-5
A_r	0.069	315.25	0.07535	0.0185	2.377E-5	1.53E-5
A_r	0.069	316.6	0.07606	0.0185	2.394E-5	1.55E-5
X_e	0.0382	314.85	0.04182	0.058	2.432E-5	4.91E-5
X_e	0.0382	316.4	0.04208	0.058	2.444E-5	4.95E-5
X_e	0.0382	314.95	0.04183	0.058	2.433E-5	4.91E-5
X_e	0.0382	316.5	0.04209	0.058	2.444E-5	4.95E-5
H_e	0.189	302.6	0.19677	0.1558	2.006E-5	1.24E-5
H_e	0.189	304.6	0.19842	0.1558	2.015E-5	1.26E-5
N_2	0.0676	314	0.07375	0.0207	1.86E-5	1.70E-5

Paraffin aerosol particles were produced by means of a monodisperse

Figure 2.5: Monodisperse aerosol generator (Mage)

aerosol generator (Minimage, see Figure 2.5), a modified version of MAGE (Prodi, 1972).

The measured value of thermal conductivity of paraffin turned out to be 0.42 W $m^{-1}K^{-1}$. The thermal conductivity of carrier gases N_2, Ar, Xe and He was found to be 0.0195, 0.0178, 0.0054, 0.153 W m^{-1} K $^{-1}$ at T =293 K, respectively.

In order to calculate the thermophoretic force and compare the experimental results with the current theories on thermophoresis (Beresnev & Chernyak, 1995; Talbot et al., 1980; Yamamoto & Ishihara, 1988) and similar terrestrial experiments (Jacobsen & Brock, 1965; Schmitt, 1959), it was necessary to consider some physical parameters, which are reported in Table 3. The mean free path was calculated from (Chen & Xu, 2002; Kennard, 1938; Saxton & Ranz,1952)

$$\lambda = (2\eta)(nmv) == (2\eta)/(\rho v) = (\eta/p)(\pi k_B T/2m)^{0.5} \qquad (2.5)$$

where m is the mass of a gas molecule; n the molecular number density; p the gas pressure; v the average thermal speed given by

$$v = [8k_BT/(\pi m)]^{0.5}, \tag{2.6}$$

where η is the gas viscosity; k_B the Boltzmann's constant; T the gas temperature; and ρ the gas density.

The values used for the viscosities of the gases are from Gray (1972).

The translational thermal conductivity was calculated from

$$k_g = (\frac{15}{4})R\eta/M = (\frac{15}{4})\eta k_B/m, \tag{2.7}$$

where M is the gas molecular weight (g mol^{-1}); and R, the universal gas constant.

The thermophoretic force, which is equal to drag force in steady state, was calculated from

$$F_{th} = 6\pi\eta r V_{th}/S, \tag{2.8}$$

where V_{th} is the experimental thermophoretic velocity, S is the slip correction;

$$S = 1 + Kn[A_1 + A_2 exp(-A_3/Kn)]. \tag{2.9}$$

Experiments on different gases (Ar, N_2, CO_2, H_2) and substances (paraffin, silicon oil) show that A_1, A_2 and A_3 values can be considered independent of gases (Schmitt, 1959).

In order to calculate the experimental reduced thermophoretic force $F_{th}/(r^2 dT/dy)$, we assumed $A_1 = 1.155$; $A_2 = 0.471; A_3 = 0.596$ for all the gases (Allen & Raabe, 1982).

2.4 Results

Figs. 2.6 and 2.7 and report the thermophoretic velocity (Eq.), normalized to 315 K, vs. Knudsen number, obtained from microgravity experiments

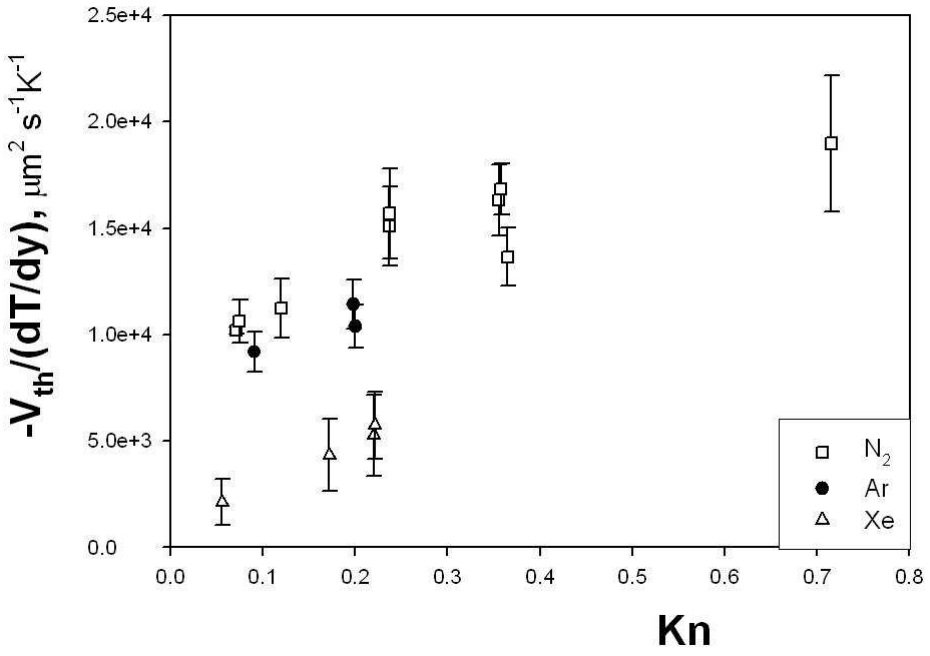

Figure 2.6: Experimental data for the normalized thermophoretic velocity vs. Knudsen number (Ar, Xe, and N2 as carrier gas).

performed on different gases. It can be observed that the thermophoretic velocity decreases from He, N_2, A_r, X_e.

In order to explain this trend, it must be borne in mind that one of the factors determining the movement of an aerosol particle in the presence of a thermal gradient is thermal creep. Utilizing gas kinetic theory, Maxwell (1879) predicted that the tangential temperature gradient ∇T at a gas-solid surface would cause a thin layer of gas adjacent to the surface to move with

$$u = c_s \nabla T / T, \tag{2.10}$$

where ν is the kinematic viscosity of the gas, and c_s is the thermal slip coefficient.

The thermal creep turns out to be proportional to the kinematic viscosity of the gas. The present experimental data show that the thermophoretic velocity has the same trend as ν, i.e. the highest value is for He with the highest kinematic viscosity, and the lowest for Xe, which has the lowest ν.

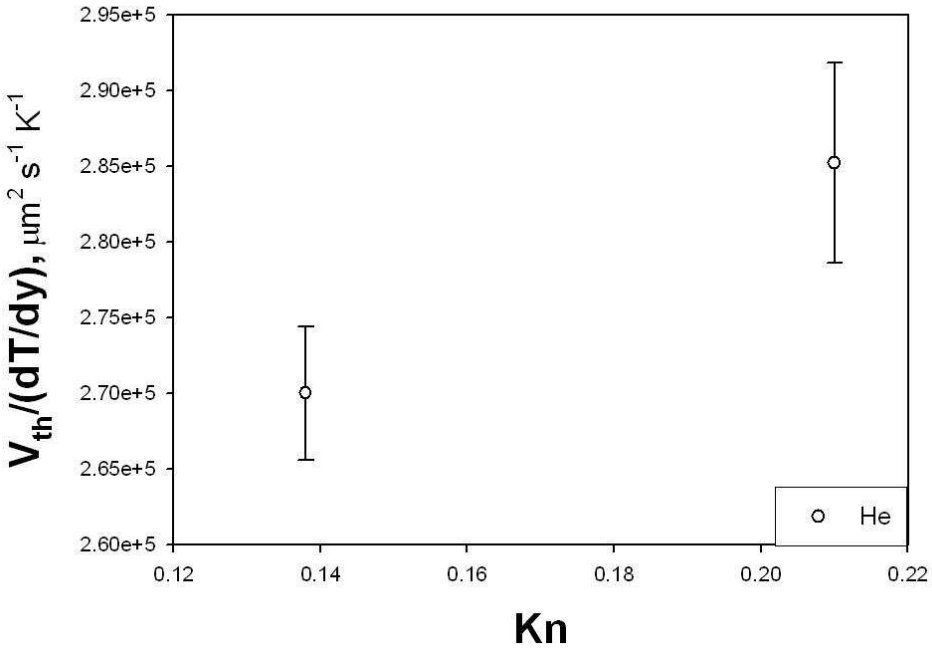

Figure 2.7: As in Fig. 1 (He as carrier gas).

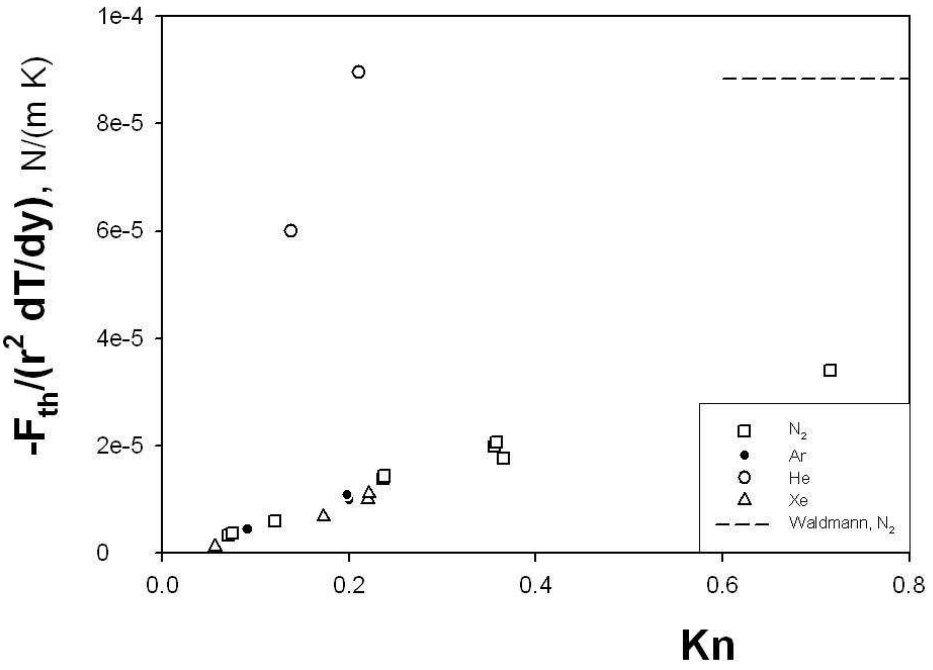

Figure 2.8: Experimental data and Waldmann's solution for the normalized thermophoretic force.

Fig.2.8 shows the experimental reduced thermophoretic force $F_{th}/(r^2 dT/dy)$ vs. Knudsen number, and the theoretical equation of Waldmann for N_2 in the free-molecule regime (8.8 x $10^{-5} N m^{-1} K^{-1}$ at T = 293 K).

In the Waldmann region ($Kn \gg 1$), where drag force is proportional to velocity and the square of the particle radius, and the thermophoretic force is proportional to the square of the radius, the thermophoretic velocity is independent of K_n and of the thermal conductivity of the particles.

Experimental data show that the reduced thermophoretic force (F_{th-r}) can be considered a unique function of the K_n number (range 0.05-0.8) for N_2, Ar and Xe.

This can be explained if it is considered that, by equating F_{th} and drag force, it turns out that

$$F_{th-r} = (6\pi\eta/Sr)[V_{th}/(dT/dy)], \tag{2.11}$$

is inversely proportional to the aerosol particle radius and directly proportional to V_{th} per unit temperature gradient (UTG). From the values of the mean free path of molecules reported in Table 3, it can be seen, for example, that the ratio between $\lambda_{Ar}/\lambda_{Xe}$ is about 1.8.

As V_{th} per UTG for Ar is about twice with respect to Xe (considering the same Knudsen number), the same value of F_{th-r} is obtained for both Ar and Xe.

A similar evaluation can be made considering N_2 with respect to the other gases. Concerning H_e, the F_{th-r} is much higher with respect the other gases.

The ratio between the F_{th-r} measured with He and the values obtained with the other gases considered, is about 7.6 and 7.86 ($K_n = 0.14$ and 0.21, respectively). This trend depends on the much higher values of the mean free path, kinematic viscosity and thermal conductivity of He as compared to N_2, Ar and Xe.

Fig.2.9 reports the comparison between experimental data obtained by Schmitt (1959) with silicone oil drops (k = 0.125 W $m^{-1}K^{-1}$), and by Jacobsen and Brock (1965) with NaCl particles (k$\cong$ 6 W $m^{-1}K^{-1}$), with argon as carrier gas and at 1g.

As the Schmitt definition of λ is

$$\lambda = \eta/(0.491\rho v) \tag{2.12}$$

instead of

$$\lambda = 2\eta/(\rho v) \tag{2.13}$$

the necessary corrections were made. Schmitt's experimental data can be considered in agreement with the values obtained in experiments at 0g with the same gas.

Figs.2.10-2.13 report the reduced thermophoretic velocity vs. Knudsen for the gases examined.

Each dot is the mean value of V_{thr} of individual particles in the drops performed. With aerosol having a given diameter maximum of three runs were performed, and in each run the velocity of about 30 monodisperse aerosol particles was measured. The error bars reported for each dot in the graphs are the standard deviation of V_{thr} of monodisperse particles examined.

Figs. 2.10-2.13 show the values of V_{thr} calculated using the Talbot et

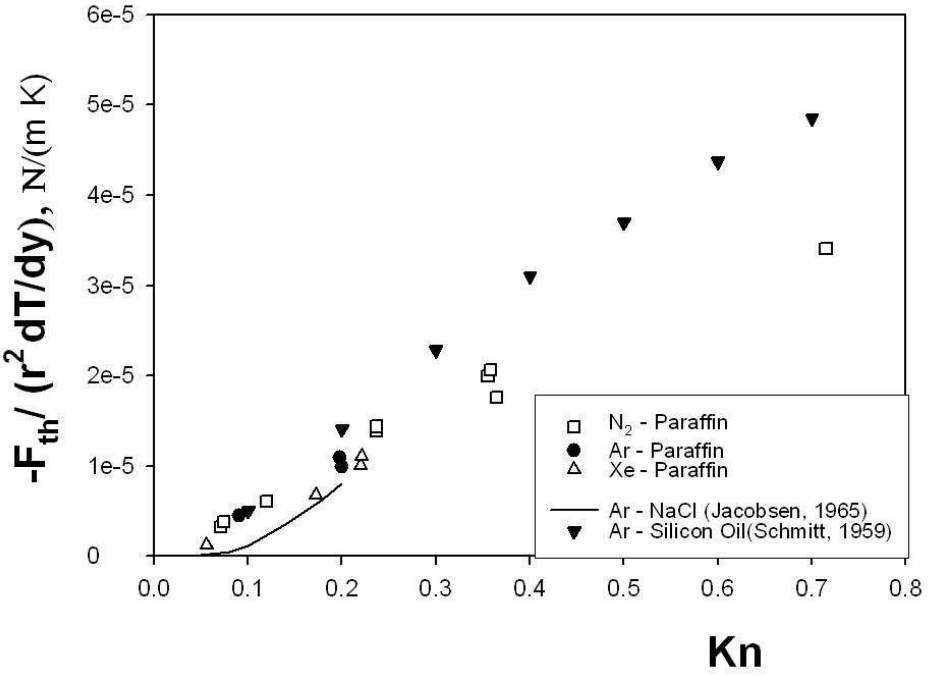

Figure 2.9: Experimental data compared with the data of Schmitt (silicon oil in Ar), and Jacobsen and Brock (NaCl particles in Ar).

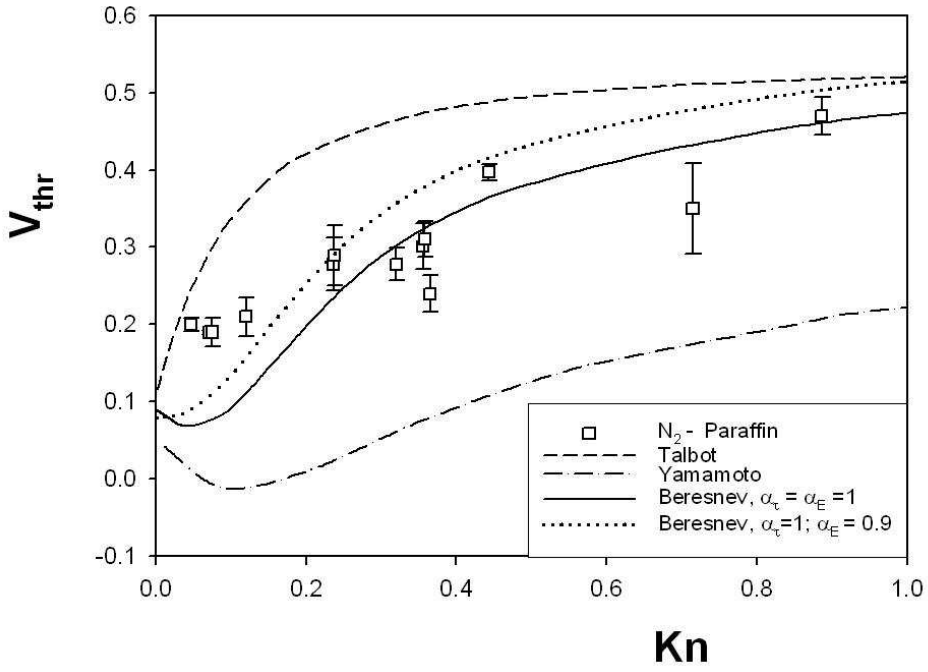

Figure 2.10: Comparison of theoretical models with the experimental reduced thermophoretic velocity (N2 as carrier gas).

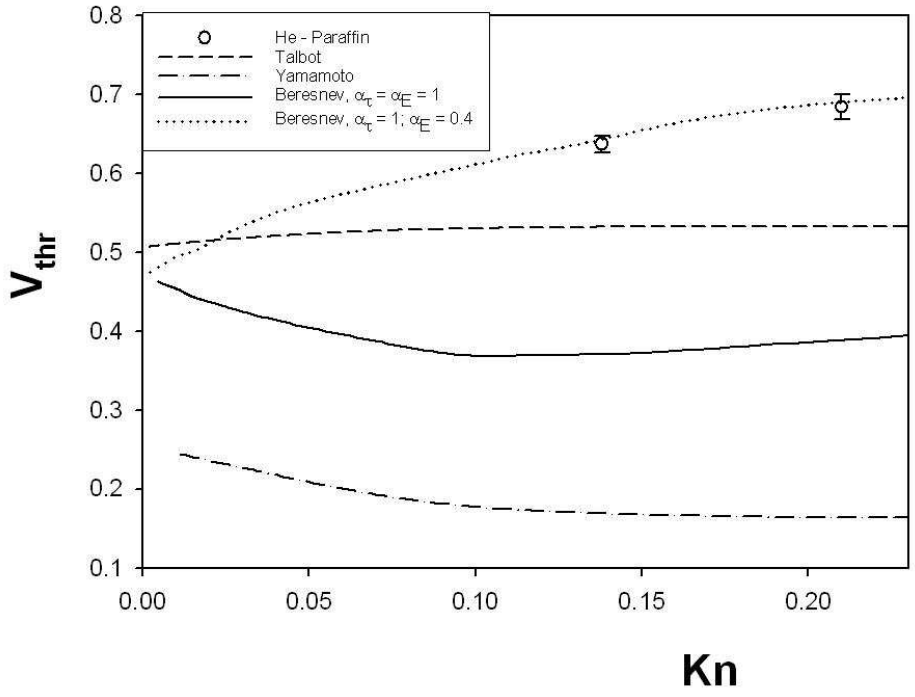

Figure 2.11: Comparison of theoretical models with the experimental reduced thermophoretic velocity (He as carrier gas).

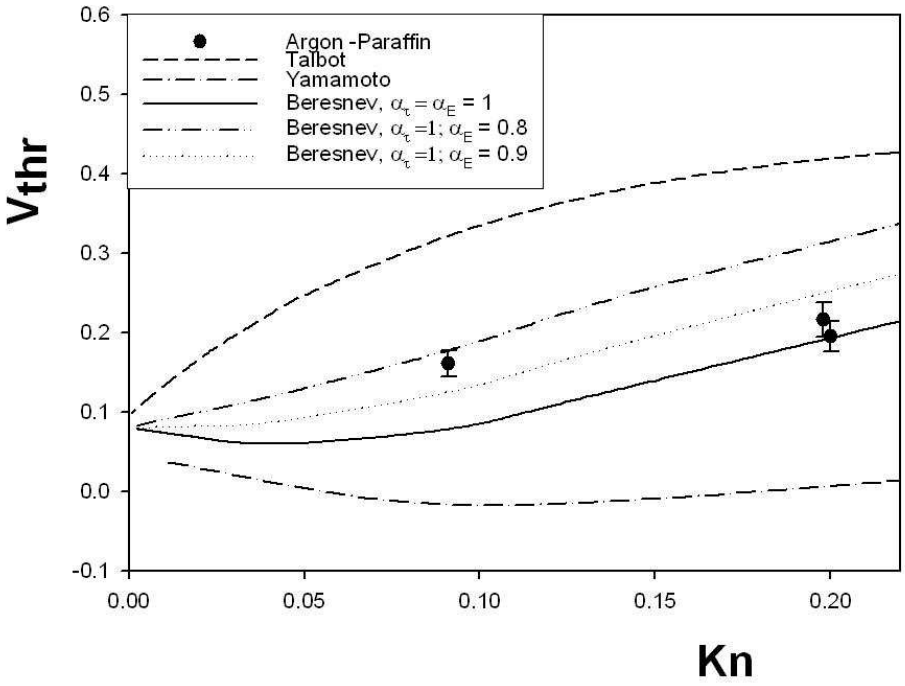

Figure 2.12: Comparison of theoretical models with the experimental reduced thermophoretic velocity (Ar as carrier gas).

al., Yamamoto and Ishihara, Beresnev and Cernyak equations. These theories, as shown above, have a different approach to the thermophoresis phenomenon.

In addition, all these authors provide a formula for the thermophoretic force, and then deduce the thermophoretic velocity, by equating drag and thermophoretic forces. Talbot et al. calculated the viscous drag by using the Millikan formula, in which A, B, and C are 1.20, 0.41 and 0.88, respectively. Yamamoto and Ishihara calculated the drag force acting on the sphere as

$$F_{drag} = 4\pi\eta r V_{th} A_s \tag{2.14}$$

where values of A_s parameter vs. $K = (\pi)^{0.5} K_n/2$ is given in Table 1 of their paper.

The ratio between F_{drag} calculated with the Millikan and Yamamoto

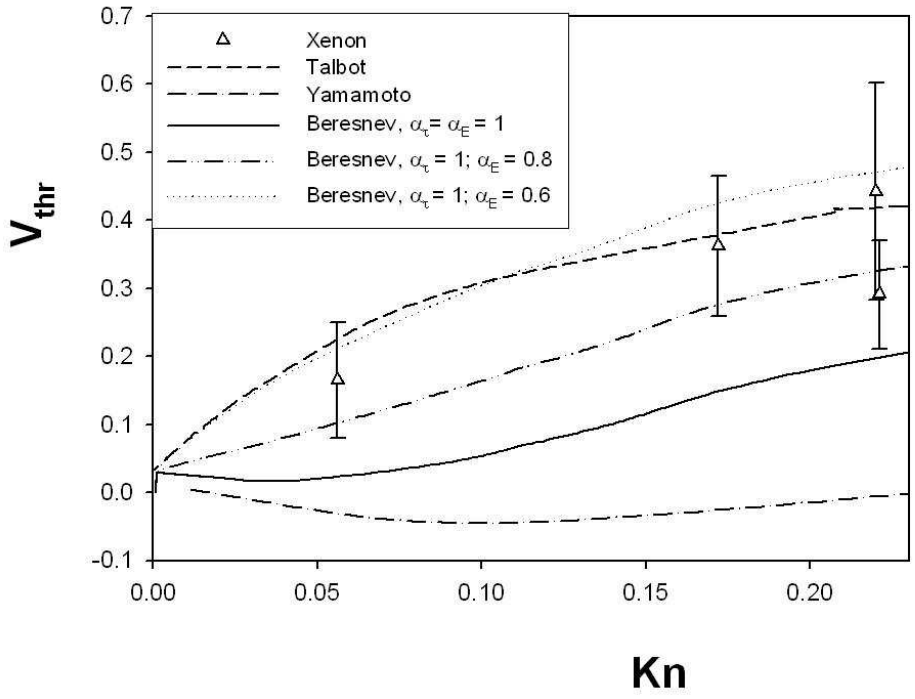

Figure 2.13: omparison of theoretical models with the experimental reduced thermophoretic velocity (Xe as carrier gas).

formulas, respectively, varies from 1 to 1.09 in the considered Knudsen range (0.05-0.8), assuming the same particle velocity. Therefore this is not the factor which determines the difference in thermophoretic velocities provided by the two models (Figs.2.10-2.13), mainly due to the theoretical approach.

The viscous drag in the thermophoretic theory of Beresnev, Chernyak, and Fomyagin (1990) is based on the same gas kinetic S-model equation as the solution for the thermophoretic force problem. The theory for viscous drag is developed for an arbitrary Knudsen number, and includes as parameters the same momentum and energy accommodation coefficients.

In the case of complete accommodation, the results of Beresnev agree with those obtained with Millikan formula. Following Beresnev the drag coefficient should depend first of all on α_τ.

As the comparison reported in Figs.2.10-2.13 assumes $\alpha_\tau = 1$, it can be deduced that the different trends of the V_{th} and V_{thr} curves for the considered models do not depend on the evaluation of the drag force, but on the different theoretical approaches to the thermophoresis phenomenon.

It can be observed that Talbot forecasts higher values than the experimental ones for N_2 and A_r, comparable values for X_e, and lower ones for H_e. For the comparison, use was made here of the values c_s, c_t and c_m suggested by the author, who assumes a complete thermal and momentum accommodation for the thermophoresis of aerosol particles. In the Talbot formula the most important parameter is c_s(1.17 for complete thermal accommodation), while variations of c_t and c_m have a small influence.

Yamamoto's equation, obtained by assuming that the gas obeys the so-called BGK equation, and that the molecules are reflected diffusely ($\alpha_E = \alpha_\tau = 1$), always gives lower values than the experimental ones, and also negative values of thermophoretic velocities for N_2, Ar, Xe.

Beresnev's theory consider in the boundary conditions the possibility of arbitrary energy (α_E) and tangential momentum accommodation (α_τ) of the gas molecules on the particle surface.

Beresnev's theory fits the experimental data to a satisfactory degree if a tangential momentum accommodation coefficient of unity and an energy accommodation coefficient less than one are assumed.

The difference between the Yamamoto theory and Beresnev theories also for $\alpha_E = \alpha_\tau = 1$, results from the fact that they are based on the linearized BGK model and S-model, respectively.

2.5 Conclusions

The aim of the experiments presented here is to evaluate the influence of the physical parameters of different gases on the thermophoretic velocity and thermophoretic force of aerosol particles.

Previous experiments in microgravity conditions (Prodi et al., 2006) did not evidence a clear dependence of V_{th} on the thermal conductivity of the aerosol. This outcome disagrees with Talbot and Yamamoto theories, but agrees with data obtained in 1g experiments (Keng & Orr, 1966; Li & Davis, 1995; Santachiara, Prodi, & Cornetti, 2002; Schadt & Cadle, 1961) and theoretically by Loyalka (1992).

Experiments performed in the same experimental conditions in the Bremen drop tower facility evidence that the V_{th} decreases from He to N_2, Ar and Xe. The presented experimental data show that the thermophoretic velocity has the same trend of ν. The highest value is for H_e , with the highest kinematic viscosity and thermal conductivity, and the lowest is for Xe, which has the lowest values.

In the considered range of Knudsen number (0.05-0.8) the experimental data disagree with the Talbot and Yamamoto theories. Talbot et al.(1980) predict thermophoretic velocities that are nearly equal to the observed values in Xenon, larger than observed ones in N_2 and Ar, and smaller than observed values in He.

The Yamamoto equation always gives lower values than the experimental ones, and also negative values of thermophoretic velocities for N_2, Ar, Xe.

Beresnev's theory fits the experimental data to a satisfactory degree in the considered Knudsen range, if a tangential momentum accommodation coefficient of unity and energy accommodation coefficient of less than one are assumed.

Concerning the reduced thermophoretic force (F_{th-r}), it can be considered a unique function of the Knudsen number for N_2, Ar and Xe. [1].

[1] Reprinted from Santachiara G., Di Matteo L., Prodi F. and Belosi F., *Measurements of thermophoretic velocities of aerosol particles in microgravity conditions in different carrier gases*, Aerosol Science 38 (2007) 645-655, with permission from Elsevier

Chapter 3

NUCLEATION OF WATER VAPOR CONDENSATION

3.1 Introduction

Raindrops and snowflakes are among the smallest meteorological entities observable without special equipment(From Wallace & Hobbs, 2006). Typical raindrops show diameters between 1 and 3 mm; however drop sizes up to 8 mm have been observed while still larger drops break up (Szakáll et al., 2010).

To form raindrops, cloud particles have to increase in mass a million times or more, and these same cloud particles are nucleated by aerosol as small as 0.01 μm. To account for growth through such a wide range of sizes in time periods as short as 10 min or so for some convective clouds, it is necessary to consider a number of physical processes.

Clouds form when air becomes supersaturated with respect to liquid water (or in some cases with respect to ice). The most common means by which supersaturations is produced in the atmosphere is through the ascent of air particles, which results in the expansion of the air and adiabatic cooling. Under these conditions, water vapor condenses onto some of the particles in the air to form a cloud of small water droplets or ice particles (From Wallace & Hobbs, 2006).

In order to measure CCN, we carried out an experimental campaign (February, 2008). During this campaign, cloud condensation nuclei were measured in a rural area (S. Pietro Capofiume, near Bologna).

3.2 Theory

Considering first the hypothetical problem of the formation of a pure water droplet by condensation from a supersaturated vapor without the aid of particles in the air (i.e., in perfectly clean air). In this process, which is referred to as *homogeneous nucleation* of condensation, the first stage is the chance collisions of a number of water molecules in the vapor phase to form small embryonic water droplets that are large enough to remain intact.

Supposing that a small embryonic water droplet of volume V and surface area A forms from pure supersaturated water vapor at constant temperature and pressure. If μ_l and μ_v are the Gibbs free energies per molecule in the liquid and the vapor phases, respectively, and n is the number of water molecules per unit volume of liquid, the decrease in the Gibbs free energy of the system due to the condensation is nV(μ_v-μ_l). Work is done in creating the surface area of the droplet. This work may be written as Aσ, where σ is the work required to create a unit area of vapor-liquid interface (called the *interfacial energy* between the vapor and the liquid, or the *surface energy* of the liquid). Writing:

$$\Delta E = A\sigma - nV(\mu_v - \mu_l) \tag{3.1}$$

then Δ E is the net increase in the energy of the system due to the formation of the droplet. It can be shown that:

$$\mu_v - \mu_l = kT \ln \frac{e}{e_s} \tag{3.2}$$

where e and T are the vapor pressure and temperature of the system and e_s is the saturation vapor pressure over a plan surface of water at temperature T. Therefore,

$$\Delta E = A\sigma - nVkT \ln \frac{e}{e_s} \tag{3.3}$$

For a droplet of radius R, (3.3) becomes

$$\Delta E = 4\pi R^2 \sigma - \frac{4}{3}\pi R^3 nkT \ln \frac{e}{e_s} \tag{3.4}$$

Under subsaturated conditions $e < e_s$. In this case, $\ln(e/e_s)$ is negative and ΔE is always positive and increases with increasing R (see Fig 3.1).

In other words, the larger the embryonic droplet that forms in a sub-

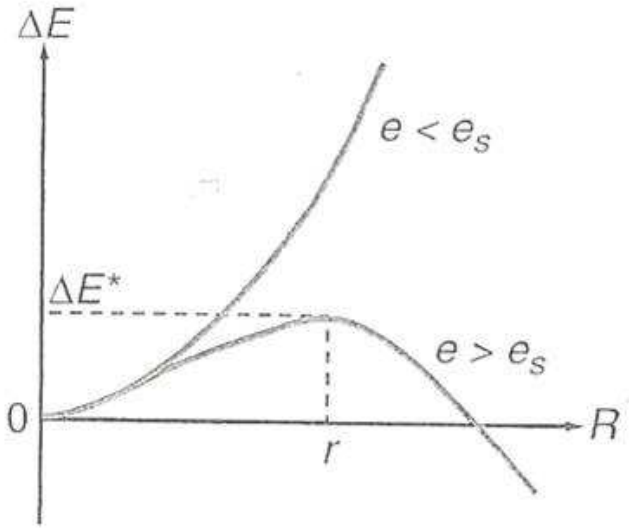

Figure 3.1: The Gibbs free energies[From Wallace & Hobbs, 2006]

saturated vapor, the greater the increase in the energy, ΔE, of the system. Because a system approaches an equilibrium state by reducing its energy, the formation of droplets is clearly not favored under subsaturated conditions. Even so, due to random collisions of water molecules, very small embryonic droplets continually form (and evaporate) in a subsaturated vapor, but they do not grow large enough to become visible as a cloud of droplets.

Under supersaturated conditions, $e > e_s$, and $\ln(e/e_s)$ is positive. In this case, ΔE in eq. (3.4) can be either positive or negative depending on the value of R. The variation of ΔE with R for $e > e_s$ is also shown in Fig 3.1, where it can be seen that ΔE initially increases with increasing R, reaches a maximum value at R=r, and then decreases with increasing R. Hence, under supersaturated conditions, embryonic droplets with R$< r$ tend to evaporate, since by so doing they decrease ΔE.

However, droplets that manage to grow by chance collisions to a radius that just exceeds r will continue to grow spontaneously by condensation from the vapor phase, since this will produce a decrease in ΔE.

At R=r, a droplet can grow or evaporate infinitesimally without any change in ΔE. It can be obtained an expression for r in terms of e by

setting $d(\Delta E)/dR = 0$ at R=r. Hence, from eq. (3.4),

$$r = \frac{2\sigma}{nkT \ln \frac{e}{e_s}} \tag{3.5}$$

Equation (3.5) is referred to as *Kelvin's equation*, after Lord Kelvin who first derived it.

Equation (3.5) can be used to calculate the radius r of a droplet that is in unstable equilibrium with a given water vapor pressure e. Alternatively, it can be used to determine the saturation vapor pressure e over a droplet of specified radius r. It should be noted that the relative humidity at which a droplet of radius r is in unstable equilibrium is 100 e/e_s, where e/e_s is by inverting eq.(3.5). A pure water droplet of radius 0.01 μm requires a relative humidity of $\sim$ 112% (i.e., a supersaturation of $\sim$ 12%) to be in (unstable) equilibrium with its environment, while a droplet of radius 1 μ m requires a relative humidity of only 100.12% (i.e., a supersaturation of $\sim$ 0.12 %). Because the supersaturations that develop in natural clouds due to the adiabatic ascent of air rarely exceed a few percent, it follows that even if embryonic droplets of pure water as large as 0.01 μ m in radius formed by the chance collision of water molecules, they would be well below the critical radius required for survival in air that is just a few percent supersaturated. Consequently, droplets do not form in natural clouds by the homogeneous nucleation of pure water.

Instead they form on atmospheric aerosol by what is known as *heterogeneous nucleation*. The atmosphere contains many particles that range in size from submicrometer to several tens of micrometer (see Chapter 3). Those particles that are *wettable* can serve as centers upon which water vapor condenses. Moreover, droplets can form and grow on these particles at much lower supersaturations than those required for homogeneous nucleation. For example, if sufficient water condenses onto a completely wettable particle 0.3 μm in radius to form a thin film of water over the surface of the particle, the water film will be in unstable equilibrium with air that has a supersaturation of 0.4%. If the supersaturation were slightly greater than 0.4%, water would condense onto the film of water and the droplet would increase in size.

Some of the particles in air are soluble in water. Consequently, they dissolve, wholly or in part, when water condenses onto them, so that a

solution droplet is formed.

The saturation vapor pressure of water adjacent to a solution droplet is less than that adjacent to a pure water droplet of the same size. The fractional reduction in the water vapor pressure is given by *Raoult's law*

$$\frac{e'}{e} = f \tag{3.6}$$

where *e'* is the saturation vapor pressure of water adjacent to a solution droplet containing a mole fraction f of pure water and e is the saturation vapor pressure of water adjacent to a pure water droplet of the same size and at the same temperature. The *mole fraction of pure water* is defined as the number of moles of pure water in the solution divided by the total number of moles in the solution.

Consider a solution droplet of radius r that contains a mass m (in kg) of a dissolved material of molecular weight M_s. If each molecule of the material dissociates into i ions in water, the effective number of moles of the material in the droplet is i(1000 m)$/M_s$. If the density of the solution is ρ' and the molecular weight of water M_w, the number of moles of pure water in the droplet is

$$f = \frac{(\frac{4}{3}\pi r^3\rho' - m)/M_w}{[(\frac{4}{3}\pi r^3\rho' - m)/M_w] + im/M_s} = \Big[1 + \frac{imM_w}{M_s(\frac{4}{3}\pi r^3\rho' - m)}\Big]^{-1} \tag{3.7}$$

Combining (3.5)-(3.7) (but replacing σ and n by σ' and n' to indicate the surface energy and number concentration of water molecules, respectively, for the solution) we obtain the following expression for the saturation vapor pressure *e'* adjacent to a solution droplet of radius r

$$\frac{e'}{e_{s'}} = \Big[exp\frac{2\sigma'}{n'kTr}\Big[1 + \frac{imM_w}{M_s(\frac{4}{3}\pi r^3\rho' - m}\Big]^{-1} \tag{3.8}$$

Equation (3.8) may be used to calculate the saturation vapor pressure *e'* adjacent to a solution droplet as a function of its radius, we obtain what is referred to as a *Köhler curve*. Several such curves, derived from 3.8, are shown in Fig 3.2. Below a certain droplet radius, the relative humidity adjacent to a solution droplet is less than that which is in equilibrium with a plane surface of pure water at the same temperature.

As the droplet increase in size, the solution becomes weaker, the Kelvin

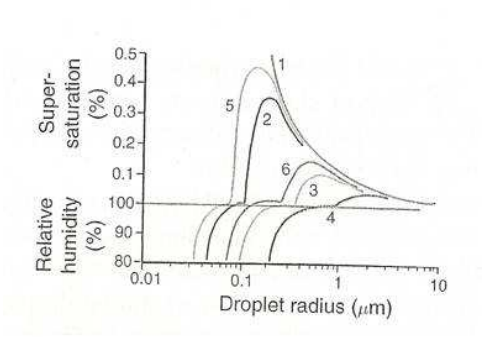

Figure 3.2: Köhler curves[From Wallace & Hobbs, 2006].

curvature effect becomes the dominant influence, and eventually the relative humidity of the air adjacent to the droplet becomes essentially the same as that adjacent to a pure water droplet of the same size (From Wallace & Hobbs, 2006).

3.3 Cloud Condensation Nuclei

A small subset of the atmospheric aerosol serves as particles upon which water vapor condenses to form droplets that are activated and grow by condensation to form cloud droplets at the supersaturations achieved in clouds ($\sim 0.1 - 1$ %). These particles are called *cloud condensation nuclei* (CCN).

The origin and nature of CCN has become a central issue in climate change due to their strong ability to modulate cloud microstructure (Sun & Ariya, 2006).

CCN are prevalently hygroscopic/water soluble inorganic, organic or mixed particles, primary (natural or anthropogenic) or secondary (Santachiara et al., 2009). The larger the size of a particle, the more readily it is wetted by water, and the greater its solubility, the lower will be the supersaturation at which the particle can serve as a CCN.

For example, to serve as a CCN at 1% supersaturation, completely wettable but water-insoluble particles need to be at least $\sim 0.1\mu$ m in radius, whereas soluble particles can serve as CCN at 1% supersaturation even if they are as small as $\sim 0.01\mu$ m in radius. Most CCN consist of a mixture of soluble and insoluble components (called *mixed nuclei*).

Worldwide measurements of CCN concentrations have not revealed any systematic latitudinal or seasonal variations. However, near the Earth's surface, continental air masses generally contain larger concentrations of CCN than marine air masses. The ratio of CCN (at 1% supersaturation) to the total number of particles in the air (CN) is $\sim$ 0.2-0.6 in marine air; in continental air this ratio is generally less than $\sim$ 0.01 but can rise to $\sim$ 0.1. The very low ratio of CCN to CN in continental air is attributable to the large number of very small particles, which are not activated at low supersaturations. Concentrations of CCN over land decline by about a factor of five between the planetary boundary layer and the free troposphere. Over the same height interval, concentrations of CCN over the ocean remain fairly constant or may even increase with height, reaching a maximum concentration just above the mean cloud height. Ground-based measurements indicate that there is a diurnal variation in CCN concentrations, with a minimum at about 6 a.m and a maximum at about 6 p.m.

The observations just described provide clues as to the origins of CCN. First of all it appears that the land acts as a source of CCN because the concentrations of CCN because the concentrations of CCN are higher over land and decrease with altitude. Some of the soil particles and dusts that enter the atmosphere probably serve as CCN, but they do not appear to be a dominant source. The rate of production of CCN from burning vegetable matter is on the order of $10^{12} - 10^{15}$ per kg of material consumed. Thus, forest fires are a source of CCN. About 80% of the particles emitted by idling diesel engines are CCN at 1% supersaturation. About 70% of the particles emitted by the 1991 Kuwait oil fires were CCN at 1% supersaturation. Although sea-salt particles enter the air over the oceans by other mechanisms, they do not appear to be a dominant source of CCN, even over the oceans.

There appears to be a widespread and probably a fairly uniform source of CCN over both the oceans and the land, the nature of which has not been definitely established. A likely candidate is gas-to-particle conversion, which can produce particles up to a few tenths of a micrometer in diameter that can act as CCN if they are soluble or wettable. Gas-to-particle conversion mechanisms that require solar radiation might be responsible for the observed peak in CCN concentrations at $\sim$ 6 p.m. Many CCN consist of sulfates. Over the oceans, organic sulfur from the ocean provides a source of CCN, with the DMS and MSA being converted to sulfate in the atmo-

sphere. Evaporating clouds also release sulfate particles (From Wallace & Hobbs, 2006).

3.4 Experimental

An experimental campaign (February 2008) were carried out in order to measure CCN, i.e. the fraction of aerosol that can become droplets in ambient clouds. CCN measurements were performed about 1 h later than the various aerosol fraction samplings.

Instruments that measure CCN can be classified according to how they generate water vapour supersaturation, based on (1) the nonlinear dependence of water vapour pressure upon temperature, or (2) the difference between water vapour diffusivity and thermal diffusivity. The first type have an applied temperature gradient perpendicular to the flow and include static diffusion cloud chambers (Twomey, 1963; Lala et al., 1977), and continuous flow parallel plate diffusion chambers (VanReken et al., 2004). The second type requires continuous laminar flow and a temperature gradient in the streamwise direction (Roberts et al., 2005).

The device used in the present investigation was a thermal diffusion chamber consisting of two parallel circular aluminium plates (D = 8 cm) joined together by a non-conducting glass wall (h = 1 cm). The ratio D/h is higher than 5, to avoid convective motion. The cloud chamber volume is about 50 cm^3. The chamber is illuminated by a laser beam (He-Ne, λ = 632 nm ; 0.6 mm beam diameter; P = 20 mW) centered in the chamber and oriented at an angle of 90 ° D1-Allied). It detects the droplets in a volume of approximately 6x10^{-3} cm^3 and register images every second during the supersaturation cycle. The optical system can detect droplets of at least 0.5 μm.

A temperature difference is applied by cooling the bottom plate thermoelectrically, while the upper plate is maintained at ambient temperature. The temperature of each plate is monitored separately by means of a thermocouple. The upper surface of the chamber is covered with a sintered porous glass imbued with water. Thus a thermal and vapour density linear gradient is created within the chamber, with a maximum supersaturation near the center of the chamber. A sample of the outside air is admitted into the thermal diffusion chamber, after which the valves are closed and

the supersaturation profile is established.

Those particles that can act as CCN are activated to grow to droplets and the time to attain steady state is about 3 s. The supersaturation experienced by the particle can be adjusted by changing the temperature difference across the chamber. The maximum supersaturation between the plates is given by the following approximate relation:

$$S_{max} = \Big(\frac{(e_w(T_t) + e_w(T_b))/2}{e_w((T_t + T_b)/2)} \Big) \cdot 100\% \tag{3.9}$$

where S_{max} is the maximum supersaturation expressed as a percentage, T_t and T_b are the top and bottom plates temperature $^\circ$ C, and e_w is water vapour saturation pressure(Katz et al., 1975).

3.5 Cloud condensation nuclei measurements

Fig.3.3 shows the trend of CCN measured at two supersaturations (S=0.03% and S=0.36%) during the experimental campaign . Generally, the diurnal trend of CCN depends on the sampling site (e.g. rural, urban or industrialized areas), local meteorological parameters (temperature, r.h., wind speed, solar radiation, diurnal convective cycle, thermal inversion), absence or presence of precipitation, and air mass type.

The present measurements reveal a diurnal trend with lower values at around midday and higher ones during the night, a similar trend between CCN (S = 0.36%) and r.h., and opposite to the mixing layer height (Fig. 3.4,3.5). The trend between temperature and r.h. is opposite.

The trend between r.h. and mixing layer seems to confirm the statement of Stroud et al. (2002), who suggest that relative humidity can be used qualitatively as an indicator of the surface mixing layer height. Saxena and Grovenstein (1994) observed peaks in CCN within and above the cloud-top, noting that the mechanism for enhancing the CCN concentration is strongly dependent upon relative humidity.

The observed trend appears to be weakly related to anthropogenic activity and excludes the hypothesis of CCN originating from photochemical nucleation process, as in this case a maximum should appear in the early afternoon.

The trend could depend on the presence of an inversion layer at night

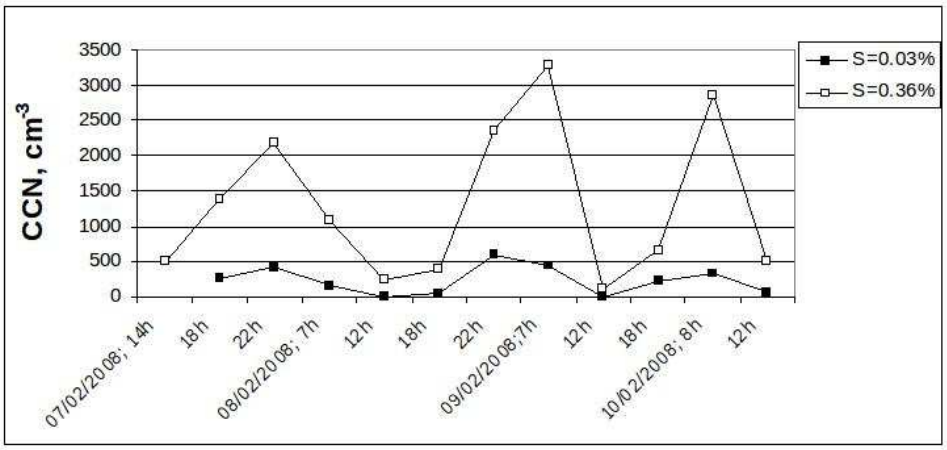

Figure 3.3: Time series of CCN concentration (cm^{-3}).

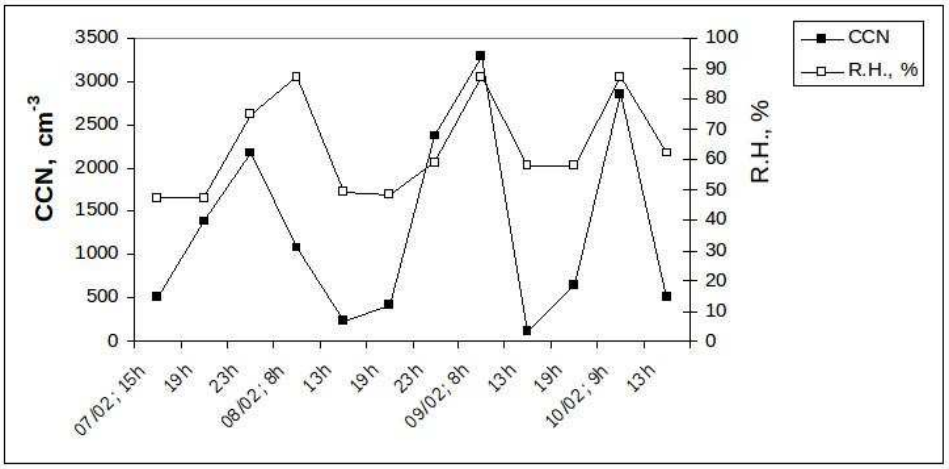

Figure 3.4: Trend of CCN concentration and relative humidity (S=0.36%).

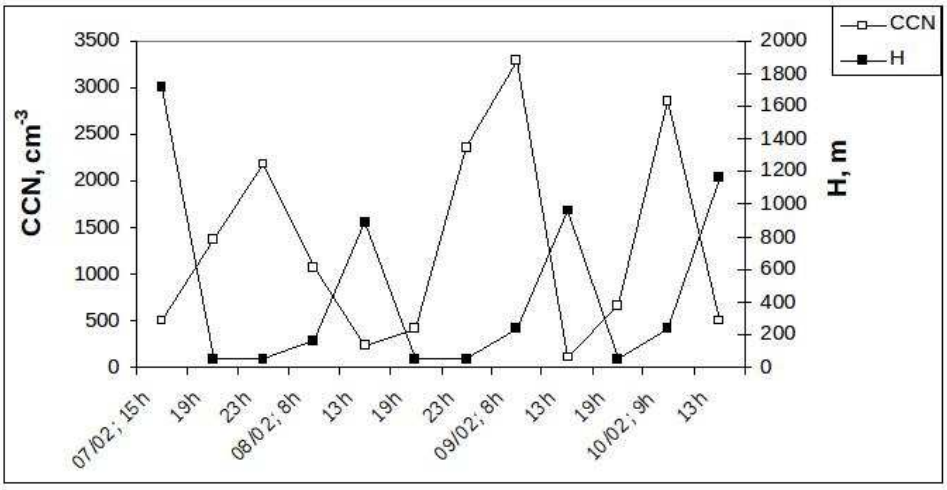

Figure 3.5: Trend of CCN concentration and mixing layer height (S=0.36%).

due to the infrared radiation emitted from the earth's surface in clear sky conditions, thus reducing the mixing layer where most of the particles are confined. In addition, sulphur dioxide can be oxidized on the surface of aerosol during night-time, due to high r.h. (about 90%), and nitrogen oxides (NO_x) can form N_2O_5 which, due to its high solubility in water, quickly dissolves into water droplets (or wetted particles) to produce nitric acid. Such processes increase the hygroscopicity of the particles.

The sharp decrease in concentration around midday is partly the result of surface heating, which raises the mixing layer height, and of an increase in wind speed, which promotes convection and the transport of aerosol to higher levels in the atmosphere. A similar trend was found by Twomey and Davidson (1975) during five-years of observations at Robertson, New South Wales, Australia (agricultural region, 700 m a.s.l.), which highlighted a repeated near-noon minimum and a well defined late-evening maximum.

Different trends are observed in populated and industrialized areas. For instance, measurements reported for Mexico City show a pattern characterized by maximum CCN concentrations with values between 6500 and 3500 cm^{-3} at 0.75% supersaturation during the first hours of sunlight, reaching values fluctuating between 600 and 2000 CCN cm^{-3} during the afternoon. The pattern was the effect of the inversion layer, and the onset of emissions from vehicular traffic in the morning, followed by the photochemical production of secondary organics that condense on the primary particles (Herrera

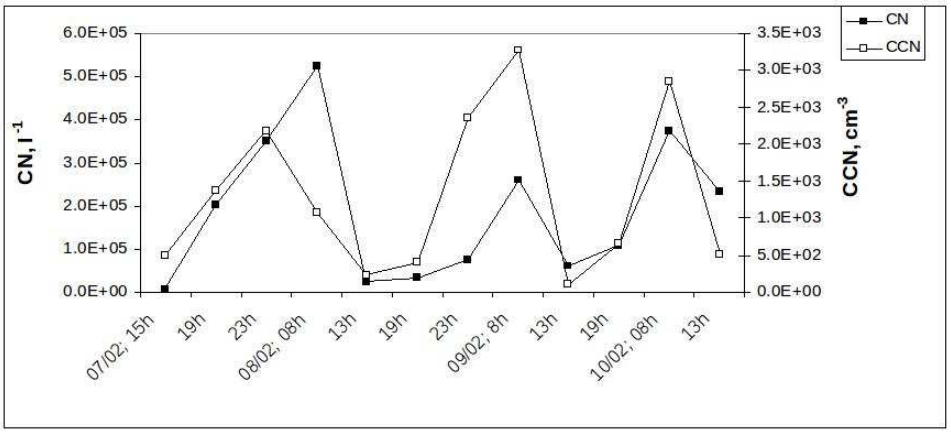

Figure 3.6: Time series of aerosol number concentration (range 0.3-1μm, l^{-1}) and CCN (cm^{-3}).

et al., 1988; Montañez et al., 1993; Baumgardner et al., 2004).

In a less densely populated city (Reno, Nevada), Hudson and Frisbie (1991) measured temperature inversions during wintertime, when concentrations are dominated by local anthropogenic sources, finding strong diurnal regular trends of CCN concentrations, with a minimum during the afternoon hours. Alofs and Liu (1981), at Rolla (Missouri), a small non-industrial town, found no seasonal variation nor diurnal pattern over a 10-month period.

Fig. 3.6 shows the time series of the aerosol number concentration in the range 0.3-1μm and the CCN concentration (S = 0.36%), showing a similar pattern, measured during the winter campaign at S.P.C. In agreement with these results, Ishizaka and Adhikari (2003) obtained in the urban atmosphere of Nakoya and in the coastal one of Mikuni (Japan) a high correlation between CCN and aerosol particles in the range 0.1-1 μm at S=0.5%. This suggests that the accumulation mode aerosol particles are activated as CCN more effectively than coarse and Aitken particles. Stroud et al. (2007) during 2-day pollution episode at Duke Forest in North Carolina observed high CCN concentrations coinciding with increases in accumulation mode particle concentrations (d_m = 100-300 nm).

Concerning CCN measurements, published papers report a wide range of CCN concentrations, from several thousand per cubic centimetre (Herrera et al., 1988; Baumgardner et al., 2004; Hobbs et al., 1985) to less than 10

cm^{-3} (Radke et al., 1969).

Fig 4.7 reports some published measurements of CCN concentrations in different areas. In unpolluted maritime air masses (Raga et al., 1995; Yum et al., 2001; Charlson et al., 1987; Hegg et al., 1991; Gras et al., 1995; Furutani et al., 2008; De Felice et al., 1996) and background sites (De Felice et al., 1996; Philippin et al., 1997; Hitzenberg et al., 1999; Roberts et al., 2001) CCN concentrations are less than 500 cm^{-3}. Unpolluted continental air-mass concentrations are usually between 200 and $\sim$ 2000 cm^{-3}, while polluted continental air-masses have concentrations above 2000 cm^{-3} (Herrera et al., 1988; Twomey et al., 1969).

The mean CCN concentrations measured during the experimental campaign at SPC (S = 0.03%, 0.36%, 0.88 %) are 231 cm^{-3}, 1294 cm^{-3} , 1566 cm^{-3}, respectively, indicating that the rural area is weakly affected by air from the surrounding plain.

Fig. 3.8 shows the ratio of the number of activated droplets ("CCN") relative to the number of condensation nuclei "C") measured during the campaign. The CCN/CN ratio shows the same trend as CCN concentrations.

The activation ratio, i.e. the number density of activated particles relative to the particle number density, reported in published papers, is highly variable, depending on the chemical and physical properties of the aerosol (organic and inorganic, primary and secondary, internally or surface mixed).

The ratio N_{CNN}/N_{CN} is usually higher for maritime aerosol than for continental aerosol, and increases with particle diameter for aerosol having the same chemical composition and mixing state, under the same meteorological conditions. In the extreme case of pure sulphate and marine aerosol particles, which are completely soluble, a sharp threshold is present, with practically 100% activation of particles above 50 nm.

Usually aged anthropogenic aerosol show a higher CCN/CN ratio than fresh aerosol (Andreae & Rosenfeld 2008; Furutani et al., 2008). Hudson and Frisbie (1991) measured (Reno, Nevada) the CCN/CN ratio of concentrations, showing a wide variation from a few per cent to more than 50%, pointing out that CN concentrations cannot be used as a surrogate for CCN concentrations. Kuwata et al. (2007) (Jeju Island, Korea) evidenced that the CCN/CN ratio strongly depends on particle diameter (almost zero at 100 nm and close to unity for 200 nm and higher; S = 0.097%).

Site		Elevation	Period	Sw	CCN, cm^{-3}	Range, cm^{-3}	Method
1-Mt. Sonnblick	Background	3104 m asl	1995-1997	0.5%	300	29-786	DH associated [model M1]
Vienna	Urban			0.5%	2448	500-3080	DH associated [model M1]
2-Cape Grimm	Coastal area		1981-1991	0.23%	90		Static thermal-gradient cloud chamber
				1.2%	1000		
3- Galway [Ireland]	Coastal area [marine air]		1994-1995	0.5%	140		DH associated [model M1]
	Coastal area [polluted air]		1994-1995	0.5%	770		
4- Toronto	Semi-rural [polluted and clean air]		2005, fall	0.32%		50-5000	Continuous parallel plate CCN counter
5-Ireland West Coast	Marine air		1994-2002	0.5%		91-144	DH associated [model M1]
	Continental air		1994-2002	0.5%		358-586	
6-New South Wales	Agriculture region	750 m	1968-1973	0.75%	150	80 - 570	Static thermal-gradient cloud chamber
7- Australia	Coastal site Southern Ocean		Winter 1993	1%	32		Desert research Institute CCN spectrometer
			Summer 1995	1%	160		
8-Irish Sea	Clean air Marine		1991-1992	0.95%	450		Static thermal-gradient cloud chamber
	Polluted air				2000		
9-Palmer Station, Antarctica			February 1994	1.3%	20	< 1-700	Fukuta-Saxena CCN spectrometer
10-Jeju Island,Korea			2005, Spring	0.97%	3996		CCN counter
11- Nagoya	Urban Industrial		Dec. 1998 Jan. 1999	0.5%		200-1400	CCN counter Mod.130 Mee
12 - Mikuni	Coastal, polluted air		Feb.March .1999	0.5%		50-700	
13- California	Coastal cruise		Nov. 2004	0.6%		1400-6000	Thermal gradient CCN counter
	Pacific Ocean		Nov.2004	0.6%		200-500	
14-Amazon Basin			March April 1998	0.15%		33	Static thermal-gradient cloud chamber
				1%		267	
15-Lamont, Oklahoma		Flights, 400-2000m	May 25, 2003	2.1%	1000		CCNC3
16-Mexixo city		2000m asl	April 1984	0.75%		600-6500	Thermal diffusion chamber

Figure 3.7: CCN concentrations in published papers.

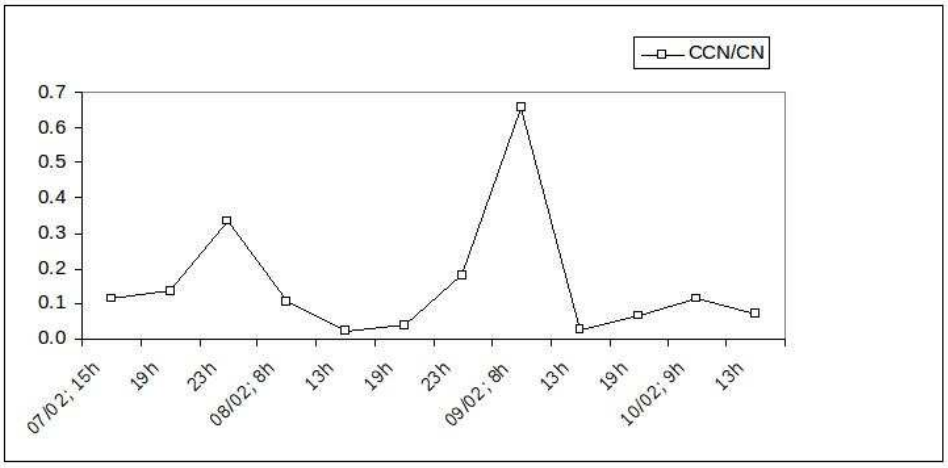

Figure 3.8: Ratio CCN/CN; S=0.36%.

The mean CCN number concentrations were 1194 cm^{-3}, 2543 cm^{-3}, and 3996 cm^{-3} (S = 0.097%; 0.27% , 0.97%, respectively). The low average CCN/CN ratio obtained during the experimental campaign at SPC (0.15 at S = 0.36%) shows a "continental" environment.

3.6 Conclusions

Condensation nuclei and cloud condensation nuclei were measured in a rural area, open to Adriatic Sea to the east, but enclosed by densely populated areas, on its southern, western and northern sides. The observations are summarized as follows:

- The mean values of CCN concentration (S = 0.03%, 0.36%, 0.88 %) are 231 cm^{-3}, 1294 cm^{-3} and 1566 cm^{-3}, respectively. The CCN/CN ratio (0.15 at S = 0.36%) shows the same trend as the CCN concentrations.

- The present measurements reveal a CCN diurnal trend with lower values at about midday and higher ones during the night, a similar trend of CCN and r.h., opposite to the mixing layer height. The trend between temperature and r.h. is opposite. The observed CCN trend appears to be weakly related to anthropogenic activity, and excludes the hypothesis of CCN originating from photochemical nucleation processes, as this would cause a maximum to appear in the early after-

noon. The sharp decrease in concentration around midday is partly due to surface heating, which raises the mixing layer height, and to an increase in wind speed, which promotes convection and the transport of aerosol to higher levels in the atmosphere. [1]

[1]The major part of the data published in this Chapter has already been published in from Santachiara G., Di Matteo L., Belosi F. and Prodi F., *Atmospheric particles acting as ice forming nuclei in different size ranges and cloud condensation nuclei measurements* Il Nuovo Cimento, 2009, Vol 124 B, N. 5, pp 565-581, with permission from Il Nuovo Cimento

Chapter 4

NUCLEATION OF ICE PARTICLES

4.1 Nucleation of Ice Particles

A supercooled droplet is in an unstable state. For freezing to occur, enough water molecules must come together within the droplet to form an embryo of ice large enough to survive and grow. The situation is analogous to the formation of a water droplet from the vapor phase discussed in Chapter 3. If an ice embryo within a droplet exceeds a certain critical size, its growth will produce a decrease in the energy of the system. However, any increase in the size of an ice embryo smaller than the critical size causes an increase in total energy. In the latter case, from an energetic point of view, it is preferable for the embryo to break up.

If a water droplet contains no foreign particles, it can freeze only by *homogeneous nucleation*. Because the numbers and sizes of the ice embryos that form by chance aggregations increase with decreasing temperature, below a certain temperature, freezing by homogeneous nucleation becomes a virtual certainty (From Wallace and Hobbs, 2006).

Homogeneous nucleation takes place only at temperatures from - 40 °C and lower; the presence of any impurity is assumed to trigger a heterogeneous freezing at a higher temperature than - 40 °C, and the wide variety of impurities which are present in natural systems con-

sequently makes homogeneous nucleation impossible (Zachariassen et al., 2004).

These impurity are special type of particle, called *ice forming nuclei*, it may freeze by a process known as *heterogeneous nucleation*; water molecules in the droplet collect onto the surface of the particle to form an ice-like structure that may increase in size and cause the droplet to freeze. Because the formation of the ice structure is aided by the ice forming nucleus, and the ice embryo also starts off with the dimensions of the freezing nucleus, heterogeneous nucleation can occur at much higher temperatures than homogeneous nucleation.

4.2 Measurement techniques

Ice nuclei can form ice through different thermodynamic mechanisms. Over the past 50 years a wide variety of measurement techniques has been developed for detecting IN and measuring their characteristics, each with different advantages and disadvantages: the drop freezing technique, particle capture on supercooled droplets, particle sampling on filters followed by processing in static or dynamic chambers, continuous-flow ice thermal diffusion chamber, and others.

The large degree of uncertainty and sometimes contradictory results in IN measurements depends on several factors: the large number of experimental devices, the fact that particles are activated in different ways and have different efficiencies, depending on the method of activation, the sensitivity of experiments to partially uncontrolled laboratory conditions, and even more unpredictable field conditions.

According to Levin and Cotton (2007), continuous-flow- device measurements (Rogers, 1982; Al-Naimi and Saunders, 1985) roughly exhibit a factor of 10 higher concentrations of IN at warmer temperatures than filter processing systems, due perhaps to the recondensation of Vaseline organic vapour onto the active ice nucleating sites of aerosol particles during filter processing.

Additional factors raise the uncertainty in measurements: the possibility of particle deactivation in the atmosphere (e.g. adsorption

of foreign gases such as SO_2, NH_3, coagulation with Aitken particles); the dependence of nucleating capability on the thermal history of particles; processes which produce organic or inorganic coating of dust, e.g. dust particles passing over the Mediterranean which can be coated with hygroscopic sea salt (Levin et al., 2005), internally mixed sulphate-organic, etc. Möhler et al. (2008b) investigated the effect of coating with secondary organic substances and sulphuric acid on the efficiency of mineral particles to act as heterogeneous ice nuclei, demonstrating a markedly reduced ice nucleation efficiency.

Even after 50 years of ice nuclei studies, a calibration ice nucleating material does not exist, and there is no general agreement on a standard technique for measuring IN. It is generally agreed that ice will form on nuclei in response to different kinds of thermodynamic forcing, the primary variables being temperature and supersaturation with respect to ice and water (S_{ice} and S_w, respectively).

The formation of ice in clouds can occur through primary processes (nucleation of ice from the liquid water or vapour phases, either homogeneously or heterogeneously), or through secondary processes (fragmentation of large drops during freezing, ice splinter formation during the riming, crystal fragmentation). The latter could explain the higher concentration of ice crystals measured in many clouds, with respect to the concentration of IN at nearby locations in clouds. The homogeneous nucleation process involves only pure water or solution droplets and depends on the mass of liquid water and its temperature. Ice will not homogeneously form from pure solution droplets, no mater how diluted, at temperatures greater than about -38 °C (Pruppacher and Klett, 1997).

Four heterogeneous nucleation mechanisms are distinguished for atmospheric ice formation: deposition (direct transition from vapour to solid on a foreign particle below water saturation), condensation-freezing (ice-phase forms as water vapour condenses on cloud condensation nuclei at $T < 0$ °C and afterwards freezes), contact-freezing (ice nuclei promote freezing on coming into contact with a supercooled droplet), and immersion-freezing (nucleation of supercooled water by a nucleus suspended in the body of water).

Heterogeneous freezing occurs at lower ice-saturation ratios than homogeneous freezing. No existing ice nucleus measuring system is capable of detecting ice formation by all known mechanisms. For example, the continuous-flow diffusion chamber (CFCD) can detect deposition and condensation- freezing, but not contact-freezing or homogeneous freezing (Rogers et al., 2001; DeMott et al., 2006). In addition an impactor needs to be inserted at the intake of the device to remove larger particles (e.g. particles with d $> 2\mu$m), in order to differentiate ice crystals from background aerosol reliably. Particle sampling on filters followed by processing in static or dynamic chambers is convenient because filter samples can be gathered and processed later without degradation of the nuclei. It also allows measurements of aerosol activation in all size ranges (Stevenson, 1968; Bigg, 1990).

Traditionally, it has been thought that good heterogeneous ice nuclei are insoluble solids. The sources can be natural (organic, such as bacteria, pollen, lichen, fungi, decaying vegetation material, marine bacteria associated with plankton, inorganics e.g. clay particles, volcanic ash, soil dust) and anthropogenic aerosol (soot, metallic oxides emitted by steel furnaces and copper smelters). Until recently, homogeneous freezing of aqueous particles was considered to be the dominant formation mechanism in upper tropospheric clouds. Consequently, homogeneous freezing of aqueous particles (e.g. binary and ternary solution of ammonium sulphate, sulphuric acid and water) was investigated extensively.

Recently, it has been shown in the laboratory that soluble species can also act as IN in both the immersion (Zuberi et al., 2001; Zobrist et al., 2006) and deposition mode (Shilling et al., 2006). Flying at altitudes as high as 15 km, Cziczo et al. (2004) measured high concentrations of sulphates and sea salt in residual ice nuclei, presumably from homogeneous freezing mechanisms. Some cirrus cloud formation observations are consistent with ammonium sulphate and other solid ammoniated sulphate particles acting as low-temperature IN.

The effects of air pollution on aerosol is still not clear. Some papers assert that air pollution can enhance the nucleus counts with respect to unpolluted regions or rural sites (Hobbs and Locatelli, 1970; Al-Naimi

and Saunders, 1985; DeMott et al., 2003). Other research involving measurements of IN made simultaneously in 44 different locations worldwide provided no evidence that pollution is an important source of nuclei (Bigg and Stevenson, 1970), while Braham and Spyers-Duran (1974), Czys (1977), and Pérez et al. (1985) measured smaller concentrations in an urban area with respect to a nearby rural site. Ardon et al. (2008) investigated the role of air pollution on ice nuclei concentration in Israel, by collecting aerosols on filter samples near the shores of Tel Aviv, upwind of pollution sources and inside the polluted area about 3 km from the sea shore. Preliminary results show some effects of the city of Tel Aviv on enhancement of effective IN.

4.3 Concentrations measurements

It should be noted that ice nucleus concentrations can sometimes vary by several orders of magnitude over several hours. On the average, the number N of ice nuclei per liter of air active at temperature T tends to follow the empirical relationship

$$\ln N = a(T_1 - T_2) \tag{4.1}$$

where T_1 is the temperature at which one ice nucleus per liter is active (typically about $-20°$ C) and a varies from about 0.3 to 0.8. For a=0.6, the concentration of ice nuclei increases by about a factor of 10 for every 4° C decrease in temperature. In urban air, the total concentration of aerosol is on the order of $10^{18}\ liter^{-1}$ and only about one particle in 10^8 acts as an ice nucleus at - 20 ° C.

The activity of a particle as a freezing or a deposition nucleus depends not only on the temperature but also on the supersaturations of the ambient air. One empirical equation for measurements is:

$$N = exp\{a + b[100(S_i - 1)]\} \tag{4.2}$$

where N is the concentration of ice nuclei per liter, S_i is the supersaturation with respect to ice, a=-0.639, and b=0.1296. Because few ground level measurements of IN in low polluted areas are re-

ported, we performed two experimental campaigns in a rural area, with the following aims: Compare IN concentrations in different size ranges,supersaturations and temperatures; check a diurnal trend in the IN concentrations; investigate the relationship between IN and particle number concentration.

4.4 Experimental:first campaign

An experimental campaign was performed at a rural site (S. Pietro Capofiume, near Bologna), in the period 09-12 July 2007.

Various aerosol fractions and total suspended particles were sampled on nitrocellulose membrane (Millipore HABG04700, nominal porosity 0.45 μm) four times a day (period 06-22 h), at 3 m above ground level. The mean flow rate was 38.3 lpm with a sampling time of 10 min.

Aerosol fractions were sampled by inserting different sampling heads (1 μm, 2.5 μm, and 10 μm cut-point-Standard EN 12341, TCR Tecora) in front of the filter. The sampling of all the fractions lasted about 1 h.

Simultaneous measurements were also performed of particle number concentrations (CNC-TSI- Mod.3020, with 50% detection at 10 nm) and particle concentration in different size classes starting from diameter d $> 0.3\mu$m (Optical Spectrometer Grimm, Mod.1.108). Meteorological data (air temperature, wind speed, pressure) were recorded and the ranges of temperature (T), relative humidity (r.h.) and wind speed (v) are reported in Table 4. The atmospheric pressure was about 1010 mbar.

Tab. 4 Details of the sampling campaign.

Date of sampling	T range, $^{\circ}C$	Range of r.h, %	Range of v, ms^{-1}
9/07/2007	25.4-32	31-39	2.3-6.4
10/07/2007	18.5-27.6	30-59	1.2-5.2
11/7/2007	13.3-22.7	43-87	1.6-3
12/07/2007	14.1-26.2	36-71	1.0-1.9

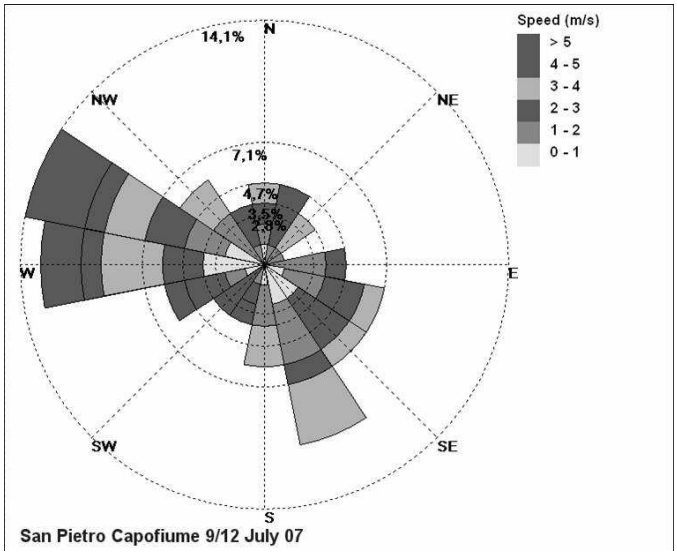

Figure 4.1: Wind rose at San Pietro Capofiume relating to the entire sampling period.

Fig 4.1 shows wind rose at San Pietro Capofiume relating to the entire sampling period.

Concentrations of IN were detected by the membrane filter technique (Bigg, 1963; Stevenson, 1968; Garland and Jiusto, 1972; Vali, 1975; Jiusto et al., 1976; Bigg, 1990; Möhler et al., 2008a).

For each sampling, PM_1, $PM_{2.5}$, PM_{10} and TSP filters were cut into four pieces, and one piece for each fraction was inserted into the same metal plate (5.5 cm diameter, 0.5 mm thick), previously covered with a smooth surface of paraffin, in order to assure good thermal contact of the filter with the supporting substrate.

Subsequently the paraffin was slightly heated and rapidly cooled in order to fill the filter pores. This allowed the simultaneous development of PM_1, $PM_{2.5}$, PM_{10} and TSP. A replica of the Langer dynamic developing chamber (Langer and Rodgers, 1975) housed in a refrigerator was used to detect and determine the concentration of aerosol particles active as IN at different supersaturations with respect to ice and water. Use of the dynamic chamber circumvents some of the problems arising with the static chamber, e.g. that the moisture supply under static conditions may be rather inadequate at a filter surface both

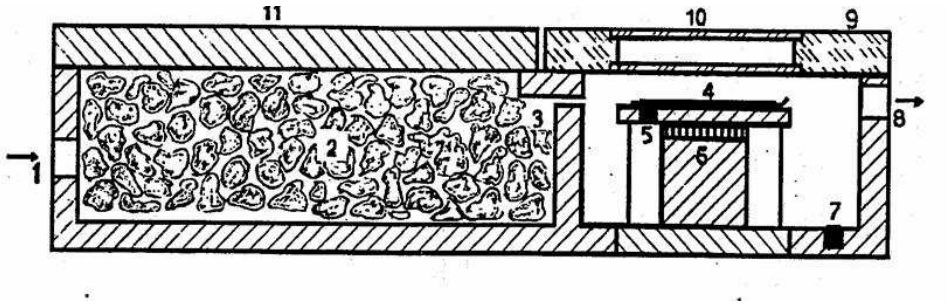

Figure 4.2: 1:Air Inlet; 2: Minced ice; 3: Slit and air temperature thermocouple"; 4: Filter; 5: Filter temperature thermocouple; 6: Peltier cooling device; 7: Thermocouple; 8: Air outlet; 9: Plexiglass cover; 10: Observation slit; 11:Aluminium plate.

in overcoming the effect of hygroscopic particles and in activating all potential ice nuclei (Bigg, 1963). Fig 4.2 shows the schematics of the chamber. Filtered air is forced by a pump to flow through the chamber in a closed loop (flow rate 150 l h^{-1}). Air enters the chamber through a perforated plate, spreads into the ice bed and becomes saturated with respect to ice, which is cooled by the base plate.

The temperature of the air is measured just in front of the nozzle (80 mm x 1 mm) aiming the air at the sample, which is placed on a top of a Peltier cooled surface coated with a small amount of Vaseline, to enhance heat transfer. The temperature of the air and of the Peltier cooled surface is measured with identical resistance temperature sensors (PT 100).

By controlling the temperatures of the filter and of the air, saturated with respect to finely minced ice and flowing continuously grazing the filter, it was possible to obtain different supersaturations S_{ice} and S_w. The supersaturations are calculated theoretically from vapour pressures of ice and water at the considered temperatures (Perry, 1963). Taking into account the accuracy of the air and sample temperature sensors, and of temperatures control system, an experimental uncertainty of about 6% for S_{ice} and S_w was estimated.

Runs were performed in order to evaluate the filter background ice nuclei, by developing blank filters at the considered temperatures and supersaturations. The average concentration was about 0.5 crystal

per filter at all considered temperatures. An average of 1 crystal per filter will be considered. The nucleation event was visually followed by counting on a monitor the number of ice crystal growing on the sampled filter, lighted with a grazing light. The minimum detectable size is about 100 μm.

The four pieces of different filters (PM_1, $PM_{2.5}$, PM_{10} and TSP) were exposed to water vapour for about half an hour at constant supersaturation. The exposition time was long enough for the IN concentration to reach the maximum at the given r.h. and temperature. Fig 4.3 shows an example of ice crystals grown on different aerosol size ranges in the diffusion chamber and an unexposed filter as a blank test, on which no ice crystal is observed.

Measurements were made also at high supersaturation (Table 5), even though the common understanding is that maximum supersaturation rarely exceeds 1% or 2% in natural clouds.

Tab.5 Operating conditions.

T_{air},°C	T_{filter}, °C	S_{ice} %	S_w,%
-15	-17	20	2
-15	-18	32	10
-17	-19	21	0

In fact, the discrepancy between the concentration of ice nuclei and ice crystals observed in clouds could be attributed to an occasional occurrence of very high supersaturations in clouds.

For instance, throughout the freezing process, the drop temperature is 20 °C, heat and water vapour are released into the surrounding air, whose temperature is lower than 0 °C, and a region of supersaturated water vapour surrounds the drop. Within this region of high supersaturation aerosol particles can act as CCN or even IN (Rosinski, 1979). Hobbs and Rangno (1990) suggested that the rapid production of ice particles in the ascending top of maritime cumulus congestus may be due to the presence of pockets of high supersaturation with respect to water. Fukuta (1993) showed that supersaturations up to 10% may be expected near cloud base due to the slower diffusional growth of droplets as predicted by the diffusion-kinetic droplet growth theory. If

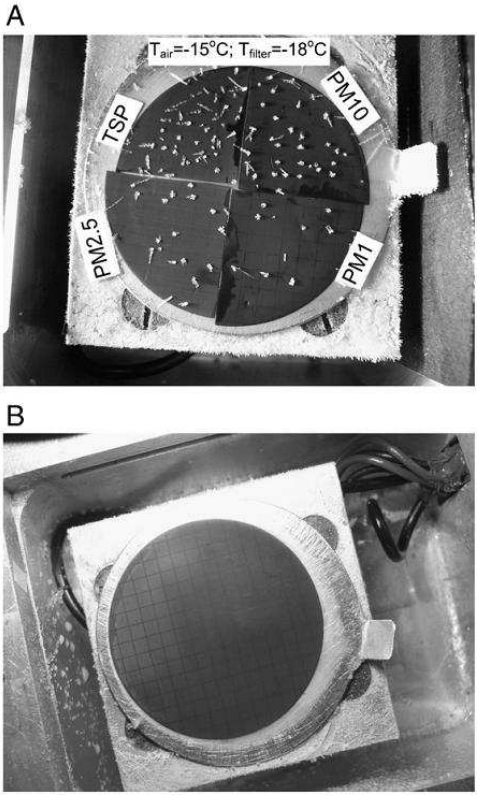

Figure 4.3: (A)Picture of ice crystals grown on different aerosol size range; (B) Blank filter developed at T_{air} = -15 °C; at T_{filter} = -18 °C

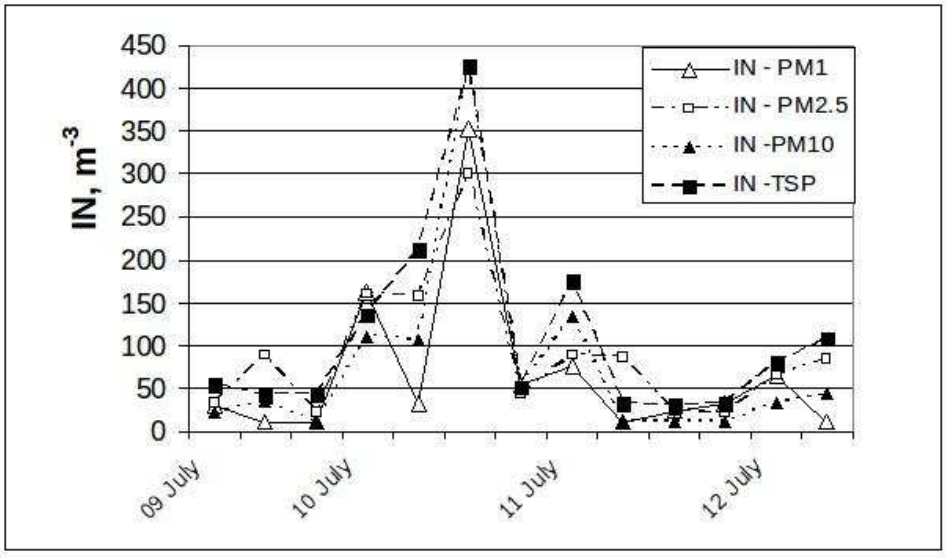

Figure 4.4: Time series of concentrations of IN ($m^{-}3$) active at T_{air} = -15 °C, T_{filter} = -17 °C.

local updrafts are created near cloud top, then pockets of high supersaturation may be a possibility. Jensen et al. (2001) measured near the tropical tropopause ice-saturation ratios ranging from 1.1 to 1.7 (i.e. supersaturations of 10-70%).

4.4.1 Results and discussion

Figs 4.4, 4.5 and 4.6 show the time series of concentrations of aerosol particles active as IN under the conditions reported in Table 5.

Measurements below water saturation should allow the detection of deposition (sorption) nuclei, while those above water saturation should allow the detection of deposition and condensation-freezing nuclei, with higher efficiency as the S_w increases. According to Rosinski (1995), the concentration of IN activated by condensation followed by freezing is very low at $S_w = 0\%$.

Table 6 shows that aerosol in the PM_1 fraction contributes about 50% of the measured ice nuclei number concentration. Since the concentration of aerosol particles in the fine fraction is much higher than in the coarse one, it can be inferred that the nucleation efficiency, i.e.

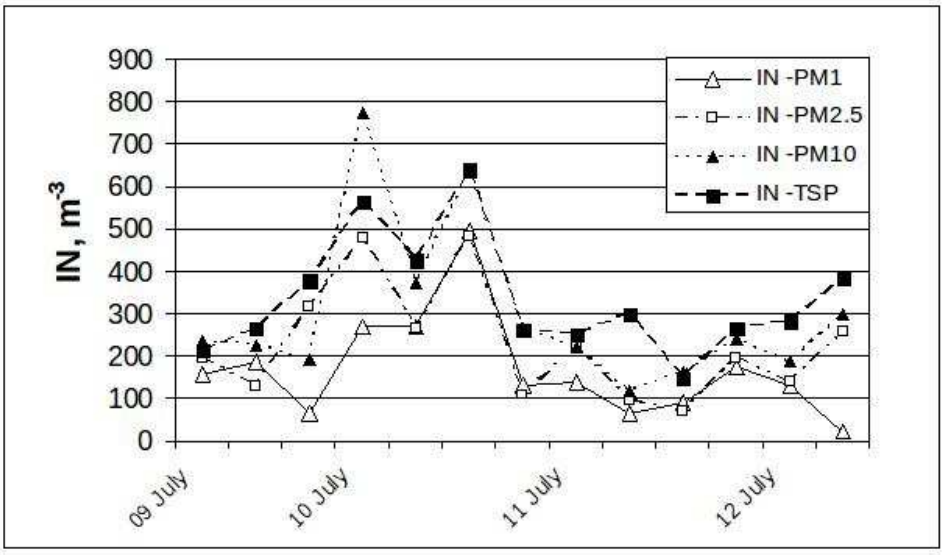

Figure 4.5: Time series of concentrations of IN (m^-3) active at T_{air} = -15 °C, T_{filter} = -18 °C.

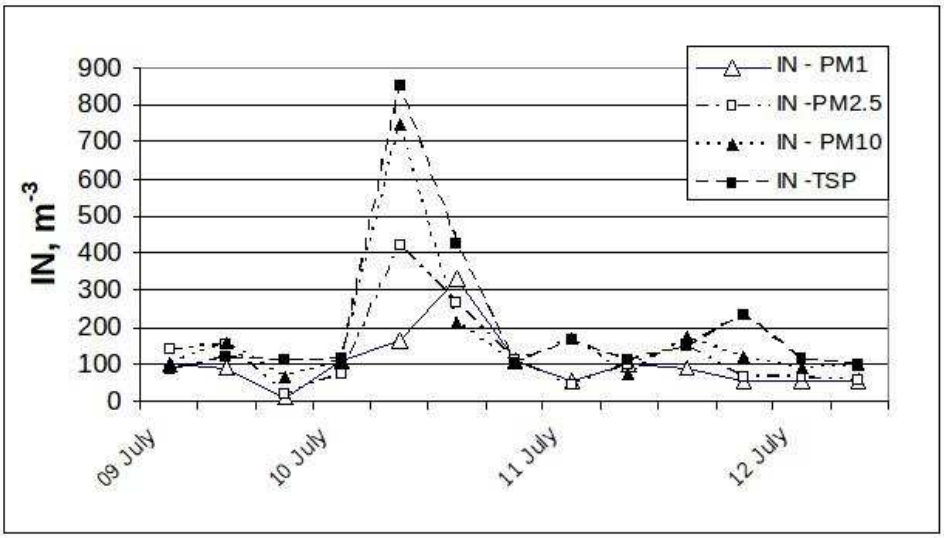

Figure 4.6: Time series of concentrations of IN (m^-3) active at T_{air} = -17 °C, T_{filter} = -19 °C.

the fraction of natural aerosol particles nucleating ice at some given temperature and supersaturation, increases with increasing particle size.

Tab. 6 Percentage of IN obtained in PM_1, $PM_{2.5}$, PM_{10} fraction with respect to IN measured in the total suspended aerosol.

	IN_{PM_1} / IN$_{TPS}$ %	IN $_{PM_{2.5}}$ / IN $_{TPS}$ %	IN $_{PM_{10}}$ / IN $_{TPS}$ %
S_{ice} = 20%; S_w = 2%	61	82	70
S_{ice} = 32%; S_w = 10%	50	67	90
S_{ice} = 21%; S_w = 0%	49	62	83

The greater ability of larger particles to act as freezing nuclei is counteracted in nature by the decrease in the aerosol particles concentration with increasing size. The average ratio between IN measured in the PM_{10} fraction and those in the TSP ranges from 70 to 90%, i.e. the dominant fraction of aerosol activated involves particles with aerodynamic diameter less than 10 μm. A positive correlation is observed between S_w and S_{ice} values and IN concentration. The average and the standard deviation (S.D.) of all measurements performed at T_{filter} = - 17 °C and T_{air} = -15 °C, i.e. S_w = 2%, S_{ice} = 20%, is (110 ± 112) m^{-3}, while for the measurements at T_{filter} = -18 °C, i.e. S_w = 10%, S_{ice} = 32%, is (337 ± 139) m^{-3}. Moreover, the average of the difference between IN concentrations at -18 °C and at -17 °C obtained from simultaneously sampling is 227 m^{-3} (S.D. = 90). As a matter of fact there is an evident increase of IN concentration with increasing S_w and S_{ice}. Fig 4.7 highlights the strong impact of S_w on the number of aerosol particles activated as IN. In Figs 4.4, 4.5 and 4.6 a sharp decrease is noted of IN concentration between samplings performed at 17-18 h (10 July) and 21-22 h. The variations in wind speed (from 1.2 to 3.2 m s^{-1}), r.h. (from 50 to 59%) and temperature (from 19 to 23 °C) are small.

Particle number concentration decreases from about 10^4 to 5 x 10^3, while particle concentration measured by Grimm (d > 0.3μm) increases from about 4000 to 7000 l^{-1}. As wind direction changes from prevalently W-NW (polluted area) to NE-E (Po river delta and Adri-

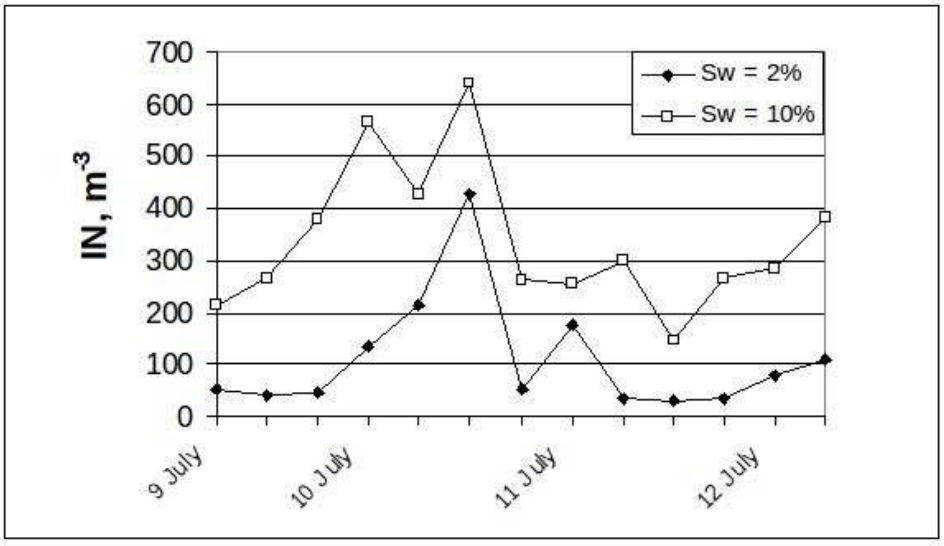

Figure 4.7: Time series of concentrations of IN (m^{-3}) active at T_{air} = -15 °C; S_w = 2% and S_w = 10%.

atic Sea), a change in the size distribution and chemical composition of the aerosol can be inferred. Prevalently, the IN concentration turns out to be higher when the wind direction is from W-NW, i.e. from urban and industrial areas, and lower when wind direction is from N-NE, i.e. from less polluted areas. This is true in all experimental conditions, even at S_{ice} = 32% S_w = 10%; S_{ice} = 21% and S_w = 0%(Fig 4.8).

In the present measurements there is no correlation between particle number measured with the optical counter and CN concentration (Fig 4.9).

Furthermore, none is found between IN measured in the different size ranges, either with the counter spectrometer (d> 0.3μm) or with the condensation nuclei counter (Fig. 5.5). The correlation coefficient was found to be 0.07, 0.34 and 0.03, respectively, by considering separately three sets of data.

It can be observed that the highest IN concentrations, measured when air masses came from West (10/07/2007), are coupled with high values of CN. No correlations between IN and CN concentrations are reported by Vychuzhanina et al. (1989) in industrial and rural areas

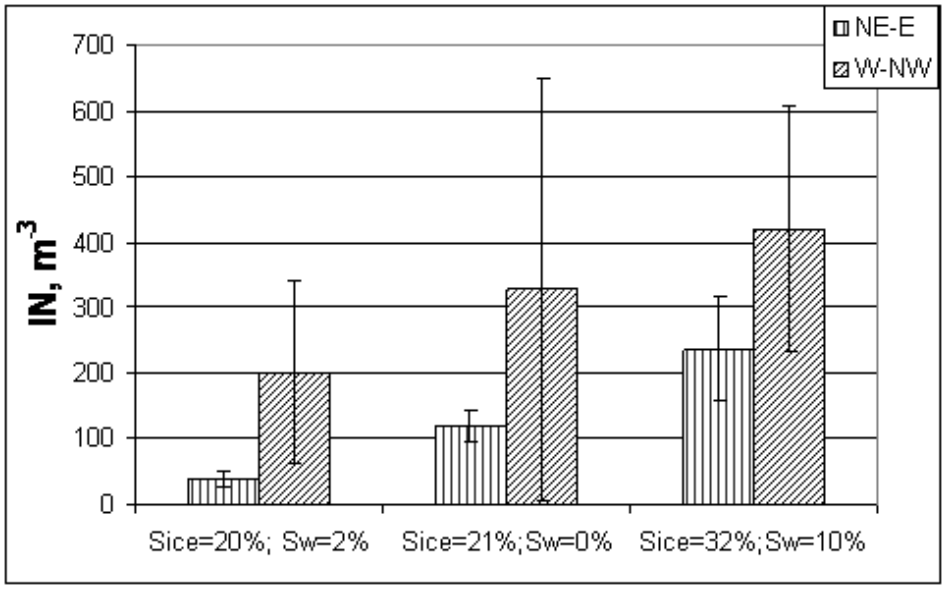

Figure 4.8: IN concentration (m^{-3}) in TSP averaged over two wind sectors.

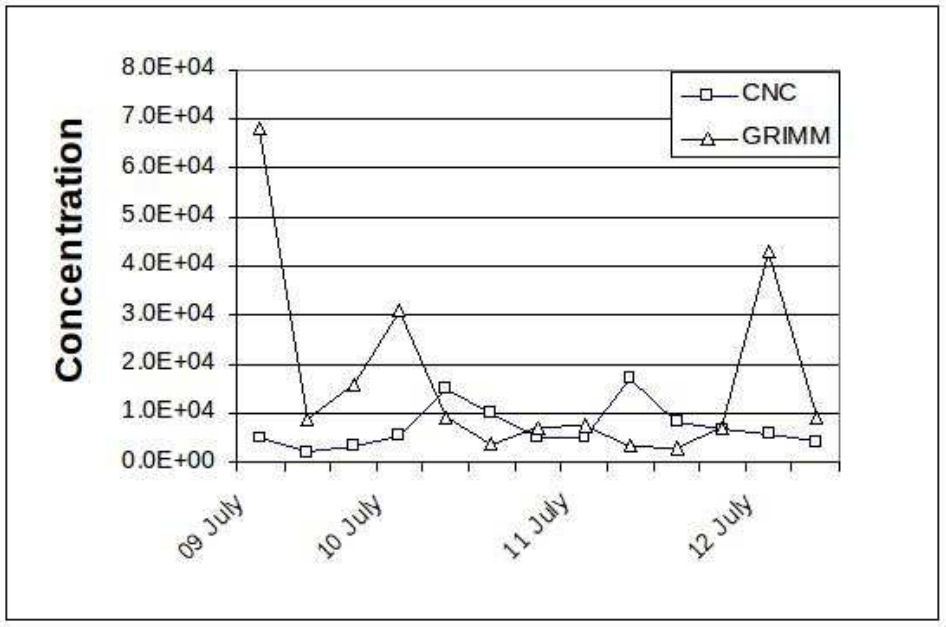

Figure 4.9: Time series of particle concentration measured with optical (l^{-1}) and CN counters (cm^{-3}).

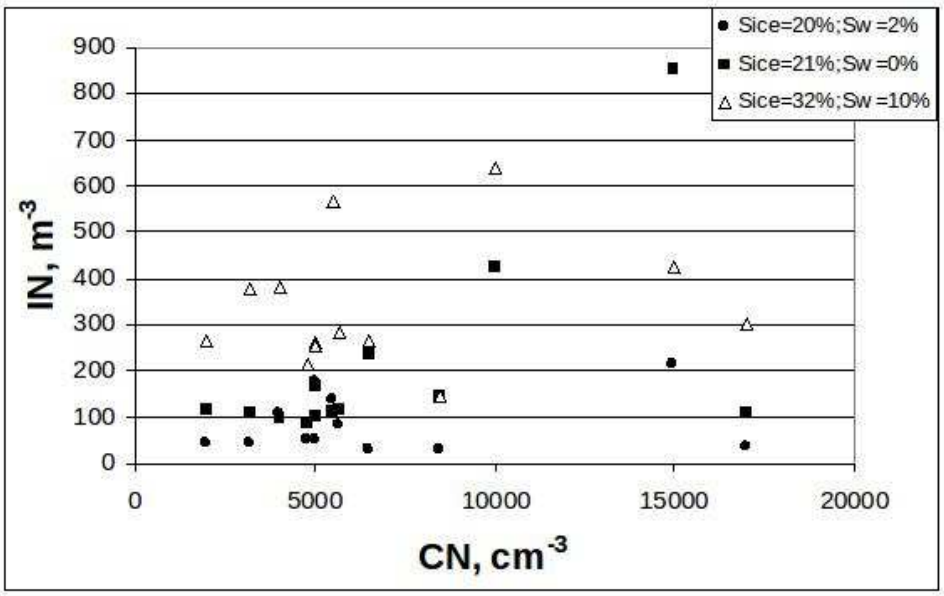

Figure 4.10: Correlation between IN (m^{-3}) in total suspended aerosol and CN concentration (cm^{-3}).

of Moldavia, Rogers et al. (1998) in background and aircraft exhausts plumes, or Klein et al. (2008) at the Taunus Observatory on Mt. Kleiner Feldberg (825 m above sea level), about 25 km north of Frankfurt/M, Germany. Richardson et al. (2007) in a campaign at Storm Peak Laboratory in Northwestern Colorado (3210 masl, April-May 2004), found a correlation between IN and aerosol concentration only when particles with d> 0.3μm and concentration higher than about 5 cm^{-3} were considered. The fraction of all particles active as IN constitutes a very small fraction of the aerosol population. In the present measurements, the ratio of IN to CN concentration, depending on T, S_{ice} and S_w, ranges from about 1:10^8 to 1:10^7. Rosinski (1979) suggests an approximate ratio of 1:10^6, and Szyrmer and Zawadzki (1997) suggest that the concentration of IN in a typical cloud (T = -10 °C) is about seven to nine orders of magnitude less than the total aerosol. A few measurements of IN at the ground level in low polluted areas are reported in the literature. Soulage (1958), and Soulage and Admirat (1962) report measurements made in several parts of Aquitaine near the ocean, at T = -15 °C using a mixing-type cloud chamber. The mean values reported are high. Near the ocean the frequency of mean

daily values of IN concentrations is 40% in the range 1-10 l^{-1}, and about 10% in the range 10-$10^2 l^{-1}$. In land (near Toulouse) 60% of the frequency is in the range 10-100 l^{-1}. Castro et al. (1998) in a rural area, far from any potential source of pollution (Leon, Spain) measured at ground level a background concentration of IN active at -15 °C, -19 °and -23 °C at water saturation, of 7, 35 and 95 l^{-1}, while Pérez et al. (1985) in Valladolid (Spain) obtained IN values in the range 0.1-300 l^{-1} at -21 °C (mean value 14 l^{-1}), much higher than those obtained in our measurements.[1].

4.5 Experimental:second campaign

The second experimental campaign was performed in the period 07-10 February 2008, at San Pietro Capofiume (SPC), a rural site located at 11 m a.s.l. (44 °39', 11 °37'W). The site is situated about 30 km northeast of the city of Bologna, in the Po Valley, which is the largest industrial, trading and agricultural area in Italy with a high population density (fig.4.11). The station is in a sparsely inhabited area open to the Adriatic Sea on the eastern side, but enclosed by densely populated areas, on its southern, western and northern sides. There are power plants and industrial areas along the Po River and close to the ports of Venice and Ravenna.

Various aerosol fractions and total suspended particles were sampled on nitrocellulose membrane (Millipore HABG04700, nominal porosity 0.45 μm) four times a day (period 06-22 h, Local Time, corresponding to 05-21 GMT), at 3 m above ground level. The mean flow rate was 38.3 lpm with a sampling time of 10 min. Aerosol fractions were sampled by inserting different sampling heads (1μm, 2.5μm, and 10μm cut-point) in front of the filter. The sampling of all the fractions lasted about 1 h. Simultaneously, measurements were also performed of condensation nuclei (aerosols d>10nm) with a butanol type instrument (CNC-TSI-3020), and of particle concentrations in different size classes starting from diameter d> 0.3μm (Optical Spectrometer Grimm, Mod.1.108). Meteorological data (air temperature, relative humidity, wind speed, pressure) were recorded and the ranges of temperature, relative humidity (r.h.) and wind speed are reported in Table

[1]A part of this Chapter is reprinted from Santachiara G., Di Matteo L., Prodi F. and Belosi F., Atmospheric particles acting as Ice Forming Nuclei in different size ranges, Atmospheric Research 96 (2010), 266-272 with permission from Elsevier

Figure 4.11: Map of Po Valley showing the observation site

7. Temperature and r.h. show a similar diurnal trend. The atmospheric pressure at surface level on sampling days was about 1040 hPa, i.e. there was a persistent high pressure, with prevalently sunny days.

Tab. 7 Details of the sampling campaign.

Date of sampling	T, °C, range	Range r.h., %	Range v, m s^{-1}
7/02/2008	5.5÷ 14	47÷ 75	1.3÷ 2.4
8/02/2008	1.1÷ 9.9	49÷ 87	1.5÷ 3.9
9/02/2008	-1.5÷ 9.1	58-87	1.9÷ 3.2
10/02/2008	-1÷7.5	62÷ 87	2.6÷ 2.8

A replica of the Langer dynamic developing chamber (Langer et al., 1975) housed in a refrigerator was used to detect and determine the concentration of aerosol particles active as IN at different supersaturations with respect to ice and water. The dynamic chamber should overcome some of the problems arising with the static chamber, e.g. the fact that the moisture supply under static conditions may be somewhat inadequate at a filter surface both in overcoming the effect of hygroscopic particles and in activating all potential ice nuclei. For each sampling of PM_1, $PM_{2.5}$, PM_{10} and TSP, filters were cut into four pieces, and one piece for each fraction was inserted into the same metal plate, which was placed on a top of a Peltier cooled surface coated with a small amount of Vaseline, to enhance the heat transfer. In

this way, different aerosol fractions could simultaneously develop. By controlling the temperatures of the filter and of the air, saturated with respect to finely minced ice and flowing continuously grazing the filter, it was possible to obtain different supersaturations S_{ice} and S_w. The nucleation event was visually followed by counting on a monitor the number of ice crystal growing on the sampled filter, lighted with a grazing light. The air and filter temperatures, and consequently supersaturation, were kept constant during each run. The four pieces of different filters (PM_1, $PM_{2.5}$, PM_{10} and TSP) were exposed to water vapour for about half an hour. The exposure time was long enough for the IN concentration to reach the maximum at the given r.h. and temperature. In fact runs performed with exposure up to 1h did not produce any additional ice crystals. Measurements were made at S_{ice} from 9.6 to 34%, and S_w from -8% to 10% (Table 4.5). Readings were made also at high supersaturation, even though the common understanding is that maximum supersaturation rarely exceeds 1% or 2% in natural clouds. In fact the discrepancy between the concentration of primary ice nuclei and ice crystals observed in clouds could depend also on an occasional occurrence of very high supersaturations in clouds (onset of droplets coalescence, droplet freezing process).

Tab. 8 Experimental conditions

T_{air}, °C	T_{filter}, °C	S_{ice}, %	S_w, %
-15	-17	20	2
-15	-18	32	10
-17	-18	9.6	-8
-17	-19	21	0
-17	-20	34	9.6

4.5.1 Results and discussion

Fig. 4.12, 4.13, 4.14 show the time series of concentrations of aerosol particles activated as IN. A prevalently uniform trend of the IN concentration was measured during the campaign, although higher values of IN were found for the TSP and PM_{10} fraction (08/02/2008; 07 h; $S_{ice} = 34\%$; $S_w = 9.6\%$). At this time the wind direction was NW and the optical counter gave the highest value measured during the campaign , i.e. 5.2 x10^3 l^{-1} in the

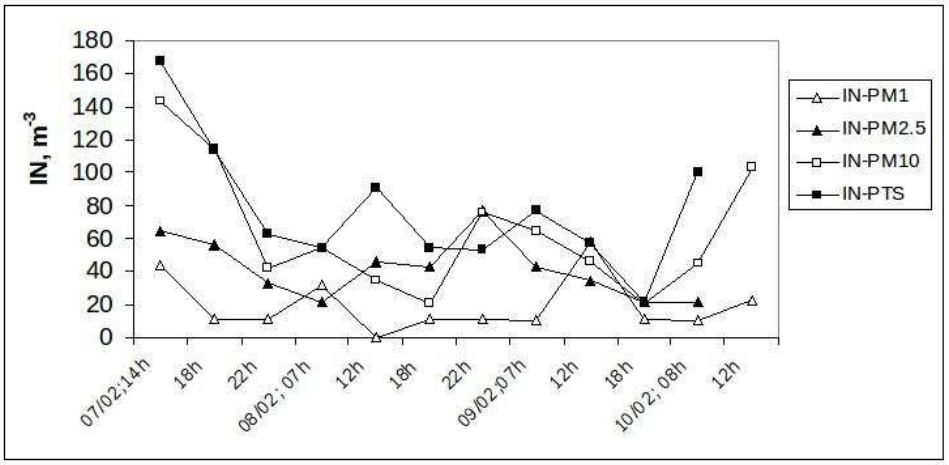

Figure 4.12: Time series of concentrations of IN (m^{-3}) active T_{air} = -15 $^{\circ}C$; T_{ice} = -17 $^{\circ}C$ (S_{ice} = 20%; S_w = 2%).

range 0.3-10 μm. Measurements made with the optical counter show that almost all particles have a diameter lower than 10 μm. The similar values of IN concentration in the PM_{10} and TSP fraction confirm the previous statement. Figure 4.15 shows the mean wind rose referring to the sampling days, showing that during experimental campaign wind was from WNW and N-NNE. No correlation can be found between IN concentration and wind direction.

Fig. 4.16 shows the mean value of IN measured at different S_{ice} and S_w. IN concentrations at S_{ice}= 32%, S_w = 10% (T_{air} = -15° C; T_{filter} = - 18° C) and at S_{ice} = 34% , S_w = 9.6% (T_{air} = -17 °C; T_{filter} = - 20 °C) (i.e. with near equal values of supersaturation), indicate that they are higher at lower temperature. Furthermore, experiments with S_{ice} = 21% , S_w = 0%, T_{filter} = -19 °C, gave IN concentrations slightly higher than the values obtained at S_{ice} = 20% , S_w = 2 % , T_{filter} = -17 °C. The IN concentrations measured at S_{ice} = 21% , S_w = 0% (T_{filter} = -1 °C) and S_{ice} = 9.6 % , S_w = -8 % (T_{filter} = -18 °C) show a small increase in IN, in spite of a strong increase in S_{ice} and S_w. Even if runs performed at S_{ice} = 9.6%; S_w = -8%, and at S_{ice} = 21%; S_w = 0%, should activate aerosol only in the deposition nucleation, while runs performed at S_w >0 could allow a condensation-freezing nucleation, the above data underscore that the aerosol temperature has a stronger impact on the activation process than S_{ice} and S_w. Rosinski and Morgan (1988), and Rosinski (1995) measured in continental air masses IN concentrations

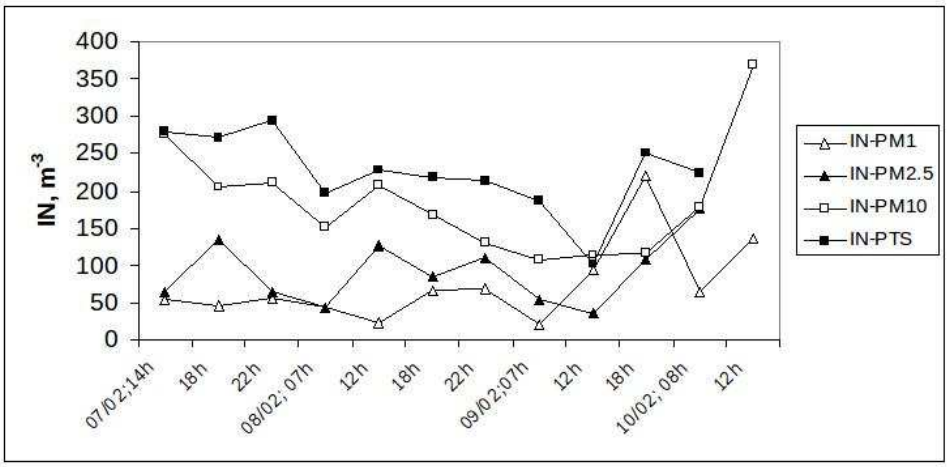

Figure 4.13: Time series of concentrations of IN (m^{-3}) active T_{air} = -15 $°C$; T_{ice} = -18 $°C$ (S_{ice} = 32%; S_w = 10%).

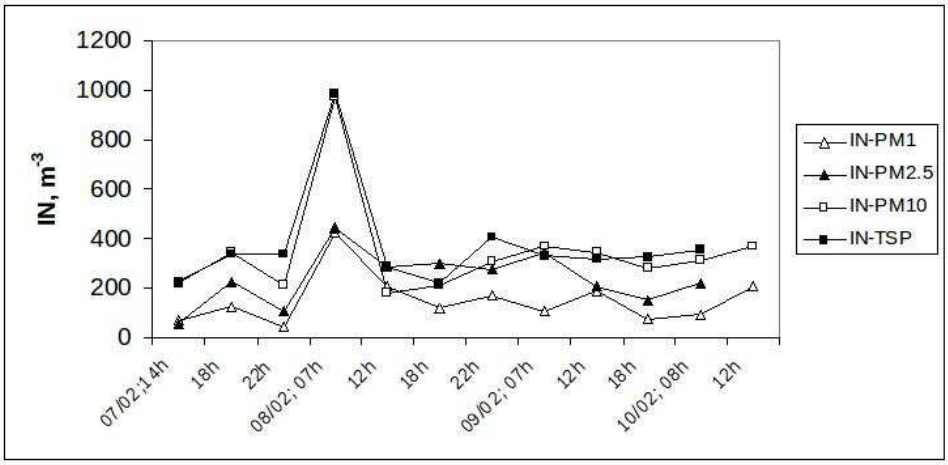

Figure 4.14: Time series of concentrations of IN (m^{-3}) active T_{air} = -17 $°C$; T_{ice} = -20 $°C$ (S_{ice} = 34%; S_w = 9.6%).

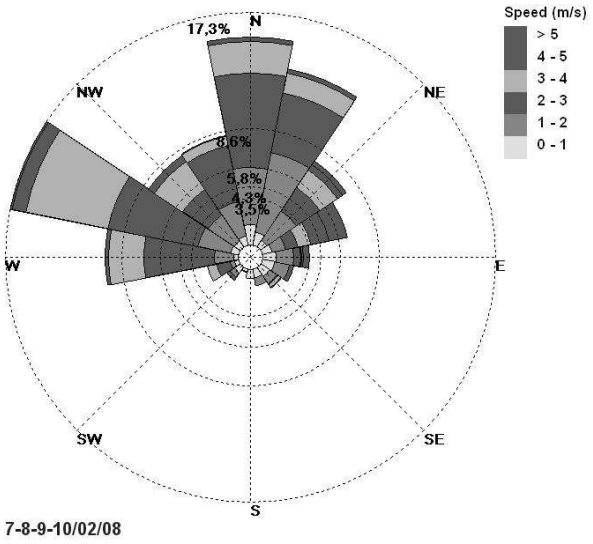

Figure 4.15: Wind rose of 7-8-9-10 February.

independent of S_w (in the range 0-6 %) at a constant temperature. Fig. 4.17 shows the concentration of active IN (m^{-3}) in the PM_{10} fraction vs. T_{filter} (T_{air} = -17 °C). The mean IN concentration is 49, 107, 341 m-3 for the three experimental temperatures of -18 °C, -19 °C and -20 °C, respectively. The results reveal an exponential dependence of IN on temperature, in agreement with Fletcher (1962). In the present measurements particle number concentrations measured with the optical counter and IN measured in the different size ranges are not correlated with number concentrations obtained with condensation counter. Such results agree with those obtained in the previous summer campaign performed of July 2007 (Santachiara et al., 2009). Fig. 4.18 shows the relationship between IN measured at T_{air} = -17 ° C, T_{filter} = -20 ° C, and aerosol particle concentration measured with the optical counter. The correlation is mainly a consequence of the IN concentration measured on 8 February, 7h (fig. 4.14); although weak, it is much higher than the one between IN and CN, thus confirming that IN are prevalently in the accumulation and coarse fraction.

No correlations between IN and CN concentrations are reported by Vychuzhanina et al. (1989) in industrial and rural areas of Moldavia, Rogers et al. (1998) in background and aircraft-affected air during SUCCESS project, and Klein et al. (2008) at the Taunus Observatory on Mt. Kleiner Feldberg (825 m above sea level), about 25 km north of Frankfurt/M, Germany.

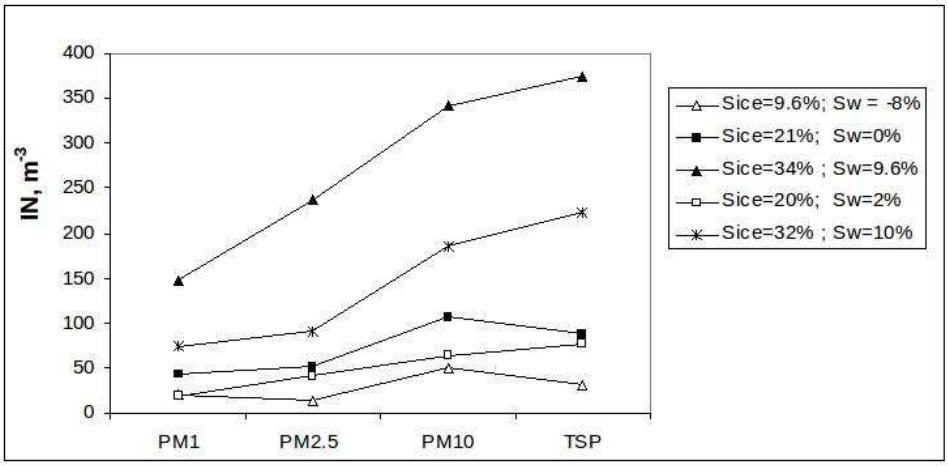

Figure 4.16: Mean value of IN concentration vs. S_{ice} and S_w

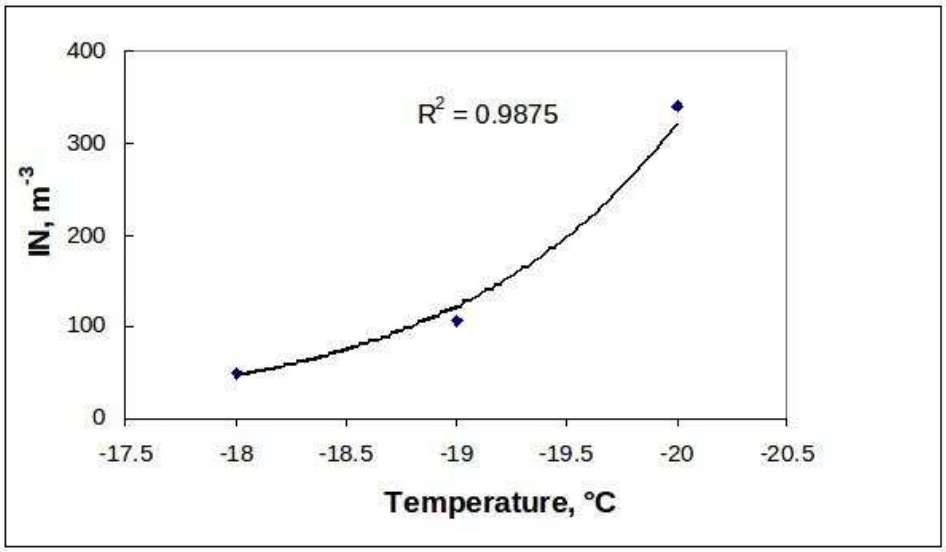

Figure 4.17: Mean concentration of IN concentration at T_{filter} = -18, -19, -20 $°C$, T_{air} = -17 $°C$ (PM_{10} fraction).

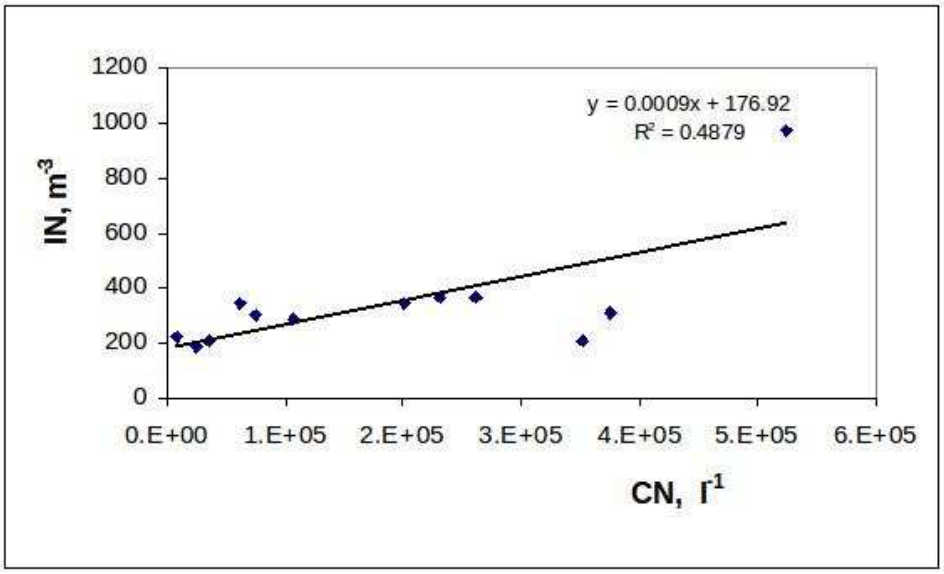

Figure 4.18: Correlation between IN concentration (m^{-3}) measured at (T_{air} = -17 ° C; T_{filter} = -20 °C) in total suspended aerosol and aerosol concentration, $d > 0.3\mu m(m^{-3})$.

Richardson et al. (2007) in a campaign at Storm Peak Laboratory in Northwestern Colorado (3210 meters a.s.l., April-May 2004), found a correlation between IN and aerosol concentration only when particles with $d > 0.3\mu m$ and concentration higher than about 5 cm^{-3} were considered. It is known that the fraction of all particles active as IN constitutes a very small part of the aerosol population. The reason for this selectivity lies in the fact that an aerosol particle must have a number of specific characteristics in order to serve as an ice forming nucleus (Pruppacher & Klett, 1997). In the present measurements the IN/CN ratio ranged between 1:5x108 and 1:2x105 (T_{air} = -15 °C; T_{filter} = -18°C). By comparing mean values of IN concentrations during summer and winter campaigns, we note that higher values were measured in the first campaign (Table 9).

Tab. 9 - IN concentrations (m^{-3}) during summer (2007) and winter campaigns (2008)

Period	T_{air} °C	T_{filter} °C	S_{ice} %	S_w %	IN_{PM1}	$IN_{PM2.5}$	IN_{PM10}	IN_{PTS}
July 07	-15	-17	20	2	67	90	77	110
	-15	-18	32	10	169	227	302	337
February 08	-15	-17	20	2	19	42	64	78
	-15	-18	32	10	74	91	186	224

A few measurements of IN at ground level in low polluted areas are reported in the literature. Soulage (1958), and Soulage and Admirat (1962) report measurements made in several parts of Aquitaine near the ocean using a mixing-type cloud chamber. The mean values reported are high. Near the ocean the frequency of mean daily values of IN concentrations is 40% in the range 1-10 L^{-1} , and about 10% in the range 10-10^2 l^{-1} (T=-15° C). In land measurements near Toulouse give 60% frequency in the range 10-100 L^{-1} (T= -21 °C). Castro et al.(1998) in a rural area distant from any potential source of pollution (Leon, Spain) measured at ground level background concentration of IN active at -15 °C, -19 °C and -23 °C at water saturation, of 7, 35 and 95 l^{-1}. Perez et al. (1985) in an urban area (Valladolid, Spain) obtained IN values in the range 0.1-300 l^{-1} at -21 °C (mean value 14 L^{-1}), much higher than those obtained in the present measurements, and no significant diurnal variations were observed. Bigg (1996), by detecting IN at temperatures of -12.5 °C, -15 °C, -17.5 °C in the high Arctic, obtained mean concentration in the range 3-13 m^{-3}.

4.6 Conclusions

The main conclusions of the first campaign are:

- The PM_1 aerosol fraction accounts for about 50% of the total measured IN for air sampled. Since the concentration of aerosol particles in the fine fraction is much higher than in the coarse one, it can be inferred that the nucleation efficiency, increases with increasing particle size. The increased ability of larger particles to act as freezing nuclei is counteracted in nature by the decrease in the aerosol particle

concentration with increasing size.

- The ratio between IN measured in the PM_{10} fraction and those in the TSP ranges from 70 to 90%, i.e. the dominant fraction of aerosol activated involves particles with aerodynamic diameter of less than 10 μm.

- A positive correlation between higher S_w and S_{ice} values and IN concentration numbers is observed. The average and standard deviation of all measurements performed at T_{filter} = -17 °C and T_{air} = -15, i.e. S_w = 2%, S_{ice} = 20%, is (110± 112) m^{-3}, while for measurements at T_{filter} = -18 °C, i.e. S_w = 10%, S_{ice} = 32%, it is (337 ± 139) m^{-3}.

- Experiments show that at S_{ice} = 21% and S_w = 0% (prevalent deposition nuclei) the average concentration is 205 m^{-3}, at S_{ice} = 20%; Sw = 2% is 110 m^{-3}, and at S_{ice} = 32%; S_w = 10% is 337 m^{-3}. There is no correlation between IN measured in the different size ranges, either with the particle number concentration measured with the counter spectrometer (d> 0.3μm). The observations about the second campaign are summarized as follows:

  A positive correlation is observed between higher supersaturation with respect to ice and water values and ice nuclei number concentration, and an exponential dependence of IN on temperature. Particle number concentrations measured with the optical counter and IN measured in different size ranges are not correlated with aerosol number concentrations obtained with a condensation counter.

- Mean IN concentration at Tair = -17 °C, and T_{filter} = -18 °C, -19 °C and -20°C, are respectively 49, 107, 341 m^{-3}. These values are lower than those measured by Soulage (1958), Soulage and Admirat (1962), and Castro et al.(1998) in low polluted and rural areas. A uniform trend is noted in the IN concentration measured during the campaign, meteorogically characterized by a high pressure. [2]

[2]Part of the data published in this Chapter has already been published in from Santachiara G., Di Matteo L., Belosi F. and Prodi F., *Atmospheric particles acting as ice forming nuclei in different size ranges and cloud condensation nuclei measurements* Il Nuovo Cimento, Vol 124 B, N. 5, pp 565-581

Chapter 5

BELOW-CLOUD SCAVENGING

5.1 Introduction

The scavenging of aerosol particles in the atmosphere by precipitation is one of the major mechanisms for maintaining a balance between the sources and sinks of the atmospheric aerosol (McGann & Jennings, 1991; Chang et al., 2003).

Wet deposition is generally split in two categories: in-cloud scavenging and below-cloud scavenging (Zhang et al., 2006).

Aerosols wet scavenging by precipitation is generally named as below-cloud scavenging. The falling raindrops collide with aerosols and collect them(Zhao et al., 2006).

The efficiency with which small aerosol particles ($r < 0.5\mu$m) collide with water drops due to simultaneous effect of Brownian, phoretic and electrical force was determined by Wang et al., 1978 (McGann B. T. & Jennings S. G., 1991).

There are several difficulties in quantifying the aerosol transfer into raindrops, because this process undergoes too many influence (e.g dry deposition and chemical reactions), so the aerosol removal by precipitations remains an open subject for the scientific community (Mircea et al., 2000). The aerosol wet removal mechanisms depends on aerosol and raindrops distribution, shape and diameter of the crystal, water content, rainfall or snow-fall intensity, environmental parameters (e.g temperature, r.h), physical and

chemical properties of aerosol.

Humidity can affect aerosol particle size distribution because the hygroscopic chemical components in aerosol, such as sulfate, nitrate and some organic matters can take up water vapor to grow in size (Yan et al., 2009).

In my Ph.D I studied indoor and outdoor $PM_{2.5}$ distribution and its removal. The primary sources of outdoor $PM_{2.5}$ are fuel combustion processes in transportation and energy production while cooking, smoking and cleaning activities contribute primarily to the indoor $PM_{2.5}$ concentrations (Martuzevicius et al., 2008). The aim of the study is to improve this topics, relating aerosol removal with r.h.

5.2 Measurement techniques

First of all it's important characterize the particulate matter; so many studies about aerosol distributions were made indoor, measuring meteorological data, first of all, relative humidity (r.h).

In studying aerosol distributions, one technique is based on the light scattering principle. Light scattering from particles is based on Mie light scattering theory.

Instruments can be classified into two classes: photometers and optical particle counters (OPC). In the first class, the instrument measures the total amount of light scattered inside the measuring chamber by the sampled aerosol. Another measurement technique is based on the detection of the light scattered by each single aerosol particle. In an OPC, aerosol is drawn through a light beam, and light flashes scattered by single particles are received by a photodetector (Santi et al., 2010).

$DUSTTRAK^{TM}$ (TSI, Inc., model 8520-hereinafter DT) is hand-held; it uses light scattering measurements to determine mass concentration in real time. The light emitted from the laser diode is scattered by particles drawn through the unit in a constant stream; the amount of light scatter determines the particle mass concentration, based on a calibration factor(Kingham et al., 2006; Liu et al., 2002).

Impaction inlets are available with 1 μm, 2.5 μm and 10 μm cuts.

The P-DustMonit unit is an instrument for measuring and registering in continuation particles present in the air; the used method is laser scattering. This method allows measuring in $\mu g/m^3$ the fine particulate concentrations

Figure 5.1: DustTrak, TSI

expressed as PM_{10}, $PM_{2.5}$, PM_1.

Studies about aerosol distributions were made outdoor during different rainy days.

Instruments that quantify rainfall can spit in instruments that count and measure individual drops, and those that don't. Instruments that count and measure drop sizes are defined as disdrometers. Instruments that don't count drops measure an average quantity proportional to the integrated volume of an ensemble of raindrops; these instruments are normally called rain gauges.(Michaelides et al., 2009)

The Pludix is a rain-gauge/disdrometer based on the analysis of an X-band continuous wave radar signal backscattered by hydrometeors (Caracciolo et al.,, 2006). It provides hydrometeor size distribution and precipitation type identification (rain, snow, hail, drizzle); they both play an important role in aerosol wet removal mechanisms.

5.3 Experimental: indoor measurements

The measurements were performed from 18/02/10 to 22/02/10 at the CNR research area of Bologna, which can be considered an urban background site.

The DustTrak was positioned in the laboratory and was used to measure $PM_{2.5}$ aerosol fractions during day and night. The aim of this experiment was to obtain a typical indoor distribution of $PM_{2.5}$. During this first ex-

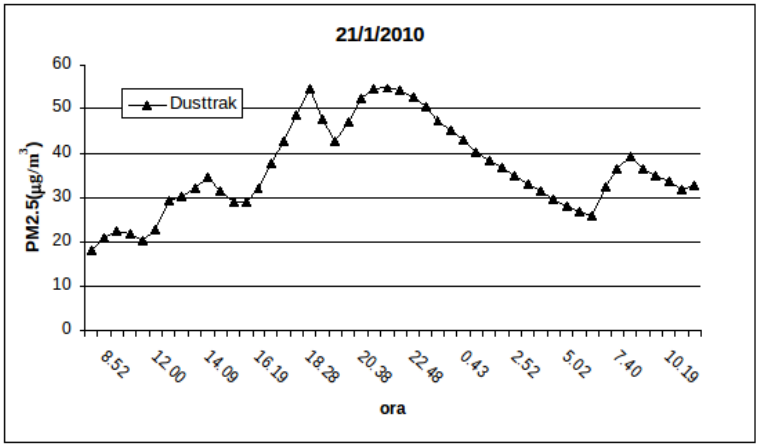

Figure 5.2: Measurements of $PM_{2.5}$ indoor

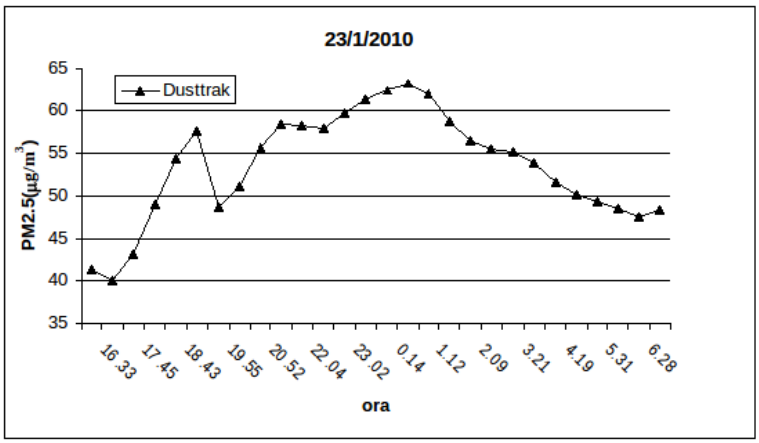

Figure 5.3: Measurements of $PM_{2.5}$ indoor

perimental campaign relative humidity was not measured. Fig 5.2 and fig 5.3shows the concentration of $PM_{2.5}$ ($\mu g/m^3$) during the day. The measurements reveal a diurnal trend with lower values at about midday and higher ones during the night. The observed trend appears to be related to relative humidity. In fact, as the air cools during the night, the relative humidity increase. The $PM_{2.5}$ concentrations measured during the day are comparable to those found by others (Martuzevicius et al., 2008).

Then, another campaign was performed using simultaneously DustTtrak and DustMonitor (March 2010). The gravimetric measurements was performed by means of manual sampling line equipped with a standard inlet

(Zambelli) and by a vacuum pump (Tecora, Bravo H-Plus) operating at a constant flow-rate of 2.3 m^3/h (Mean value 34 $\mu g/m^3$. During this campaign r.h was monitored. Table 10 shows the details of the campaign.

Time	DT ($\mu g/m^3$)	DustMonit ($\mu g/m^3$)	h.r (%)
16	35.6	32.8	37.2
17	39.5	35.7	43.2
18	38.1	34.8	49.9
19	36	39.8	52.8
20	42.2	42.9	58.3
21	47.0	45.4	67.6
22	69.6	54.5	78.3
23	91.8	59.9	83.4
0	112.6	65.5	86.7
1	139.7	72.1	90.0
2	161.8	80.5	91.8
3	174.7	110.4	93.0
4	154.1	97.0	92.8
5	129.3	59.8	89.7
6	102.5	37.3	81.8
7	77.0	37.3	67.4
8	119.1	72.4	62.5

Tab. 10 Details of the campaign

It is possible to see that concentration is high for both instruments from 23 p.m to 6 a.m when r.h is $> 80\%$. Fig 5.4 show a good correlation between concentration and r.h.(R^2=0.82); in particular fig. 5.5 show that this correlation is very high when r.h is $> 80\%$ (R^2=0.93). Values recorded by DustMonit show an increase for particles with diameters 350-450 nm and then for particles with diameters 650 nm.

5.4 Experimental: outdoor measurements

Measurements were made outdoor using the DustTrak in different meteorological conditions. These measurements were performed in Turin from May to September 2010 using DustTrak for $PM_{2.5}$ and Pludix for precip-

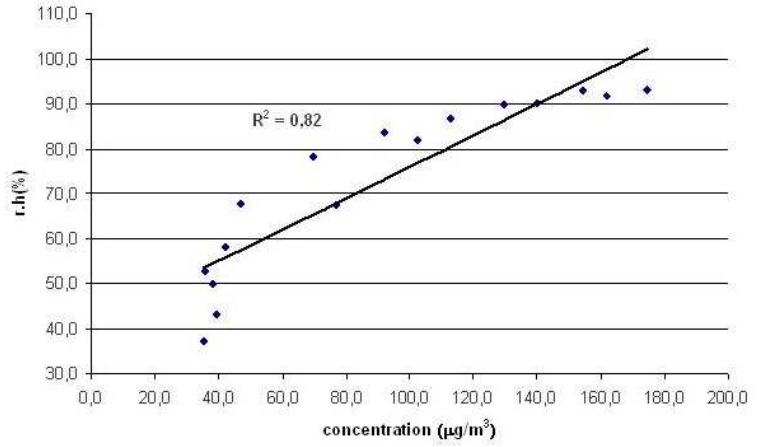

Figure 5.4: Scatter plot between r.h and concentration

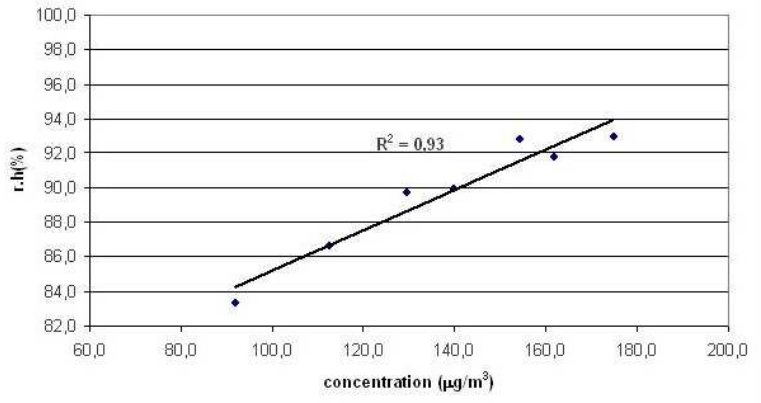

Figure 5.5: Scatter plot between r.h and concentration (r.h > 80%)

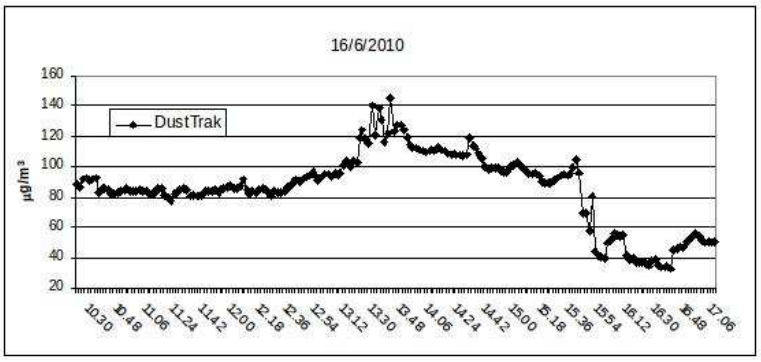

Figure 5.6: $PM_{2.5}$ concentration(June 16, 2010)

itations (also recorded in a station near the University). Moreover, data of r.h are available. During rainfall $PM_{2.5}$ concentration decreases. Fig. 5.6 highlights that $PM2.5$ concentration has high value (140 $\mu g/m^3$) before the rainfall; at the end of the rainfall the value is 70 μg/ m^3. The rainfall during this day was intense and prolonged (about 3 hours). Values of r.h remain high for one hour after the rainfall event and then these values begin to decrease. The rainfall mainly removes coarse particles, that are few but important for mass concentration ($PM_{2.5}$ is about 60% of PM_{10}). It can be hypothesized that the increase in the relative humidity has lead to hygroscopic growth of particles, facilitating gravitational settling. $PM2.5$ concentration remains low even after the rainfall. A similar trend was found by Casazza & Piano (2003), even if the decrease in r.h is faster. Fig 5.7 shows the spectrum of precipitation.

Fig. 5.8 shows that during 20 June 2010, the rainfall was short and the $PM_{2.5}$ concentration remain high; r.h presents lower values and drops quickly, due to meteorological conditions. Fig 5.9 shows the spectrum of precipitation.

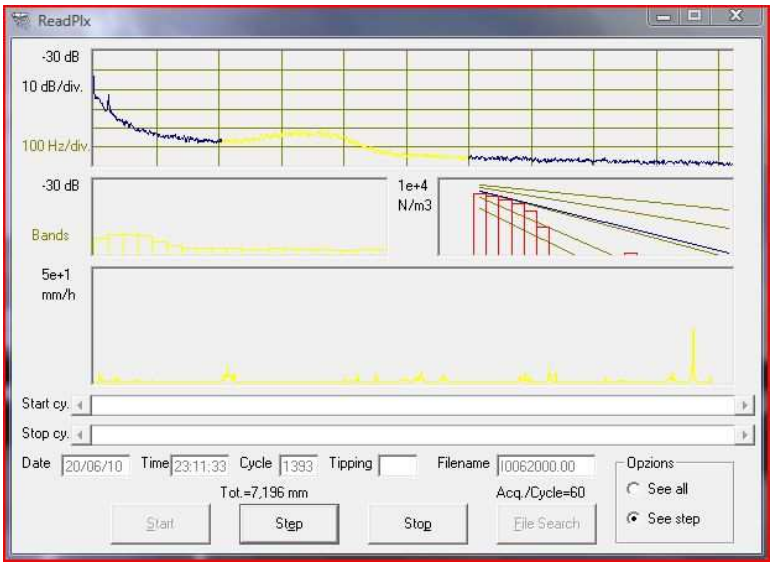

Figure 5.7: Output of Pludix (June 20, 2010)

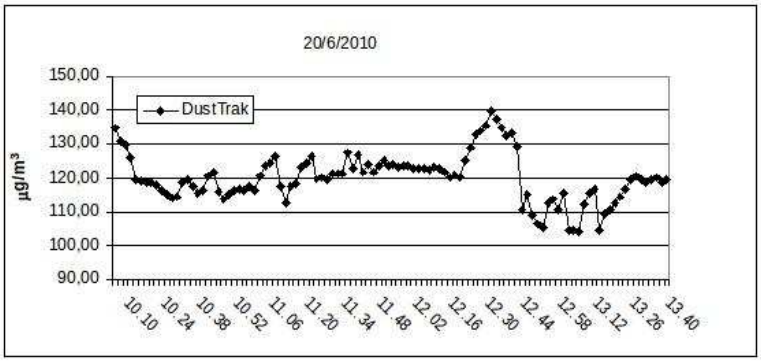

Figure 5.8: $PM_{2.5}$ concentration (June 20, 2010)

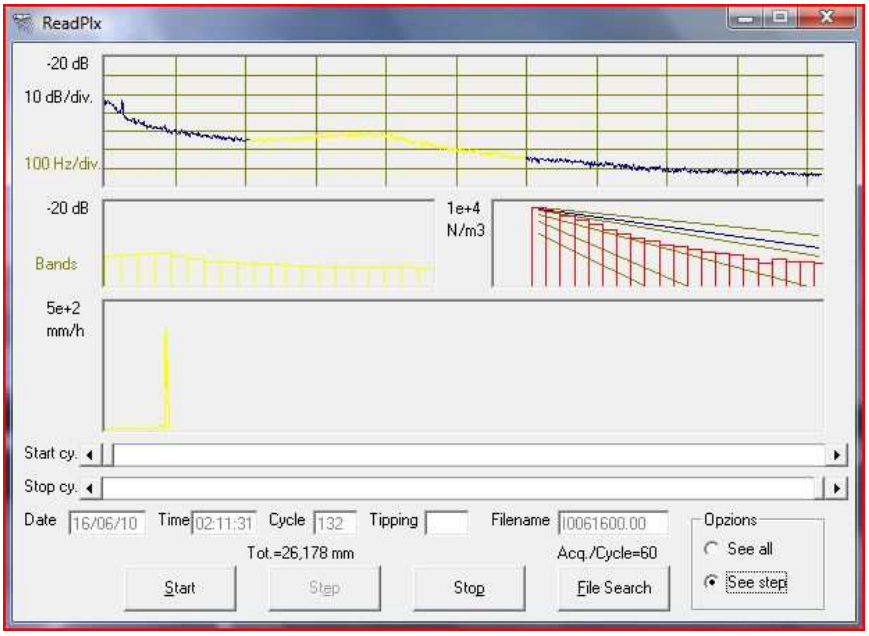

Figure 5.9: Output of Pludix (June 16, 2010)

5.5 Conclusions

It is well known that rain removes particulate. But the aerosol wet removal system is very complex because wet scavenging process is influenced by many factors: aerosol size distribution, raindrop size distribution, rainfall intensity, water content, physical and chemical properties of aerosol and raindrops and meteorological parameters (e.g., relative humidity).

The difficulty for the description of aerosols wet scavenging lies in that the process of aerosols wet scavenging is related to not only aerosol size distribution (ASD) but also raindrop size distribution (RSD). The hypothesis that links change in size distributions with variations in relative humidity seems to be confirmed. Indeed the removal seems to be linked with this parameter.

It appears that it is important to characterize both the size distribution and the chemical nature because the particle hygroscopicity depends on this parameter. Obviously it is important also characterize raindrop size distribution.

The Pludix provides hydrometeor size distribution and precipitation type identification (rain, snow, hail, drizzle); they both play an important role

in aerosol wet removal mechanisms; for such purpose Pludix seems to be an excellent instrument.

CONCLUSIONS

Aerosol has impact on human health, on visibility, and direct and indirect effects on climate. In this context, the aerosol removal has a fundamental role, also because some of the scavenging processes are closely linked to the indirect effects of aerosol on climate (aerosol acts as condensation center for cloud droplets and ice crystals changing cloud properties). The overall role of aerosol and clouds is also a critical factor for climate models, only means available to obtain the possible future scenarios with a certain reliability.

In this thesis, different removal processes of aerosol have been studied experimentally with the aim to obtain a global study of these processes.

Studies about thermophoresis in microgravity conditions, thus making convective motions negligible, allowed to study phoretic forces, that play a crucial role in particles removal in clouds. The aim of the experiments presented here was to evaluate the influence of the physical parameters of different gases on the thermophoretic velocity and thermophoretic force of aerosol particles.

The main goal was to obtain thermophoretic velocities in microgravity conditions for gases with different thermal conductivities because such experiments were never done before. The experiments show that the thermophoretic velocity decreases from helium to nitrogen, argon, and xenon. Some test regarding *diffusiophoresis* (not reported in this thesis because they are incomplete) were carried out; at present there are few studies on this topic. A competition between thermo and diffusiophoresis exists in the scavenging of atmospheric aerosol during growing or evaporating processes of ice crystals and droplets; then it would be important to test simultaneously these processes in order to obtain clarity.

Studies on formation of IN and CCN permitted to improve knowledge about these phenomena.

Concerning the importance of surface CCN measurements, the substitution of surface CCN for airborne measurements would secure the advantage of cost reduction and the possibility of continuous measurements, which could lead to a complete climatology. From surface measurements of CCN concentration and others parameters, it is possible to retrieve the vertical profile of CCN (if the aerosol composition and size distribution below cloud are uniform). Measurements related to CCN, reveal diurnal trend with lower values at about midday and higher ones during the night. The observed CCN trend appears to be weakly related to anthropogenic activity and excludes the hypothesis of CCN originating from photochemical nucleation processes, as this would cause a maximum to appear in the early afternoon. The sharp decrease in concentration around midday is partly due to surface heating, and to an increase in wind speed, which promotes convection and the transport of aerosol to higher levels in the atmosphere.

Few measurements of IN at the ground level in low polluted areas are reported in the literature. It was found that the fraction of all particles active as IN constitutes a very small fraction of the aerosol population. A positive correlation is observed between higher supersaturation with respect to ice and water values and ice nuclei number concentration, and an exponential dependence of IN on temperature. Measurements were made also at high supersaturation, even though the common understanding is that maximum supersaturation rarely exceeds 1% or 2% in natural clouds, because the discrepancy between the concentration of IN and ice crystals observed in clouds could be attributed to an occasional occurrence of high supersaturations in clouds.

Even though, the amount of new information acquired in the course of this study, spread some light on processes, which still maintain an evident grade of uncertainty.

As far as the studies concerning impaction are concerned, it remains to establish the role of r.h. and the correlations with different types of precipitations (For instance,the period under review does not include snow and aerosol wet removal also depends on shape and diameter of the crystal). Moreover, aerosol wet removal mechanisms is also related on aerosol and raindrops environmental parameters, physical and chemical properties of aerosol. In order to obtain more exhaustive results, it would be proper to carry out further experimental campaigns.

Bibliography

[1] Allen, M. D., & Raabe, O. G. (1982). *Re-evaluation of Millikan's oil drop data for the motion of small particles in air.* Journal of Aerosol Science, 13, 537-547.

[2] Al-Naimi, R., Saunders, C.P.R., 1985. *Measurements of natural deposition and condensation-freezing ice nuclei with a continuous flow chamber.* Atmospheric Environment 19, 1871-1882.

[3] Alofs D. J. and Liu T.H., J. Atmos. Sci., 38 (1981) 2772.

[4] Andreae M. O. and Rosenfeld D., Earth-Science Reviews, 89 (2008) 13.

[5] Ardon, K., Levin, Z., Ganor, E., Klein, H., Bingemer, H., 2008. *The effect of air pollution on nuclei concentration in Israel. 14th International Confer ence on Clouds and Precipitation*, Cancun, 7-11 July.

[6] Arimoto R., *Eolian dust and climate: relationship to sources, tropospheric chemistry, transport and deposition* Earth-Sciences Review 54 (2001) 29-42

[7] Baumgardner D., Raga G. B. and Muhlia A., Atmos. Environ., 38 (2004) 357.

[8] Beresnev, S., Chernyak, V., & Fomyagin, G. A. (1990). *Motion of spherical particle in a rarefied gas. Part 2. Drag and thermal polarization.* Journal of Fluid Mechanics, 219, 405-421.

[9] Beresnev, S., & Chernyak, V. (1995). *Thermophoresis of a spherical particle in a rarefied gas: Numerical analysis based on the model kinetic equations.* Physics of Fluids, 7, 1743-1756.

[10] Bhatnagar, P. L., Gross, E. P., & Krook, M. (1954). *A model of collision process in gases.* Physical Review, 94, 511-525.

[11] Bigg, E.K., 1963. *The measurements of ice nucleus concentrations by means of Millipore filters.* Journal of Applied Meteorology 2, 226-269.

[12] Bigg, E.K., 1990. *Measurement of concentrations of natural ice nuclei.* Atmospheric Research 25, 397-408.

[13] Bigg, E.K., Stevenson, C.M., 1970. *Comparison of concentrations of ice nuclei in different parts of the world.* Journal Recherches Atmosphériques 4, 41-58.

[14] Bigg E. K., Tellus, 48B (1996) 223.

[15] Borbèly-Kiss et al., *Saharan dust episodes in Hungarian aerosol: elemental signatures and transport trajectories* Aerosol Science 35 (2004) 1205-1224

[16] Braham Jr., R.R., Spyers-Duran, P., 1974. *Ice nucleus measurements in an urban atmospheres.* Journal of Applied Meteorology 13, 940-945.

[17] Bretchel F. J., Flagan R. C. and Seinfeld J. H., J. Geophys. Res., 111 (2006) D05S11, doi:10.1029/2004JD005695.

[18] Brock, J. R. (1962). *On the theory of thermal forces acting on aerosol particles.* Journal of Colloid Science, 17, 768-780.

[19] Cameron J. H and Goerg-Wood, 1999 *Role of thermophoresis in the deposition of fume particles resulting from the combustion of high inorganic containing fuels with reference to kraft black liquor* Fuel Processing Technology 60 (1999) 49-68.

[20] Caracciolo C., Prodi F., and Uijlenhoet R., *Comparison between Pludix and impact/optical disdrometers during rainfall measurements campaigns* Atmospheric Research 82 (2006) 137-163.

[21] Casazza M., and Piano A., *Some remarks on* $PM_{2.5}$ Annals of Geophysics, Vol. 46, N. 2, April 2003.

[22] Castro, A., Marcos, J.L., Dessens, J., SÃ¡nchez, J.L., Fraile, R., 1998. *Concentration of ice nuclei in continental and maritime air masses in León (Spain).* Atmospheric Research 47-48, 155-167.

[23] Chang H. Jung et al., 2003 *A moment model for simulating raindrop scavenging of aerosols* Aerosol Science 34 (2003) 1217-1233

[24] Chang, R.Y.W., Liu P. S. K., Leaitch W.R. and Abbatt J. P. D., Atmos. Environ., 41, (2007) 8172.

[25] Charlson R. J., Lovelock J. E., Andreae M. O. and Warren S. G., Nature 326 (1987) 655.

[26] Chen, X., & Xu, D.Y. (2002). *Thermophoresis of a near-wall particle at great Knudsen number.* Aerosol Science and Technology, 36, 39-47.

[27] Curtius J., et al., *Observations of meteoric material and implications for aerosol nucleation in the winter Arctic lower stratosphere derived from in situ particle measurements* Atmos. Chem. Phys. 5 (2005) 3053-3069.

[28] Curtius J., *Nucleation of atmospheric aerosol particles*, C. R. Physique 7 (2006) 1027-1045.

[29] Cziczo, D.J., Murphy, D.M., Hudson, P.K., Thomson, D.S., 2004. *Single particle measurements of the chemical composition of cirrus ice residue during CRYSTAL-FACE.* Journal Geophysical Research 109, D04201. doi:10.1029/ 2003JD004032.

[30] Czys, R.R., 1977. *University of Chicago measurements of ice-forming nuclei from Metromex.* Preprints. Sixth Conference on in-advertent and Planned Weather Modification, Champaign-Urbana, IL, American Meteorology Society, 29-32.

[31] De Felice T.P., Atmos. Res., 41 (1996) 229.

[32] DeMott, P.J., Sassen, K., Poellot, M.R., Baumgardner, D., Rogers, D.C., Brooks, S.D., Prenni, A.J., Kreidenweis, S.M., 2003. *African dust aerosols as atmospheric ice nuclei.* Geophysical Research Letters 30, 1732. doi:10.1029/ 2003GL017410.

[33] DeMott, P.J., Prenni, A.J., Kreidenweis, S.M., Twohy, C.H., Rogers, D.C., 2006. *Ice nuclei variability and ice formation in mixed-phase clouds.* Sixteenth ARM Science Team Meeting Proceedings, Albuquerque, NM, March 27-31.

[34] Dressler, R. F. (1981). *Transient thermal convection during orbital spaceflight*. Journal of Crystal Growth, 53, 523-533.

[35] Dubois, F., Joannes, L., & Legros, J. C. (1999). *Improved three-dimensional imaging with digital holography microscope using a partial spatial coherent source*. Applied Optics, 38, 7085-7094.

[36] Dwyer, H. A. (1967). *Thirteen-moment theory of the thermal force on a spherical particle*. Physics of Fluids, 10, 976-984.

[37] Fletcher N. H. (1962), Phisics of rain and clouds, Cambridge University Press, London.

[38] Fuentes E. et al., *Laboratory generated primary marine aerosol via bubble-bursting and atomization* Atmos. Meas. Tech., 3, 141-162, 2010.

[39] Fukuta, N., 1993. *Water supersaturation in convective clouds*. Atmospheric Research 30, 105-126.

[40] Furutani H., Dall'Osto M., Roberts G. C. and Prather K. A., Atmos. Environ., 42 (2008) 3130.

[41] Garland, G.G., Jiusto, J.E., 1972. Numerical estimates of humidity in a membrane-filter ice nucleus chamber. Journal of Applied Meteorology 11, 674-683.

[42] Gras J. L. Atmos. Res., 35 (1995) 233.

[43] Gray, D.E. (Ed.). (1972). *American Institute of Physics Handbook (3rd ed.)*. New York: McGraw-Hill.

[44] Hagen L. J. et al., 2010 *Estimating the saltation and suspension components from field wind erosion* Aeolian Research 1 (2010), 147-153.

[45] Hegg D. A., Radke L F.and Hobbs P. V., J. Geophys. Res., 96 (1991) D(10), 18,727.

[46] Herrera J. R. and Castro J. J., , J. Appl. Meteorol., 27 (1988) 1189.

[47] Hitzenberger R., Berner A., Giebl H., Kromp R., Larson S. M., Rouc A., Koch A., Marischka S. and Puxbaum H., Atmos. Environ., 33 (1999) 2647.

[48] Hobbs P. V., Bowdle D. A.and Radke L. F., J. Clim. Appl. Meterol., 24 (1985) 1344.

[49] Hobbs, P.V., Locatelli, J.D., 1970. *Ice nucleus measurements at three sites in western Washington.* Journal of the Atmospheric Sciences 27, 90-100.

[50] Hobbs, P.V., Rangno, A.L., 1990. *Rapid development of high ice particles concentrations in small polar maritime cumuliform clouds.* Journal of the Atmospheric Sciences 47, 2710-2722.

[51] Horvath H; Metzig G., Preining O., and Pueschel R. F., *Observation of a blue sun over New Mexico U. S.A., on 19 April 1991* Atmospheric Environment Vol 28, No4, pp 621-630, 1994

[52] Hudson J. G. and Frisbie P. R., Atmos. Environ., 25A (1991) 2285.

[53] Ian M. Kennedy *The health effects of combustion-generated aerosols* Proceedings of the Combustion Institute 31 (2007) 2757-2770

[54] IPCC (2007). Intergovernmental panel on climate change. *Aerosols, their Direct and Indirect Effects* Cambridge: Cambridge University Press.

[55] Ishizaka Y. and Adhikari M., J. Geoph. Res., 108 (2003) (D4), 4138, doi:10.1029/2002JD002085

[56] Ivchenko, L. N., & Yalamov, Yu. I. (1971). *The hydrodynamical method for the thermophoretic velocity of moderate large non-volatile particles.* Russian Journal of Physical Chemistry, 45, 317.

[57] Jacobsen, S., & Brock, J. R. (1965). *The thermal force on spherical sodium chloride aerosols.* Journal of Colloid Science, 20, 544-554.

[58] Jaenicke R., *Tropospheric aerosols, in: P.V. Hobbs (Ed.), Aerosol-Cloud-Climate Interactions*, Academic Press, San Diego, CA, 1993, pp. 1-31.

[59] Jennings S.G., Geever M. and O'Connor T. C., Atmos. Res., 46 (1998) 243.

[60] Jensen, E.J., Toon, O.B., Vay, S.A., Ovarlez, J., May, R., Bui, T.P., Twohy, C.H., Gandrud, B.W., Pueschel, R.F., Schumann, U., 2001. *Prevalence of ice-supersaturated regions in the upper troposphere: implications for optically thin ice cloud formation.* Journal of Geophysical Research 106,17253-17266.

[61] Jiusto, J.E., Lala, G.G., Zamurs, J., 1976. *Filter measurements of ice nuclei concentrations and selected comparisons.* International Conference on Cloud Physics, Boulder, Colorado. July 26-30.

[62] Katz J. L.and Mirabel P., J. Atmos. Sci., 32 (1975) 646.

[63] Keng, E. Y. H., & Orr, C., Jr. (1966). *Thermal precipitation and particle conductivity.* Journal of Colloid Interface Science, 22, 107-116.

[64] Kennard, E. H. (1938). *Kinetic theory* (pp. 311-327). New York: McGraw-Hill.

[65] Kingham, S., et al., *Winter comparison of TEOM, MiniVol and DustTrak PM_{10} monitors in a woodsmoke environment* Atmospheric Environment 40 (2006) 338-347.

[66] Klein, H., Bundke, U., Nillius, B., Schütz, L., Wetter, T., Bingemer, H., 2008. *The variability of ice nucleating aerosols over Central Europe.* 15th International Conference on Clouds and Precipitation, Cancun, July 7-13.

[67] Kousaka, Y., Endo, Y., 1993 *Experiments on diffusiophoresis of aerosol particles at low Knudsen number* J. Aerosol Sci. 24, 611-617.

[68] umar A. et al, *Mineral and anthropogenic aerosol in Arabian Sea-atmospheric boundary layer: Sources and spatial variability* Atmospheric Environment 42 (2008) 5169-5181.

[69] Kuwata M., Miyazaki Y., Komazaki Y., Kondo Y., Kim J. H. and Yum S. S., *Nucleation and atmospheric aerosols*, 17th Intn. Conf., Galway, Ireland 2007, C.D. ÓDowd and P.Wagner Editors.

[70] Lala G. G. and Jiusto J. E., J. Appl. Meteorol., 16 (1977) 413.

[71] Langer, G., Rodgers, J., 1975. *An experimental study of ice nuclei on membrane filters and other substrata*. Journal of Applied Meteorology 14, 560-571.

[72] Law, W. R. (1986). *Motion of a sphere in a rarefied gas: drag and thermophoresis*. Ph.D. thesis, University of Missouri, Columbia.

[73] Leck, C., and Bigg, E. K. (2005a). *Biogenic particles in the surface microlayer and overlaying atmosphere in the central Artic Ocean during summer*. Tellus, 57B, 305-316.

[74] Leck, C., and Bigg, E. K. (2005b). *Evolution of the marine aerosol-a new perspective*. Geophysical Research Letters, 32, L19803.

[75] Levin, Z., Cotton, W.R., 2007. *Aerosol pollution impact on precipitation: a scientific review*. The WMO/IUGG International Aerosol Precipitation Science Assessment Group (IAPSAG). InWorld Meteorological Organization, Geneva.

[76] Levin, Z., Teller, A., Ganor, E., Yin, Y., 2005. *On the interactions of mineral dust, sea salt particles and clouds-a measurement and modelling study from the MEIDEX campaign*. Journal of Geophysical Research 110, D20202. doi:10.1029/2005JD005810.

[77] Li, W., & Davis, E. J. (1995). *The effects of gas and particle properties on thermophoresis*. Journal of Aerosol Science, 26, 1085-1099.

[78] Liu, L.J.S. et al., 2002 *Comparison of light scattering devices and impactors for particulate measurements in indoor, outdoor, and personal environments* Environmental Science & Technology 36, 2977-2986.

[79] Lohmann, U. and Feichter, J.: 2005, *Global indirect aerosol effects: A review*, Atmos. Chem. Phys. 5, 715-737.

[80] Loyalka, S. K. (1968). *Momentum and temperature slip-coefficient with arbitrary accommodation at the surface*. Journal of Chemical Physics, 48, 5432-5436.

[81] Loyalka, S. K. (1992). *Thermophoretic force on a single particle-I. Numerical solution of the linearized Boltzmann equation*. Journal of Aerosol Science, 23, 291-300.

[82] Loyalka, S. K., & Ferziger, J. H. (1967). *Model dependence of the slip coefficient*. Physics of Fluids, 10, 1833-1839.

[83] Malm, W. C., Pitchford, M.L., 1997. *Comparison of calculated sulfate scattering efficiences as estimated from size resolved particle measurements at three national locations*, Atmospheric Environment 31, 1315-1325

[84] Martuzevicius D., et al., *Traffic-related $PM_{2.5}$ aerosol in residential houses located near major highways: Indoor versus outdoor concentrations* Atmospheric Environment 42 (2008) 6575-6585

[85] Maxwell, J. C. (1879). *On stresses in rarefied gases arising from inequalities of temperature*. Philosophical Transactions of the Royal Society, 170, 231-240.

[86] McGann B. T & Jennings S. G., *The efficiency with which drizzle and precipitations sized drops collide with aerosol particles* Atmospheric Environment Vol 25A, N 3/4, pp. 791-799, 1991.

[87] McMurry P. H., 2000 *A review of atmospheric aerosol measurements* Atmospheric Environment 34 (2000) 1959-1999

[88] Michaelides et al., *Precipitation: Measurement, remote sensing, climatology and modeling* Atmospheric Research 94 (2009) 512-533

[89] Mircea et al., *Precipitation scavenging coefficient: influence of measured aerosol and raindrop size distributions* Atmospheric Environment 34 (2000) 5169-5174

[90] Möhler, O., DeMott, P.J., Stetzer, O., and the AIDA team, 2008a. *The fourth international ice nucleation workshop ICIS-2007. 15th International Conference on Clouds and Precipitation*. Cancun, 7-11 July.

[91] Möhler, O., Schneider, J., Walter, S., Heymsfield, J., Schmitt, C., Ulanowski, Z.J.,and the AIDA team, 2008b. *How coating layers influence the deposition mode ice nucleation on mineral particles*. 14th International Conference on Clouds and Precipitation. Cancun, 7-11 July.

[92] Montañez R. A. and García-García F., Atmósfera, 6 (1993) 39.

[93] Morawska L., et al., *Experimental study of the deposition of combustion aerosol in the human respiratory tract* Aerosol Science 36 (2005) 939-957.

[94] Ohwada, T., & Sone, Y. (1992). *Analysis of thermal stress slip flow and negative thermophoresis using the Boltzmann equation for hard-sphere molecules.* European Journal of Mechanics B, 11, 389-414.

[95] Oostra, W. (1998). *An experimental approach into the phenomenon of thermophoresis.* Ph.D. thesis, Delft University of Technology, The Netherlands.

[96] Parker C. Reist. *Introduction to Aerosol Science*, Macmillian Publishing Company, New York, 1984

[97] Pérez, P.G., García, J.A., Casanova, J., 1985. *Estudio de la variación temporal de una población de IN y análysis de posibles anomalías.* Revista de Geofísica 41, 237-242.

[98] Perez P.G., García J. A. and Casanova J., Atmos. Environ., 19 (1985) 993.

[99] Perry, J.H., 1963. *Chemical Engineers' Handbook.* McGraw-Hill Company, New York.

[100] Philippin S. and Betterton E. A., Atmos. Res., 43 (1997) 263.

[101] Prodi, V. (1972). *A condensation aerosol generator for solid monodisperse particles.* In T.T. Mercer, P.P. Morrow, & W. Stober (Eds.), Assessments of airborne particles (pp. 169-181).

[102] Prodi, F., Santachiara, G., Cornetti C.(2002). *Measurements of diffusiophoretic velocities of aerosol particles in the transition region.* J. Aerosol Sci. 33, 181-188.

[103] Prodi, F., Santachiara, G., Travaini, S., Vedernikov, A., Dubois, F., & Legros, J. C. (2006). *Measurements of phoretic velocities of aerosol particles in microgravity conditions.* Atmospheric Research, 82, 183-189.

[104] F. Prodi, G. Santachiara, L. Di Matteo, A. Vedernikov, S.A. Beresnev, V.G. Chernyak: *Measurements of Thermophoretic Velocities of Aerosol*

Particles in Microgravity Conditions in Different Carrier Gases, Journal of Aerosol Science 38 (2007)pag 645-655

[105] Pruppacher, H.R., Klett, J.D., *Microphysics of Clouds and Precipitation*. Kluwer Academic Publishers, 2003.

[106] Radke L. F. and Hobbs P. V., J. Atmos. Sci., 26 (1969) 281.

[107] Raga G. B. and Jonas P. R., Atmos. Environ., 29 (1995) 673.

[108] Reade L., Jennings S. G. and McSweeney G., Atmos. Res., 82, (2006) 610.

[109] Richardson, M.S., DeMott, P.J., Kreidenweis, S.M., Cziczo, D.J., Dunlea, E.J., Jimenez, J.L., Thomson, D.S., Ashbaugh, L.L., Borys, R.D., Westphal, D.L., Casuccio, G.S., Lersch, T.L., 2007. *Measurements of heterogeneous ice nuclei in the western United States in springtime and their relation to aerosol characteristics*. Journal of Geophysical Research 112, D02209. doi:10.1029/2006JD007500.

[110] Rissman T. A., VanReken T. M., Wang J., Gasparini R., Collins D. R., Jonsson H. H., Bretchel F. J., Flagan R. C. and Seinfeld J. H., J. Geophys. Res., 111 (2006) D05S11, doi:10.1029/2004JD005695.

[111] Roberts G. C. and Nenes A., Aeros. Sci. Tech., 39 (2005) 206.

[112] Roberts G. C., Andreae M. O., Zhou J. and Artaxo P. , Geophys. Res. Lett., 28 (2001) 2807.

[113] Rogers, D.C., 1982. *Field and laboratory studies of ice nucleation in winter orographic clouds*, Ph.D. dissertation, Dept. of Atmospheric Science, Univ. of Wyoming, Laramie, 161 pp.

[114] Rogers, D.C., De Mott, P.J., Kreidenweis, S.M., Chen, Y., 1998. *Measurements of ice nucleating aerosols during SUCCESS*. Geophysical Research Letters 25, 9, 1383-1386.

[115] Rogers, D.C., DeMott, P.J., Kreidenweis, S.M., Chen, Y., 2001. *A continuous- flow diffusion chamber for airborne measurements of ice nuclei*. Journal of Atmospheric and Oceanic Technology 18, 725-741.

[116] Rosinski, J., 1979. *The role of natural and man-made ice-forming nuclei in the atmosphere.* Advances in Colloid and Interface Science 10, 315-367.

[117] Rosinski, J., 1995. *Cloud condensation nuclei as a real source of ice forming nuclei in continental and marine air masses.* Atmospheric Research 38, 351-359.

[118] Rosinski J. and Morgan G. M., J. Aerosol Sci., 19 (1988) 531.

[119] Salma I., Balásházy I., Winkler-Heil R., Hofmann W. and Záray G., *Journal of Aerosol Science* 33 (2002), 119-132.

[120] Santachiara G., Di Matteo L., Prodi F. and Belosi F., Atmos. Res. (2010), doi:10.1016/j.atmosres.2009.08.004.

[121] Santachiara, G., Prodi, F., & Cornetti, C. (2002). *Experimental measurements on thermophoresis in the transition region.* Journal of Aerosol Science, 33, 769-780.

[122] Santachiara G., L. Di Matteo, F. Belosi, F. Prodi, *Atmospheric particles acting as Ice Forming Nuclei in different size ranges and Cloud Condensation Nuclei measurements*, Il Nuovo Cimento, Vol. 124 B, N. 5, pp. 565-581, 2009.

[123] Santi et al., *Real-time aerosol photometer and optical particle counter comparison* IL NUOVO CIMENTO DOI 10.1393/ncb/i2010-10904-5 Vol. 125 B, N. 8

[124] Saxena V. K. and Grovenstein J. D., Atmos. Res., 31 (1994) 71.

[125] Saxton, R. L., & Ranz, W. E. (1952). *Thermal force on an aerosol particles in a temperature gradient.* Journal of Applied Physics, 23, 917-923.

[126] Schadt, C. F., & Cadle, R. D. (1961). *Thermal force on aerosol particles. Journal of Physical Chemistry*, 65, 1689-1694.

[127] Schmitt, K. H. (1959). *Untersuchungen an Schwebstoffteilchen im Temperaturfeld.* Zeitschrift fuer Naturforschung, 14a, 870-881.

[128] Shakhov, E. M. (1968). *Generalization of the Krook equation.* Fluid Dynamics, 3, 95-96.

[129] Shilling, J.E., Fortin, T.J., Tolbert, M.A., 2006. *Depositional ice nucleation on crystalline organic and inorganic solids.* Journal of Geophysical Research 111, D12204. doi:10.1029/2005JD006644.

[130] Shen, Z., Li, X., Cao, J., Caquineau, S., Wang, Y., & Zhang, X. (2005). *Characteristics of clay minerals in Asian dust and their environmental significance.* China Particuology, 3(5), 260-264.

[131] Sone, Y., & Aoki, K. (1981). *Negative thermophoresis: Thermal stress slip flow around a spherical particle in a rarefied gas.* In S.S. Fisher, (Ed.) Rarefied gas dynamics (pp. 489-503). New York: American Institute of Aeronautics and Astronautics.

[132] Sone, Y., & Aoki, K. (1983). *A similarity solution of the linearized Boltzmann equation with application to thermophoresis of a spherical particle.* Journal de Mécanique Théorique et Appliquée, 2, 3-12.

[133] Soulage, R.G., 1958. *Influence de l'aérosol atmosphérique sur la formation de la grêle.* Bulletin Observatoire Puy de Dome 4, 125-146.

[134] Soulage, R.G., Admirat, P., 1962. *Description d'anomalies estivales du pouvoir glacogéne de l'air en France.* Bulletin Observatoire Puy de Dome 4, 155-171.

[135] Stern N. *The Economics of Climate Change: The Stern Review*, Cambridge University Press 2007

[136] Stevenson, C.M., 1968. *An improved Millipore filter technique for measuring the concentrations of freezing nuclei in the atmosphere.* The Quarterly Journal of the Royal Meteorological Society 94, 35-44.

[137] Stroud C. A. et al., J. Geophys. Res., 107 (2002) No. D16, 4291, 10.1029/2001JD000959

[138] Stroud C. A., Nenes A., Jimenez J. L., DeCarlo P. F., Huffman J. A., Bruintjes R., Nemitz E., Delia A. E., Toohey D.W., Guenter A. B. and Nandi S., J. Atmos. Sci., 64 (2007) 441.

[139] Sun J. & Ariya P.A, *Atmospheric organic and bio-aerosols as cloud condensation nuclei (CCN): A review.* Atmospheric Environment 40 (2006) 795-820

[140] Szakáll M et al., *Shapes and oscillation of falling raindrops-A review* Atmospheric Research 97 (2010) 416-425

[141] Szyrmer, W., Zawadzki, I., 1997. *Biogenic and anthropogenic sources of ice- forming nuclei: a review.* Bulletin of the American Meteorological Society 78, 209-228.

[142] Talbot, L., Cheng, R. K., Schefer, R. W., & Willis, D. R. (1980). *Thermophoresis of particles in a heated boundary layer. Journal of Fluid Mechanics* ,101, 737-758.

[143] Toda, A., Ohi, Y., Dobashi, R., & Hirano, T. (1996). *Accurate measurements of thermophoretic effect in microgravity.* Journal of Chemical Physics, 105(16), 7083-7087.

[144] Toda, A., Ohnishi, H., Dobashi, R., & Hirano, T. (1998). *Experimental study on the relation between thermophoresis and size of aerosol particles.* International Journal of Heat and Mass Transfer, 41, 2710-2713.

[145] Travis D., Carleton A., Lauritsen R., 2002

[146] Trijonis, J., 1980 *Visibility in the southeast-an exploration of the historical data base*, Atmospheric Environment 13, 833-843

[147] Twomey S. et al., J. de Rech. Atmos., 1 (1963) 101.

[148] Twomey S. and Davidson K. A., J. Atmos. Sci., 32 (1975) 225.

[149] Twomey S. and Wojciechowski T. A., J. Atmos. Sci., 26 (1969) 684.

[150] Vali, G., 1975. *Workshop Summary 3rd International Workshop on ice nucleus measurements.* Bulletin of the American Meteorological Society 56, 1180-1184.

[151] VanReken T. M. , Nenes A., Flagan R. C. and Seinfeld J. H., Aer. Sci.Technol., 38 (2004) 639.

[152] Vychuzhanina, M.V., Grishina, N.P., Parshutkina, I.P., Plaude, N.O., Potapov, Ye.I., 1989. *Measurements of the atmospheric aerosol in industrial and rural areas of the USSR European territory.* Journal Aerosol Science 20 (8), 1237-1240.

[153] Waldmann, L. (1959). *Über die Kraft eines inhomogenen Gases auf kleine suspendierte Kugeln.* Zeitschrift fuer Naturforschung, 14a, 589-599.

[154] Wallace M. and Hobbs V., *Atmospheric Science*, Elsevier, 2006.

[155] Winiwarter W., Bauer H., Caseiro A., Puxbaum H., *Quantifyng emissions of primary biological aerosol particle mass in Europe* Atmospheric Environment 43 (2009) 1403-1409.

[156] Yamamoto, K., & Ishihara, Y. (1988). *Thermophoresis of a spherical particle in a rarefied gas of a transition regime.* Physics of Fluids, 31, 3618-3624.

[157] Yan P., et al., *Hygroscopic growth of aerosol scattering coefficient: A comparative analysis between urban and suburban sites at winter in Beijing* Particuology 7 (2009) 52-60.

[158] Yum S. Y. and Hudson J. H., J. Geophys. Res., 106 (2001) 15,045.

[159] Zachariassen et al., *Ice nucleation in solutions and freeze-avoiding insects-homogeneous or heterogeneous?* Cryobiology 48 (2004) 309-321

[160] Zhao H. & Zheng C., *Monte Carlo solution of wet removal of aerosol by precipitation* Atmospheric Environment 40 (2006) 1510-1525

[161] Zobrist, B., Marcolli, C., Koop, T., Luo, B.P., Murphy, D.M., Lohmann, U., Zardini, A.A., Krieger, U.K., Corti, T., Cziczo, D.J., Fueglistaler, S., Hudson, P.K., Thomson, D.S., Peter, T., 2006. *Oxalic acid as a heterogeneous ice nucleus in the upper troposphere and its indirect aerosol effect.* Atmospheric Chemistry and Physics 6, 3115-3129.

[162] Zhang L. et al, 2004 *Numerical studies of aerosol scavenging by low-level, warm stratiform clouds and precipitation* Atmospheric Environment 38 (2004) 4653-4665

[163] Zhang L. et al, 2006 *A review of current knowledge concerning size-dependent aerosol removal* China Particuology, Vol. 4, No 6, 272-282, 2006

[164] Zhang, M., Han, Z., & Zhu, L. (2007). *Simulation of atmospheric aerosols in East Asia using modeling system RAMS-CMAQ: Model evaluation*. China Particuology, 5(5), 321-327.

[165] Zheng F., *Thermophoresis of spherical and non-spherical particles: a review of theories and experiments*, Advances in Colloid and Interface Science 97 (2002) 255-278.

[166] Zheng M. et al., *Dry and wet deposition of elements in Hong Kong* Marine Chemistry 97 (2005) 124-139.

[167] Zobrist B. et al., Atmos. Chem. Phys., 6 (2006) 3115.

[168] Zuberi B., Bertram A. K., Koop T., Molina L. T. and Molina M. J., J. Phys. Chem. A, 105 (2001) 6458.

[169] Zuberi, B., Bertram, A.K., Koop, T., Molina, L.T., Molina, M.J., 2001. *Heterogeneous freezing of aqueous particles induced by crystallized* $(NH_4)2SO_4$*, ice and letovicite*. Journal of Physical Chemistry A 105, 6458-6464.

ACKNOWLEDGEMENT

Per concludere vorrei ricordare che questo lavoro è stato realizzato grazie alla preziosa collaborazione di tutti i Prof., ricercatori e tecnici con i quali ho avuto la fortuna di lavorare (dislocati tra Bologna, Ferrara e Torino).

Per quanto riguarda *Bologna* ringrazio il Prof. F. Prodi (mio relatore nei primi due anni di dottorato) che mi ha accolta a Bologna e mi ha trasmesso l'amore per la ricerca; il gruppo di ricerca composto dai ricercatori Dott. F. Belosi, Dott. G. Santachiara e dai diversi ricercatori (e cari amici) che si sono succeduti nel tempo dividendo con me l'ufficio: Silvia Ferrari, Guido Turatti, Efisio Santi; inoltre Marcello Tercon e Giuliano Trivellone per la preziosa assistenza tecnica. Ringrazio inoltre tutte le persone che ho ho avuto modo di conoscere presso il CNR, in modo particolare all'ISAC. Vorrei ricordare tutte le persone che ho conosciuto a Bologna e che non ho ancora menzionato nel precedente elenco, tra le quali tre che hanno avuto (ed hanno) un'importanza fondamentale: Greta Varchi, Dania Cescato ed Elisa Palazzi.

Per quanto riguarda la sede di *Ferrara* ringrazio il mio relatore interno F. Porcù e il Prof. F. Frontera, coordinatore del dottorato e l'Università degli Studi di Ferrara.

Infine, per quanto riguarda *Torino*, il Prof. A Piano (mio relatore esterno) e il dott. M. Casazza che mi hanno accolto nel loro gruppo di ricerca e l'Università degli Studi di Torino.

Ringrazio i miei referee: Prof. C. Sabbioni, Prof. A. Gambaro e Prof. A. Di Sarra per aver letto la tesi e avermi fornito consigli per migliorarla.

Ringrazio Ilaria per il suo supporto nella traduzione.

Ringrazio tutti i miei amici storici dislocati in varie sedi per la loro presenza continua, in particolare Francesco, Silvia e Antonella.

Un grazie speciale a Luca, che mi è stato costantemente vicino dimostrando

affetto e comprensione. Un grazie caloroso anche alla sua famiglia.

Ringrazio mia sorella Michela e Sergio per l'affetto e la grande disponibilitá nei miei confronti. In modo particolare dico ancora una volta grazie ai miei genitori che sono sempre stati presenti nella mia vita dandomi sostegno di ogni tipo.